Modelling and Analysis of Long Josephson Junctions

Timco Visser

2002

Ph.D. thesis
University of Twente

Twente University **Press**

Also available in print:
http://www.tup.utwente.nl/catalogue/book/index.jsp?isbn=9036517591

Modelling and Analysis of Long Josephson Junctions

Twente University **Press**

Publisher:
Twente University Press,
P.O. Box 217, 7500 AE Enschede, the Netherlands,
www.tup.utwente.nl

Cover design: Jo Molenaar, [deel 4] ontwerpers, Enschede
Print: Océ Facility Services, Enschede

ISBN 9036517591

MODELLING AND ANALYSIS OF LONG JOSEPHSON JUNCTIONS

PROEFSCHRIFT

ter verkrijging van
de graad van doctor aan de Universiteit Twente,
op gezag van de rector magnificus,
prof.dr. F.A. van Vught,
volgens besluit van het College voor Promoties
in het openbaar te verdedigen
op vrijdag 7 juni 2002 te 15.00 uur

door

Timco Peter Paul Visser
geboren op 3 november 1973
te Hengelo [Ov.]

Dit proefschrift is goedgekeurd door de promotor
prof.dr. E. van Groesen

en de assistent-promotor
dr. S.A. van Gils

Preface

Four years... An eternity gone by before you notice it.

This is the time to reflect on those last four years. Much has happened in that period. Not only in my work, but also in my social life, as most of you already know. Now it is also time to look back and mention some of those that have contributed to this work or otherwise deserve to be mentioned here. This list will have to be incomplete, so let me start off by thanking those that will not get mentioned below, since I will have to restrict myself somehow!

To start off, I would like to thank Brenny, for giving me the opportunity to work in his group and to benefit from his constant drive and motivation. And in the same line, Stephan. They have both contributed a lot to the contents of this thesis. It was very interesting to get a glimpse of your different mathematical worlds.

From mathematics to physics. I would also like to thank Alexey Ustinov and his group here, for letting me spend some time in Erlangen. My stay in your group has strongly influenced the directions taken in the research, resulting in this thesis. For the discussions about modelling I would like to thank Farruh from Erlangen and Gerrit Gerritsma from Applied Physics in Twente. A further word of thanks goes out to Edward Goldobin, for useful discussions.

I would also like to thank Arjen Doelman and Gianne Derks, without whom chapter four would not exist...?

A special word of thanks should be directed to Edi, for being a very nice office-mate and friend, and for being one of my "paranimfs". I really enjoyed our discussions and your sense of humour.

The financial support of NWO (the Dutch Science Foundation) is gratefully acknowledged.

To start on the more condensed lists, I would like to thank Jan Zitzmann for very interesting discussions, Kempi for the nice game-evenings and Marcus Schuster for fighting off the snowmans!

I would like to thank my colleagues at Applied Mathematics, Barbera for her always cheerful presence, Judith for her Friday-afternoon-remarks, Wilbert for starting me off on Linux, Monica and Agus for all the snacks I found in your office, and for enabling me to use the cd-writer (which proved to be of extreme importance near the end!), Helena for helping me to extend my Euro-collection, Manfred for organising

the skittles-evening (including police interrogation!) and of course Hadi for our discussions and for reading my manuscript. In general, to all of my colleagues, I enjoyed being in one group with you. I will especially remember our coffee and lunch breaks!

Apart from work there are also quite a few persons who deserve to be mentioned. To start off Guido (for getting addicted to a certain game), Vishy, Jurriaan, Ikina Bram, Martien, Mark, Lyuba and Christiaan for joining the MECCG-gang. I hope we will have many more adventures!

On more general games-ground I would like to thank Ikina, Jurriaan, Elise, and Sjoerd for our game(evenings/weekends). I would also like to thank the members of DIOK and 4 Happy Feet, badminton and dancing have been a worthwhile and welcome distraction from my work!

A warm word of thanks is directed to my parents, for being there for me and stimulating me in my studies and work! I would further like to thank my in-laws for the regular parrot-sitting. I would like to thank my sister for being my other "paranimf" and for all the fun we had.

I would like to thank all the rest of my family and friends for just being who they are. Toon and Freya, thanks for taking care of our pets, and for the pleasant evenings.

A last, but certainly not least word of thanks is reserved for my Yvonne, for her help in everything and her understanding!

Timco Visser Hengelo, mei 2002

Contents

1 Introduction **1**

1.1 The Josephson effect 1
1.2 Josephson junctions 3
1.2.1 The long Josephson junction 4
1.3 Effects of interest 5
1.4 Applications 7
1.5 Outline 7

2 Modelling **9**

2.1 Introduction 9
2.2 The long Josephson junction 10
2.2.1 General model 11
2.2.2 Ideal superconductors 13
2.2.3 Quasi-particle tunnelling 16
2.2.4 Applied bias current 16
2.2.5 Surface resistance 17
2.2.6 Further extensions 18
2.3 Stacks of long Josephson junctions 21
2.3.1 General model 23
2.3.2 Infinite surface resistance 25
2.3.3 Zero impedance in outer layers 26
2.3.4 Large surface resistance 28
2.A Detailed derivation of the equations 29
2.A.1 Derivation for the single junction 29
2.A.2 Stack of junctions 31
2.A.3 No surface resistance 32
2.A.4 Large surface resistance 34
2.B The Maple worksheet to derive the equations (2.A.27) 37

3 The single Josephson junction **43**

3.1 Travelling waves . . . 43
3.2 Unperturbed case . . . 44
3.3 Perturbation analysis . . . 45
3.4 Travelling kink-solutions . . . 48
3.5 Numerical calculations . . . 50
3.6 Heteroclinic cycle breakup . . . 52
3.6.1 Sketch of the situation . . . 52
3.6.2 Verification of the assumptions . . . 56
3.7 Other configurations . . . 61
3.A Proof of Lemma 6 . . . 61

4 Stability **63**

4.1 The spectral problem . . . 63
4.2 The essential spectrum . . . 65
4.3 The Evans function . . . 66
4.4 Analysis with zero surface resistance . . . 68
4.5 Analysis of the Evans function around $\lambda = 0$. . . . 71
4.6 Analysis of the Evans function around the points $\lambda = \pm i\sqrt{1-c^2}$ . . . 73

5 Stacks of Josephson junctions **77**

5.1 Rewriting the equations . . . 77
5.2 Symmetric solutions . . . 78
5.3 Identical junctions with a single fluxon . . . 79
5.4 Unequal junctions . . . 81
5.4.1 The case $J > 1$ . . . 82
5.5 Numerical experiments . . . 87
5.A The PDE-solver . . . 89
5.A.1 The numerical scheme . . . 89

6 Conclusions and recommendations **91**

6.1 Modelling . . . 91
6.2 Single long junction . . . 92
6.3 Stacks of junctions . . . 93

Chapter 1

Introduction

This first chapter will give a brief description of what a (long) Josephson junction is. The Josephson effect, which is the basis of the functionality of this element, will be introduced in the first section. The analysis of the Josephson effect given here, is heavily based on [6], a more elaborate discussion can be found in [1].

In section 1.2 some examples of Josephson junctions will be given. The most interesting and important effects will be discussed in section 1.3. In the last section of this chapter some applications will be discussed.

1.1 The Josephson effect

The advent of quantum mechanics has opened new possibilities to understand nature and to predict its behaviour. The Josephson effect is one of the effects which was first predicted from theory and only later could be observed in experiments [6]. It is a real quantum mechanical effect, since it cannot be explained by classical physics.

Quantum mechanics predicts that electrons belonging to a metal, actually have a small chance of being found outside of the material. This opens the possibility of the tunnelling of electrons. If two metals are brought very close, but still with a small gap in between, there is a chance that an electron of the one metal is found in the other metal. The electrons can "jump" from one metal to the other. If a potential difference is applied, a current can flow from the one metal to the other, even though there is an insulator in between. The Josephson effect is a similar effect.

The Josephson effect occurs, if two superconductors are brought close to each other. See figure 1.1. We take two (ideal) superconductors, so all electrons have condensed to the superconducting state, i.e., they have all formed Cooper pairs. Since all the electron pairs are in the same state, they can be described by a single wave function. We denote the wave function for the electrons in the left superconductor by Ψ_L and the wave function for electrons in the right hand superconductor by Ψ_R. The Schrödinger equations for this system are then given by the following expression

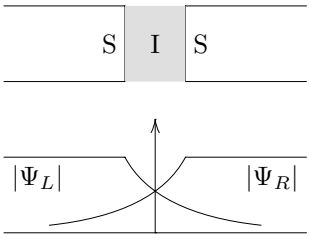

Figure 1.1: Two superconductors separated by a thin insulating barrier.

$$\begin{aligned} i\hbar\frac{\partial}{\partial t}\Psi_L &= E_L\Psi_L - K\Psi_R \\ i\hbar\frac{\partial}{\partial t}\Psi_R &= E_R\Psi_R - K\Psi_L \end{aligned} \tag{1.1.1}$$

The wave functions are complex valued functions, and can hence be written as

$$\begin{aligned} \Psi_L &= \sqrt{\rho_L}e^{i\theta_L} \\ \Psi_R &= \sqrt{\rho_R}e^{i\theta_R} \end{aligned} \tag{1.1.2}$$

The amplitude of the wave functions is the square root of the density of pairs, since $\Psi^*\Psi$ should give the density.

We apply a voltage V across the junction, where the potential of the left is raised w.r.t. the right. Since the electron has a negative charge, the energy for them is lower at the left. We take the zero level of the energy as the average of the potential energy left and right. We have, $E_L = -E_R = -eV$. We substitute (1.1.2) into the equations (1.1.1) and obtain, after solving for the real and complex part, the equations

$$\begin{cases} \dfrac{\partial\rho_L}{\partial t} = \dfrac{2}{\hbar}K\sqrt{\rho_L\rho_R}\sin\phi \\ \dfrac{\partial\rho_R}{\partial t} = -\dfrac{2}{\hbar}K\sqrt{\rho_L\rho_R}\sin\phi \end{cases} \quad \begin{cases} \dfrac{\partial\theta_L}{\partial t} = \dfrac{K}{\hbar}\sqrt{\dfrac{\rho_R}{\rho_L}}\cos\phi + \dfrac{eV}{\hbar} \\ \dfrac{\partial\theta_R}{\partial t} = \dfrac{K}{\hbar}\sqrt{\dfrac{\rho_L}{\rho_R}}\cos\phi - \dfrac{eV}{\hbar} \end{cases} \tag{1.1.3}$$

where we have introduced $\phi = \theta_L - \theta_R$ as the phase difference between the two wave functions.

From equation (1.1.3) we can derive the Josephson relations. We see that if $\phi(t)$ is positive (but less than π) ρ_L increases, so there is a flow of electron pairs from the right to the left. This means that there is a current from left to right. This is the dc-Josephson effect:

$$I = I_c\sin\phi = I_c\sin(\theta_l - \theta_R), \tag{1.1.4}$$

where I_c is, hence, a positive constant.

Due to this potential difference the phase difference $\phi(t)$ will change in time, as can be seen from (1.1.3):

$$\partial_t\phi(t) = \partial_t\theta_L(t) - \partial_t\theta_R(t) = -\frac{E_L}{\hbar} + \frac{E_R}{\hbar} = \frac{2eV}{\hbar} = \frac{2e}{\hbar}(V_L - V_R) \tag{1.1.5}$$

This equation is called the ac-Josephson relation.

The dc-Josephson relation shows that we can have a direct current tunnelling through the insulator, without any potential difference. This is in contrast to the normal tunnelling current, where a potential difference is needed to get a net current from one metal to another. On the other hand, even a very small applied current will destroy this dc current, since the phase difference will increase over time, and there will be a fast oscillating ac-current.

Since the phase difference is important, one can see that it will be impossible to explain these phenomena with a classical theory.

1.2 Josephson junctions

The device described in the previous section (figure 1.2(a)) is an example of a Josephson junction. More generally a Josephson junction is a weak link between two superconductors. One way of obtaining this is to use the setup described in the previous section. Another way is to take a strip of superconducting material and cover it with a thin layer of insulating material. Then another strip of superconducting material is put across the first one (figure 1.2(b)) creating a small overlap.

Yet another way (and a one-step procedure and hence easier to create is to take a large superconductor and make a Dayem bridge (figure 1.2(c)), in this technique, one cuts away part of the material such that there remains only a thin connection between the two parts of the superconductor. This device also behaves like a Josephson junction, if the dimensions of the connection are smaller than the coherence length.

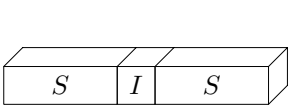

(a) point contact

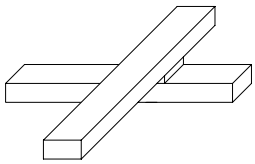

(b) cross-strip junction

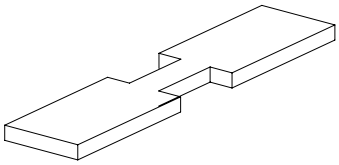

(c) Dayem bridge

Figure 1.2: Three types of Josephson junctions.

1.2.1 The long Josephson junction

A special place among the Josephson junctions, is taken by the so-called long Josephson junctions. These are the central point of interest in this thesis. The important difference with the small junctions is now that not all the dimensions are "small", but there is one direction (the x-direction) which is "large". This means that this x-direction is large compared to the Josephson penetration depth. The Josephson penetration depth is the distance over which a magnetic field can enter the junction. When a Josephson junction is put in a magnetic field, a screening current will start to flow along the surface of the superconductors. This screens the bulk of the superconductor from the the magnetic field. At the junction, this screening will be imperfect and the magnetic field can enter the barrier over a distance λ_J, the Josephson penetration depth (see figure 1.3).

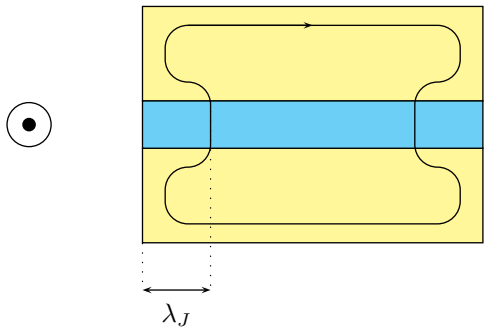

Figure 1.3: The distance over which a magnetic field penetrates a Josephson junction, is called the Josephson penetration depth λ_J.

There are several types of long Josephson junctions. Most notably one distinguishes the "in-line" and "overlap" geometry (figure 1.4). For observations and measurements it is most often convenient to use annular junctions.

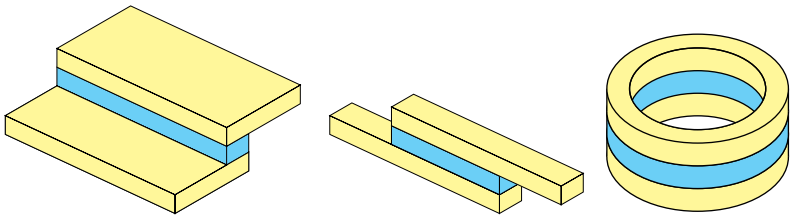

(a) Overlap junction (b) In-line junction (c) Annular junction

Figure 1.4: Types of long Josephson junctions

1.3 Effects of interest

In the long Josephson junction which we will be considering in this thesis, some special phenomena can be observed. The most important of which is the existence of a fluxon. This is a circulating current across the insulator, see figure 1.5. This fluxon can be forced to move if one applies a bias current. A bias current can be injected in the top superconductor from a current source. To study fluxons, most often a uniform bias current is used, as is indicated in figure 1.5. The current will flow along the surface of the top superconductor and then vertically down through the junction. This will influence the fluxon.

The circulating current induces a magnetic field, it will experience a Lorenz force if a bias current is applied. This will accelerate the fluxon, until it reaches a maximum velocity, due to dissipation.

A fluxon can be observed in measurements, due to the fact that it gives rise to a (localised) voltage across the junction. This fluxon corresponds to a local increase of ϕ with 2π. This means that over a local range in x, ϕ_x must be positive. If this object moves, also the time derivative of ϕ at a point the fluxon passes will be positive. This means that there will be a potential difference between the two superconductors. One can observe this as a voltage peak in the time measurement of the local voltage. It is very difficult to measure this local voltage peak, since this is a very short pulse, and hence measurements with a very high time-resolution are necessary. One can also observe the presence of a fluxon by measuring the total voltage, since the positive peak has a positive contribution to the total voltage.

The total voltage over the junction with length L is given by

$$\int_0^L V \mathrm{d}x = \frac{\Phi_0}{2\pi} \int_0^L \phi_t \mathrm{d}x \overset{travelling\ wave}{=} \frac{\Phi_0}{2\pi} \int_0^L c\phi_x \mathrm{d}x = n\Phi_0 c, \tag{1.3.1}$$

if there are n fluxons in the junction, moving with velocity c. As long as the solution is a travelling wave the total voltage is proportional to the velocity and the number of fluxons in the junctions. If the travelling wave solution becomes unstable, there is

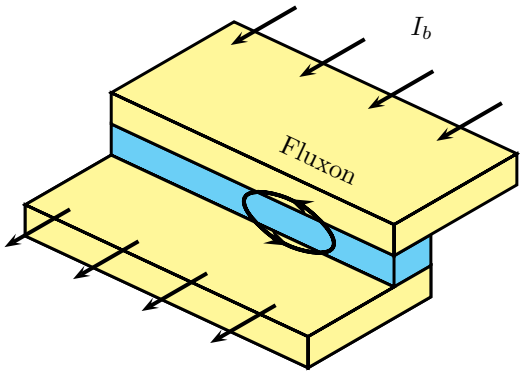

Figure 1.5: A fluxon in a long Josephson junction

a large jump in the voltage across the junction and this can not be interpreted as a velocity anymore.

If one increases the bias current the fluxon will be accelerated until a higher maximal velocity is reached due to dissipative effects. The time derivative of the phase (voltage) will be larger, if the fluxon moves at a higher speed. So the total voltage across the junction will increase. Measuring the voltage, while increasing the bias current will result in a picture like 1.6.

The fluxon corresponds to a (localised) increase of the phase ϕ by 2π, a travelling "front" solution. A different type of phenomenon is the "plasma wave". These are small amplitude waves, which travel along the junction. The fluxon and the plasma waves are two different solutions to the equation describing the Josephson junction (see chapter 3). These two solutions are the most important. There is, however, another important solution. This can also be observed in experiments and is called the resistive state. For a junction in this state, there is almost no difference between points along the junction. The gradients in space are small, but the time derivatives are very large. The whole long junction, actually acts as a single small junction. At each point the phase increases in time.

In experiments, one has to work with junctions of a finite size. Due to the high speed of these fluxons, the fluxon soon reaches the edge of the junction. On collision with the edge several things can happen, depending on the exact physical boundary conditions. The fluxon can be reflected into an anti-fluxon, which is also a circulating current, but the direction of the current is reversed. Since then also the magnetic field of the fluxon points in a different direction, the same bias current induces a force in the opposite direction, moving the anti-fluxon away from the edge. When this anti-fluxon reaches the other edge, it may be reflected in a fluxon again. The collision with the edge will dissipate some of the energy of the fluxon, but the bias current will quickly accelerate it to reach its constant velocity, again.

If, however the dissipation due to the collision with the edge is too high, there is not enough energy for the fluxon to remain, and it vanishes. In stead plasma waves may be generated, which can travel back along the junction, possibly forming a new fluxon on collision with the other edge [27]. So for a junction of finite length fluxons can

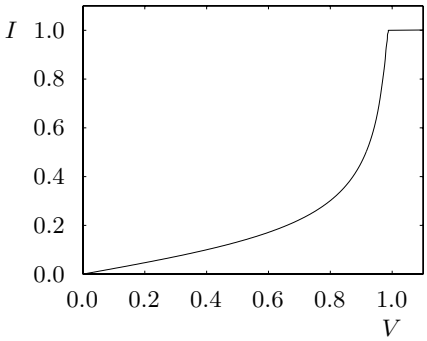

Figure 1.6: An example of what one could measure (or calculate) as an IV-characteristic

disappear and they can be created. To study the dynamics of fluxons experimentally, one quite often uses annular junctions.

The advantage of having annular junctions is that if one can create somehow this localised 2π-kink, then it can never escape (due to the periodicity induced by the geometry). This means that as soon as one has a fluxon, it will always remain (as long as the temperature is low enough).

1.4 Applications

One of the applications of the long Josephson is related to the interaction with the edge, mentioned at the end of the previous section. On collision with the edge, radiation can be emitted.The emission of radiation is partially responsible for the loss of energy when a fluxon collides with the edge of the junction. The radiation emitted can be of extremely high frequencies. This makes a long Josephson junction a very good candidate for a radiation source. For example to be used in a sub-mm wave receivers[18, 19]. A disadvantage of using a single Josephson junction as a radiation source, is that the output power is relatively low. A great improvement would be to have a stack of junctions, working in a phase locked state, to increase the power output.

Another branch of applications of Josephson junctions is their use as rapidly switching electronical elements to build logical circuits (RSFQ technology). For these circuits to operate, a clock is needed to synchronise the operation. A perfect candidate for this is a long Josephson junction, preferably an annular one [39].

The long Josephson junction can also be used to build devices with transistor-like properties [28, 29], needed to amplify the signals from, e.g., radiation detectors based on Josephson junctions. In the most passive use, the long Josephson junctions can also be used as transport channels, the "wiring" of circuits.

Long Josephson junctions (and stacks thereof) are also interesting points of research since this may shed new light on the behaviour and properties of certain types of high-temperature superconductors. (Strictly speaking this is not an application, but it is another motivation to research long Josephson junctions.) Some of these high-T_c superconductors (as e.g. $Bi_2Sr_2CaCu_2O_{8+x}$) form natural stacks of Josephson junctions. The structure of the crystal is such that superconducting and insulating layers alternate, giving rise to an intrinsic Josephson effect [17].

1.5 Outline

In chapter 2 we start off by investigating several models for the long Josephson junction. We obtain equations by taking the continuum limit of a discrete model. In the simplest case we obtain the sine-Gordon equation. By extending the discrete model, we will obtain more complicated equations. For the case of a stack of two junctions we obtain a model containing two terms which were not previously seen.

Chapter 3 will be dedicated to the existence of the aforementioned "fluxon"-solutions in a single long Josephson junction. The stability of these solutions will be investigated in chapter 4.

In the next chapter, we will investigate a stack of two junctions and some possible configurations of fluxons in this stack.

We end in chapter 6 with some conclusions and recommendations.

Chapter 2

Modelling

In this chapter we will consider some different ways to model the long Josephson junction. To this we need to obtain a description of all the currents flowing across and along the junction. These currents can be currents of quasi-particles, which experience resistance, or of electrons condensed in the superconducting state which can flow without any resistance.

To model the currents across the junction, we make use of various models proposed for the short junction: The capacitively shunted junction (CSJ) model for ideal superconductors, and the resistively and capacitively shunted junction (RCSJ) model to model the flow of quasi particles across the junction.

2.1 Introduction

The long Josephson junction has been modelled by many authors in various ways over the years. Basically two separate paths can be distinguished. On the one hand we have the model which was originally developed by Sakai, Bodin and Pederson [31]. In this article a general model is given based on the magnetic flux density and its relation to the phase of the wave function. This model has been used by several authors [30, 38].

A different approach is to model the system as a discrete system, by assuming the relevant physical properties to be constant over some interval Δx. The equations for the long junction are then obtained on taking the limit $\Delta x \to 0$. This approach was used by [11, 26, 27] and will also be the approach used here.

Most of the times this means that a discrete circuit will be posed with specific impedances to model the effect of resistance, capacitive and inductive effects. In this thesis a slightly different approach will be used. We will not immediately make specific assumptions on the impedances to model the relations between current and voltage, but will first derive the equations, for general impedances. Having derived the differential equation which still contains these operators, we will make assumptions for these operators based on physical considerations to obtain closed formulas.

In the first section we will model the long Josephson junction in this fashion. The next section will be dedicated to a stack of two long Josephson junctions.

2.2 The long Josephson junction

In this section we will derive a model for the long Josephson junction (see section 1.2.1), based on a discrete model. We will derive an equation for the phase difference between the top and bottom superconductor. This equation will result from analysing which currents flow and the dependance of these currents on the potential differences. At first the relation between the currents and potential differences is not made specific, but is assumed to be described by a (linear) operator. In later sections specific assumptions are made for these operators to derive the equations in closed form.

If we assume that the superconductors are ideal and there are no quasi-particle currents, the model we will obtain (in section 2.2.2) is given by

$$\Phi_{xx}(x,t) - \Phi_{tt}(x,t) = \sin\Phi(x,t). \tag{2.2.1}$$

This model is obtained by using the CSJ-model for the currents across the junction and an inductance for currents along the junction. This is the sine-Gordon equation, an equation with a Hamiltonian structure.

This model will only be valid for very low temperatures, and small potential differences between the top and bottom superconductor. For higher temperatures, the superconductor will contain some quasi-particles, giving rise to lossy currents. Moreover, if the potential difference between the top and bottom superconductor is large, a pair of electrons may be separated, after which one of the electrons tunnels to the other superconductor. This also results in a current with a non-zero resistance.

Lossy currents across the junction will be incorporated in section 2.2.3. The only change is that we use the RCSJ model for currents across the junction. The model will result in the equation:

$$\Phi_{xx}(x,t) - \Phi_{tt}(x,t) = \sin\Phi(x,t) + \alpha\Phi_t(x,t). \tag{2.2.2}$$

In the next subsection the energy-input through an applied bias current will be included, resulting in the equation

$$\Phi_{xx}(x,t) - \Phi_{tt}(x,t) = \sin\Phi(x,t) + \alpha\Phi_t(x,t) - \gamma(x,t). \tag{2.2.3}$$

The next important extension is to include the contribution of quasi-particles in the superconductors, that flow along the surface, due to potential differences. In section 2.2.5 we derive the equation

$$\Phi_{xx}(x,t) - \Phi_{tt}(x,t) = \sin\Phi(x,t) + \alpha\Phi_t(x,t) - \beta\Phi_{xxt}(x,t) - \gamma(x,t). \tag{2.2.4}$$

2.2.1 General model

At any point along the junction, there will be currents flowing along the junction as well as across. We will model these currents in a discrete model, as indicated in the introduction. The continuous long Josephson junction will be approximated by assuming that in a small strip of size Δx (see figure 2.1) all relevant physical properties are constant. This enables us to write down expressions for the currents. The equations for the continuous system then follow after taking the limit for $\Delta x \to 0$.

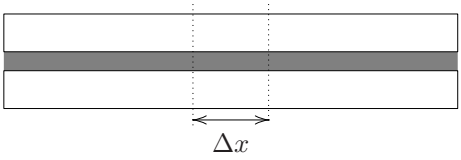

Figure 2.1: The long Josephson junction

We will assume that these currents only depend on some (constant) material properties and the phase differences across the junction and along the junction. Most of these currents only depend on potential differences, which can be related to the time derivative of the phase difference through the AC-Josephson effect. We will assume that the relation between the currents and the potential difference can be described by a linear operator

$$V = \mathsf{Z}(I) \tag{2.2.5}$$

and can be modelled by a constellation of the electronical building blocks: resistor, inductor, capacity. Our discrete model is depicted in figure 2.2. In the figure, $\theta(x,t)$ indicates the phase at the position x at time t, which is related to the voltage by the AC-Josephson relation (1.1.5). Each of the $\mathsf{Z}(I)$ is a suitably chosen combination of resistors, capacitors and inductors.

The relation between the current through each of these elements and the potential difference over it are the well known relations

$$\text{Resistor:} \qquad V = IR \tag{2.2.6a}$$

$$\text{Capacitor:} \quad \frac{\mathrm{d}V}{\mathrm{d}t} = \frac{I}{C} \tag{2.2.6b}$$

$$\text{Inductor:} \qquad V = L\frac{\mathrm{d}I}{\mathrm{d}t} \tag{2.2.6c}$$

The vertical impedance Z_S together with the Josephson junction form a model of a short junction. The model for the long junction will result from coupling these short junctions by suitable chosen impedances Z_B and Z_T, and then letting the size of the short junctions (and the distance between them) go to zero.

Of course, the impedances as depicted in figure 2.2 depend on Δx. So far we have suppressed the dependance of these impedances on Δx. For the impedances $\mathsf{Z}_T(I)$

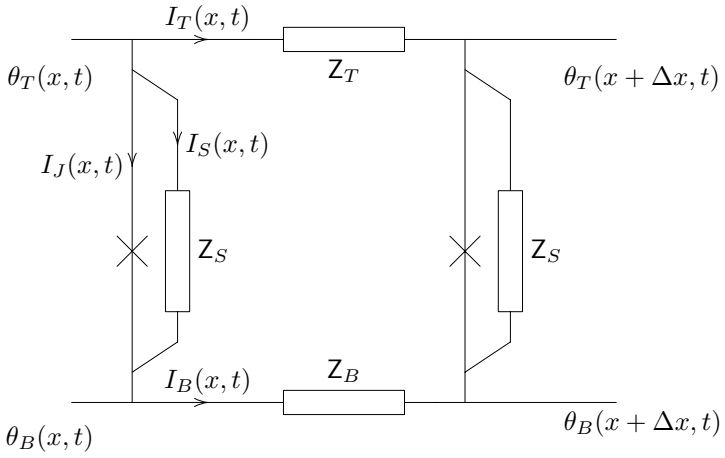

Figure 2.2: The general discrete model of the long Josephson junction

and $\mathsf{Z}_B(I)$ we must have

$$\mathsf{Z}_{T,B}(I;\Delta x) = 2\mathsf{Z}_{T,B}\left(I;\frac{\Delta x}{2}\right) \tag{2.2.7}$$

since we can think of these impedances as a series of two impedances of half the size. Hence we must have $\mathsf{Z}_{T,B}(I) = \Delta x \mathsf{z}_{T,B}(I)$.

The impedance Z_S can be thought of as two parallel impedances of half the size, so we must have

$$\frac{1}{\mathsf{Z}_S(I;\Delta x)} = \frac{2}{\mathsf{Z}_S(I;\frac{\Delta x}{2})}, \tag{2.2.8}$$

which implies that

$$\mathsf{Z}_S(I;\Delta x) = \frac{\mathsf{z}_S(I)}{\Delta x} = \mathsf{z}_S(\frac{I}{\Delta x}) = \mathsf{z}_S(J), \tag{2.2.9}$$

where J is the current density.

We will now derive an equation for the phase difference $\Phi(x,t) = \theta_T(x,t) - \theta_B(x,t)$ between the top and bottom superconductor. We will make use of two identities. The first can be described as the "conservation of phase"

$$\begin{aligned}\theta_T(x,t) - \theta_T(x+\Delta x,t) + \theta_T(x+\Delta x,t) - \theta_B(x+\Delta x,t) + \\ + \theta_B(x+\Delta x,t) - \theta_B(x,t) + \theta_B(x,t) - \theta_T(x,t) = 0.\end{aligned} \tag{2.2.10}$$

(One can object that θ is a multi-valued function and that the above expression cannot be assumed to be zero, but that it may be $2k\pi$. However, later on we will differentiate the expression with respect to time and hence this does not make any difference.)

From this identity and the AC-Josephson relation (1.1.5), we can derive a relation between the drop in the phase difference Φ along the junction and the currents flowing along the surface of the superconductors

$$\frac{\Phi_t(x+\Delta x,t)-\Phi_t(x,t)}{\Delta x}=\frac{2\pi}{\Phi_0}\Big(-\mathsf{z}_T\big(I_T(x,t)\big)+\mathsf{z}_B\big(I_B(x,t)\big)\Big). \tag{2.2.11}$$

An expression for these currents can be derived from Kirchhoff's current law on the top left node (and similarly for the bottom left node):

$$I_T(x-\Delta x,t)-I_T(x,t)-I_J(x,t)-I_S(x,t)=0. \tag{2.2.12}$$

So in this way the x-derivative of the surface currents can be related to the vertical currents (or better the current density of the vertical currents). The vertical currents are the Josephson current and currents due to potential differences between the top and bottom superconductor. These are given by

$$J_J=J_c\sin\Phi(x,t) \tag{2.2.13a}$$

$$J_S=\frac{\Phi_0}{2\pi}(\mathsf{z}_S)^{-1}\big(\Phi_t(x,t)\big) \tag{2.2.13b}$$

In the end we then obtain (a more detailed derivation can be found in the appendix 2.A to this chapter)

$$\Phi_{xxt}(x,t)=\mathsf{z}_e\left(\frac{2\pi}{\Phi_0}J_c\sin\Phi(x,t)+(\mathsf{z}_S)^{-1}\big(\Phi_t(x,t)\big)\right), \tag{2.2.14}$$

where we defined $\mathsf{z}_e(J)=\mathsf{z}_B(J)+\mathsf{z}_T(J)$.

In the next sections we will make assumptions for each of the impedances in figure 2.2 based on physical considerations.

2.2.2 Ideal superconductors

If we assume the superconductors to be ideal superconductors, we do not take into account the flow of quasi-particles. This means that in the scheme of figure 2.2 the vertical currents are only the Josephson current given by (1.1.4) and displacement currents due to capacitive effects. The impedance Z_S is a capacitor in this case (CSJ-model). The currents parallel to the junction experience no resistance and there are no capacitive effects for these currents. So there can only be an inductive effect, due to the magnetic field induced by this current. Hence we take Z_T and Z_B both to be inductors. The effective impedance $\mathsf{z}_e=\mathsf{z}_T+\mathsf{z}_B$ is hence also an inductor.

From the equations 2.2.6 we have

$$\mathsf{z}_e(J)=l\frac{\mathrm{d}}{\mathrm{d}t}J, \tag{2.2.15a}$$

$$(\mathsf{z}_S)^{-1}(V)=c\frac{\mathrm{d}}{\mathrm{d}t}V. \tag{2.2.15b}$$

Substituting these assumptions in (2.2.14) gives the model

$$\frac{1}{l}\Phi_{xx}(x,t) = \frac{2\pi}{\Phi_0}J_c \sin\Phi(x,t) + c\Phi_{tt}(x,t) + \tilde{\Phi}(x,0) \tag{2.2.16}$$

where the term $\tilde{\Phi}(x,0)$ represents the initial conditions:

$$\tilde{\Phi}(x,0) = \frac{1}{l}\Phi_{xx}(x,0) - \mathsf{z}_S^{-1}\big(\Phi_t(x,0)\big) - \frac{2\pi}{\Phi_0}J_c \sin\Phi(x,0) \tag{2.2.17}$$

We can rescale both x and t to obtain a simpler equation. Furthermore we will assume $\tilde{\Phi}(x,0)$ to be zero. (This term represents the initial conditions, not the bias current term, which will be included in section 2.2.4). Rescaling results in the sine-Gordon equation

$$\Phi_{xx}(x,t) - \Phi_{tt}(x,t) = \sin\Phi(x,t). \tag{2.2.18}$$

This is an equation with a Hamiltonian structure. Defining $\Psi(x,t) = \Phi_t(x,t)$, we define the Hamiltonian.

$$H\big(\Phi,\Psi\big)(x,t) = \int_{-\infty}^{\infty}\left(\frac{1}{2}\big(\Phi_x\big)^2 + \tfrac{1}{2}\big(\Psi\big)^2 + 1 - \cos\Phi\right)(x,t)\mathrm{d}x. \tag{2.2.19}$$

The equation of motion can now be written as

$$\partial_t\begin{bmatrix}\Phi\\ \Psi\end{bmatrix} = S\delta H, \tag{2.2.20}$$

where

$$S = \begin{bmatrix}0 & 1\\ -1 & 0\end{bmatrix} \tag{2.2.21}$$

and δ is the variational derivative.

The Hamiltonian can be related to the physical energy as follows. For the ideal superconductors, the model is shown in 2.3. The energy is given by

$$E = \int_0^t P\mathrm{d}t \tag{2.2.22}$$

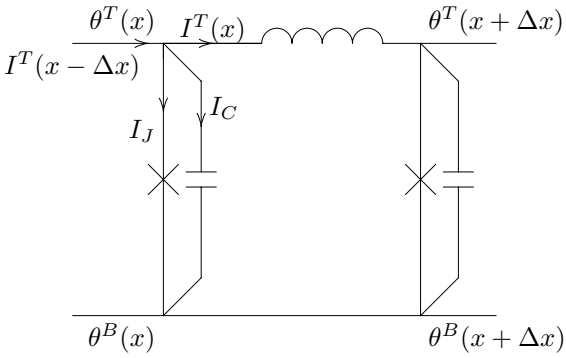

Figure 2.3: The model for ideal superconductors

where

$$P = VI \tag{2.2.23}$$

The potential difference over the left Josephson junction and capacitor is denoted by $V_v(x,t)$. The potential difference over the inductor will be denoted by $V_h(x,t)$. For the vertical impedance, the potential difference and current are equal to

$$V_v(x,t) = \frac{\Phi_0}{2\pi}\Phi_t(x,t) \tag{2.2.24}$$

$$I_v(x,t) = J_v(x,t)\Delta x = \big(J_c \sin\Phi(x,t) + c\frac{\mathrm{d}}{\mathrm{d}t}V_v(x,t)\big)\Delta x \tag{2.2.25}$$

$$= \big(J_c \sin\Phi(x,t) + c\frac{\Phi_0}{2\pi}\Phi_{tt}(x,t)\big)\Delta x \tag{2.2.26}$$

The horizontal current and potential difference are related by

$$V_h(x,t) = \frac{\Phi_0}{2\pi}\big(\Phi_t(x,t) - \Phi_t(x+\Delta x,t)\big) = -\frac{\Phi_0}{2\pi}\Delta x\Phi_{xt}(x,t) + \mathcal{O}(\Delta x^2) \tag{2.2.27}$$

$$V_h(x,t) = L\frac{\mathrm{d}I_h(x,t)}{\mathrm{d}t} \Rightarrow I_h(x,t) = -\frac{\Phi_0}{2\pi}\frac{\Delta x\Phi_x(x,t)}{L} + I_0 + \mathcal{O}(\Delta x^2). \tag{2.2.28}$$

Since the inductor L is proportional to Δx, we have $L = l\Delta x$.

Taking the limit for $\Delta x \to 0$, we obtain the expression

$$E = \int_0^t \int_{-\infty}^{\infty} \left(\frac{\Phi_0}{2\pi}\Phi_t(x,t)\left(J_c \sin\Phi(x,t) + c\frac{\Phi_0}{2\pi}\Phi_{tt}(x,t)\right) + \right. \tag{2.2.29}$$

$$\left. \frac{\Phi_0}{2\pi}\Phi_{xt}(x,t)\left(\frac{\Phi_0}{2\pi}\frac{\Phi_x(x,t)}{l} + I_0\right)\right)\mathrm{d}x\mathrm{d}t \tag{2.2.30}$$

The integration over time can be performed, and we get (after setting the initial condition $\Phi(x,0) = 0$):

$$E = \frac{\Phi_0}{2\pi}\int_{-\infty}^{\infty}\big(J_c(1-\cos\Phi) + \frac{1}{2}\frac{\Phi_0}{2\pi}c\Phi_t^2 + \frac{1}{2l}\frac{\Phi_0}{2\pi}\Phi_x^2 + \Phi_x I_0\big)(x,t)\mathrm{d}x \tag{2.2.31}$$

The last term in this expression

$$\int_{-\infty}^{\infty} I_0\Phi_x(x,t)\mathrm{d}x = I_0(\Phi(\infty,t) - \Phi(-\infty,t) \tag{2.2.32}$$

is a *constant* expression and follows from the boundary conditions. We choose the zero level of the energy in such a way that this term vanishes.

Rescaling x and t we obtain the equation

$$\frac{2\pi}{\Phi_0 J_c}E = \int_{-\infty}^{\infty}\big(1-\cos\Phi(\tilde{x},\tilde{t})\big) + \frac{1}{2}\big(\Phi_{\tilde{t}}(\tilde{x},\tilde{t})\big)^2 + \frac{1}{2}\big(\Phi_{\tilde{x}}(\tilde{x},\tilde{t})\big)^2\mathrm{d}\tilde{x} \tag{2.2.33}$$

Which is a multiple of the Hamiltonian introduced before. So, in this case there is a clear relation between the Hamiltonian introduced and the physical energy.

The rescaling is explicitly given by

$$\tilde{x} = \sqrt{\frac{2\pi J_c l}{\Phi_0}}x \qquad \tilde{t} = \sqrt{\frac{2\pi J_c}{\Phi_0 c}}t \tag{2.2.34}$$

which are, in fact, exactly the same transformations as used to obtain (2.2.18).

2.2.3 Quasi-particle tunnelling

If a potential difference exists between the two superconductors, a Cooper pair in the superconductor with the higher potential can be broken, to allow one electron to tunnel to the other superconductor [1]. This can of course, only happen if the potential difference between the two superconductors is sufficiently large to allow the energy to decrease in this process.

At temperatures above $0K$, there will also be some thermally excited quasi-particles, which can tunnel to the other side, if a potential difference (of arbitrary small size) is applied to the system. Both of these effects require a potential difference and result in a loss of energy. These effects can be modelled by a resistor across the junction. In the scheme of figure 2.2, this means that the impedance Z_S becomes a capacitor parallel to a resistor.

For the equation (2.2.14) this means that

$$\mathsf{z}_e(J) = l\frac{\mathrm{d}}{\mathrm{d}t}(J), \tag{2.2.35a}$$

$$(\mathsf{z}_S)^{-1}(V) = c\frac{\mathrm{d}}{\mathrm{d}t}V + \frac{V}{r}. \tag{2.2.35b}$$

With these relations equation (2.2.14) becomes (after rescaling and again taking the initial conditions to be zero.)

$$\Phi_{xx}(x,t) - \Phi_{tt}(x,t) = \sin\Phi(x,t) + \alpha\Phi_t(x,t). \tag{2.2.36}$$

The value of α is given by

$$\alpha = \sqrt{\frac{\Phi_0}{2\pi J_c c}}\frac{1}{r} \tag{2.2.37}$$

This is an equation with a mixed conservative and dissipative character, it can be written as

$$\partial_t \begin{bmatrix}\Phi\\ \Psi\end{bmatrix} = \begin{bmatrix}0 & 1\\ -1 & 0\end{bmatrix}\begin{bmatrix}\frac{\delta H}{\delta\Phi}\\ \frac{\delta H}{\delta\Psi}\end{bmatrix} - \begin{bmatrix}\alpha & 0\\ 0 & 0\end{bmatrix}\begin{bmatrix}\frac{\delta H}{\delta\Phi}\\ \frac{\delta H}{\delta\Psi}\end{bmatrix}, \tag{2.2.38}$$

with H being defined as in (2.2.19). So, the energy H is no longer conserved.

2.2.4 Applied bias current

The quasi-particle tunnelling described above, leads to dissipation of energy. One can also drive the system by applying a bias current to the system. A current source is connected to the two superconducting layers. This enforces a vertical current across the junction. To incorporate this in our model, we extend the model of figure 2.2 to include a bias current at the top and bottom (see figure 2.4).

The derivation does not change much. The bias current enters the model through the expression for the currents I_T and I_B, since there is an extra current into the top left node. It is easy to see that equation (2.A.8) becomes

$$\Phi_{xxt}(x,t) = \frac{2\pi}{\Phi_0}\mathsf{z}_e\big(J_J(x,t) + J_S(x,t) - J_b(x,t)\big), \tag{2.2.39}$$

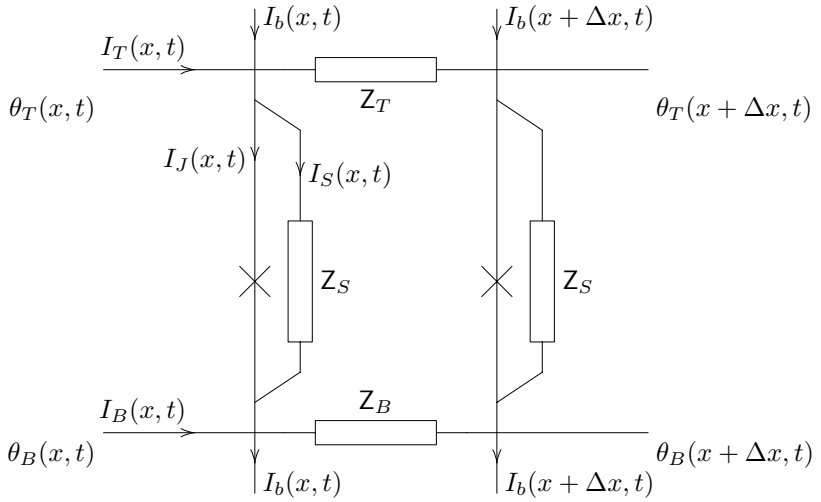

Figure 2.4: The general model of the long Josephson junction, including bias current

where we have defined $I_b = (\Delta x)J_b$.

Making the same assumptions as in the previous section for the impedances, we obtain the equation

$$\Phi_{xx}(x,t) - \Phi_{tt}(x,t) = \sin\Phi(x,t) + \alpha\Phi(x,t) - \gamma(x,t). \tag{2.2.40}$$

where

$$\gamma(x,t) = \frac{J_b(x,t)}{J_c} \tag{2.2.41}$$

2.2.5 Surface resistance

As mentioned in section 2.2.3, at non-zero temperature, there will be thermally excited quasi-particles in the superconductors. There the possibility was discussed that these particles tunnel to the other superconductor because of a potential difference across the junction. This is not the only source of energy loss. Also, if a potential gradient is present in one of the superconductors, there will be a flow of quasi-particles along the junction, resulting in an energy loss. This (normally very small) current can be modelled by placing a resistor parallel to the inductor in the superconductors. These two impedances must be in parallel, since both the quasi-particle current and the supercurrent flow independent of each other.

To incorporate this in the model, the impedance z_e will be taken to be a resistor parallel to an inductor. This means that

$$\mathsf{z}_e^{-1}(V) = \frac{V}{r_L} + \frac{1}{l}\int V\mathrm{d}t + J_0, \tag{2.2.42}$$

and a closed form for z_e cannot be found. We can still derive the equations, from the equation

$$\mathsf{z}_e^{-1}\Phi_{xxt}(x,t) = \frac{2\pi}{\Phi_0}\big(J_J(x,t) + J_S(x,t) - J_b(x,T)\big). \tag{2.2.43}$$

For z_e we use the expression (2.2.42) and we use the RCSJ-model:

$$(\mathsf{z}_S)^{-1}(V) = c\frac{\mathrm{d}}{\mathrm{d}t}V + \frac{V}{r}, \tag{2.2.44}$$

This results in

$$\frac{\Phi_{xxt}}{r_L} + \frac{\Phi_{xx}}{l} + J_0 = \frac{2\pi}{\Phi_0}J_c\sin\Phi + c\Phi_{tt} + \frac{1}{r}\Phi_t - \frac{2\pi}{\Phi_0}J_b(x,t), \tag{2.2.45}$$

which can be rescaled to the more familiar form

$$\Phi_{xx} - \Phi_{tt} - \sin\Phi = \alpha\Phi_t - \beta\Phi_{xxt} - \gamma. \tag{2.2.46}$$

where the constant β is given by

$$\beta = \frac{l}{r_L}\sqrt{\frac{2\pi J_c}{\Phi_0 c}} \tag{2.2.47}$$

2.2.6 Further extensions

The model derived in the last section seems to cater for most of the observed phenomena in physics. It gives a rather complete picture of the long junction. All currents are represented in the model. Across the junction we have a supercurrent due to the Josephson effect, a flow of quasi-particles, and a current due to capacitive effects. The currents along the surface of the superconductors are a supercurrent due to the flow of condensed electrons and a current of quasi-particles.

In the analysis it was assumed that the physical properties are independent of the position along the junction. The model can be extended in a straightforward manner to include x-dependency. In this thesis we will assume all physical properties to be independent of x.

Inductive effects of the quasi-particle flow

A more direct extension that may be of interest, is to replace the resistor, modelling the flow of quasi particle along the surface of the superconductors, by a resistor in series with an impedance. The flow of quasi-particles, although small, will also give rise to a magnetic field.

We could analyse this situation in the following way. We solve the differential equation for the current flowing due to a potential difference. If we apply a voltage $V(t)$ to the impedance depicted in figure 2.5 the current I_1 through the inductor L_1 in figure 2.5 satisfies

$$V(t) = L_1\frac{\mathrm{d}I_1(t)}{\mathrm{d}t} \Rightarrow I_1(t) = \frac{1}{L}\int_0^t V(t)\mathrm{d}t + I_0(x). \tag{2.2.48}$$

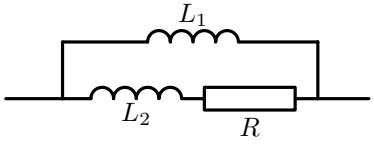

Figure 2.5: An extension for z_e

The current I_2 through the bottom inductor and resistor satisfies

$$V(t) = L_2 \frac{\mathrm{d}I_2(t)}{\mathrm{d}t} + RI_2(t) \Rightarrow I_2(t) = e^{-\frac{Rt}{L_2}} \left(\int_0^t e^{\frac{R\tau}{L_2}} \frac{V(x,\tau)}{L_2} \mathrm{d}\tau + f(x) \right). \quad (2.2.49)$$

So, the total current along the surface is given by

$$I(t) = \frac{1}{L} \int_0^t V(\tau)\mathrm{d}\tau + I_0(x) + \int_0^t e^{\frac{R\tau - Rt}{L_2}} \frac{V(x,\tau)}{L_2} \mathrm{d}\tau + e^{-\frac{Rt}{L_2}} f(x). \quad (2.2.50)$$

One could also use this expression to obtain an integro-differential equation for the phase $\Phi(x,t)$. Using the RCSJ-model for the vertical currents (assuming the initial conditions $I_0(x)$ and $f(x)$ to be zero as usual), we obtain the equation

$$\frac{\Phi_{xx}}{l_1} + \int_0^t e^{\frac{r\tau - rt}{l_2}} \frac{\Phi_{xxt}(x,\tau)}{l_2} \mathrm{d}\tau = \frac{2\pi}{\Phi_0} \left(J_c \sin \Phi(x,t) - J_b(x,t) \right) + \\ + c\Phi_{tt}(x,t) + \frac{1}{r}\Phi_t(x,t). \quad (2.2.51)$$

The equation (2.2.46) can be obtained from this equation, by using integration by parts once on the integral, and neglecting the remaining integral.

Alternatively, we could analyse this along the same lines as has been done in this chapter so far, and write the effective impedance as

$$\mathsf{z}_e^{-1} = \mathsf{z}_1^{-1} + \mathsf{z}_2^{-1}, \quad (2.2.52)$$

where z_1 is an inductor and z_2 is a series connection of an inductor with a resistor. Formally we can then write

$$\mathsf{z}_e^{-1}(V) = \frac{1}{l_1} \int V \mathrm{d}t + J_0 + \frac{V}{r} + \frac{1}{r} \left(\sum_{i=1}^{\infty} (-1)^i \left(\frac{l_2}{r} \right)^i \frac{\mathrm{d}^i}{\mathrm{d}t^i} V \right). \quad (2.2.53)$$

Writing this will result in an infinite number of terms in the differential equation. These terms will be of the form

$$c_i \beta^i \partial_t^i \Phi_{xx}, \qquad i \geq 2 \quad (2.2.54)$$

where β is proportional to $\frac{1}{r}$. As β multiplies the term with the highest derivative, the equation for $\beta \neq 0$ is a singular perturbation of the equation for $\beta = 0$.

For the ODE obtained for travelling waves assumption, the theory of Fenichel [5, 14] relates the dynamics for $\beta \neq 0$ to the situation for $\beta = 0$, as long as there is a *finite*

number of terms. For $\beta = 0$ there exists a two-dimensional invariant manifold. For $\beta \neq 0$ there exists an invariant manifold close to the one for $\beta = 0$. If the two-dimensional manifold (for $\beta = 0$) is normally hyperbolic, off the manifold there is exponential attraction or repulsion, so that for connections between equilibria — i.e. fluxons — only dynamics on the manifold is of interest.

For the present case where there are an infinite number of terms, the theory of Fenichel does not hold immediately. Still, it is believed that these extra terms will not result in essentially different dynamics. Although these terms may of course influence the stability of solutions.

The term $\beta\Phi_{xxt}$, which will result in a term $\beta c\phi'''$ in the ODE, can become very important. The ODE for equation (2.2.46) is given by

$$\beta c\phi''' - (1 - c^2)\phi'' - \alpha\phi' - \sin\phi + \gamma = 0 \tag{2.2.55}$$

If β is small and c approaches 1, then both the coefficients of the second and the third derivative are small. Analysing the situation $\beta \to 0$ and $c \to 1$ is rather involved, since one should be careful how one approaches the limit $\beta = 0, c = 1$.

Z_e as sum of two impedances

One can also question the assumption that z_e is a resistor parallel to an inductor. The effective impedance z_e was defined to be the sum of the surface impedances of the top and bottom superconductor. For each of these two separate impedances, this appears to be an acceptable assumption. The sum of these two impedances, does not need to be of the same form.

Let us take a look at what it would mean for the equations. We take two impedances, each consisting of an inductor in parallel to a resistor in series (see figure 2.6). If we assume that

$$\frac{L^A}{R^A} = \frac{L^B}{R^B} = F \tag{2.2.56}$$

the replacement impedance will again be an inductor parallel to a resistor, and the equation (2.2.46) will remain unchanged. Assuming that the two fractions in (2.2.56) are not equal, but that in fact

$$\frac{L^A}{R^A} = F \qquad \frac{L^B}{R^B} = \kappa F \tag{2.2.57}$$

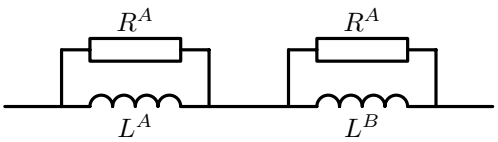

Figure 2.6: z_e is the sum of two impedances, both consisting of an inductor parallel to a resistor.

will result in extra terms in (2.2.46). We will have that

$$\mathsf{Z}_e^{-1}(V) = \frac{1}{L_{\text{eff}}} \int V \mathrm{d}t + \frac{FV}{R_{\text{eff}}} + F \sum_{i=1}^{\infty} C_i(\kappa) F^i \frac{\mathrm{d}^i}{\mathrm{d}t^i} V, \tag{2.2.58}$$

where for all i it holds that $C_i(1) = 0$.

Now, again, we obtain an equation with an infinite number of terms. These terms are comparable to the terms obtained in the previous paragraph. Also in this case the coefficients in front of these terms will vanish if the resistance goes to ∞. If we assume that R^A and R^B scale with $\frac{1}{\epsilon}$, F will scale with ϵ, and the extra terms resulting from (2.2.58) will be of order $\mathcal{O}(\epsilon^2)$. The same remarks about the invariant manifold also hold in this case. It is believed that also in this case there will not be essential different dynamics for the surface resistance large enough. Again, the stability may be influenced by these terms.

2.3 Stacks of long Josephson junctions

In this section we will extend the model of the previous section to include multi-layered (stacked) junctions. More specifically we will restrict to a stack of two junctions.

If in such a stack the middle superconductor is very thick, these two junctions are decoupled. One junction is formed by the top superconductor, the insulator and the top of the middle superconductor the other junction consists of the bottom of the middle superconductor, the second insulator and the bottom superconductor. Currents flowing in the top layer of the middle superconductor do not influence the lower junction.

If, on the other hand the middle superconductor is not so thick, a coupling between these junctions occurs. The magnetic field induced by the currents flowing at the surfaces can penetrate through the superconductor and influence currents on the other surface.

The model is then extended to the one in figure 2.7. One can recognise in this picture two separate Josephson junctions, where the only interaction is the aforementioned magnetic coupling.

Having seen in the last section what the influence is of using different assumptions for the currents across the junction(s), we will use the RCSJ-model throughout this whole section.

We will discuss three different assumptions in this section. Given the model in figure 2.7, and the fact that if the temperature is not too large, the density of quasi-particles in the superconductors is very small, we will first assume that there is no flow of quasi-particles along the surface of the superconductors: $z_O^T = z_I^T = z_I^B = z_O^B = \infty$. This will result in the equation

$$\begin{cases} \Phi_{xx}^T(x,t) + \sigma \Phi_{xx}^B(x,t) = \sin \Phi^T(x,t) + \Phi_{tt}^T(x,t) + \alpha \Phi_t^T(x,t) - \gamma_T, \\ \Phi_{xx}^B(x,t) + \Delta\sigma \Phi_{xx}^T(x,t) = \\ \qquad \Delta \dfrac{\sin \Phi^B(x,t)}{J} + \Delta C \Phi_{tt}^B(x,t) + \Delta R \alpha \Phi_t^B(x,t)\big) - \gamma_B, \end{cases} \tag{2.3.1}$$

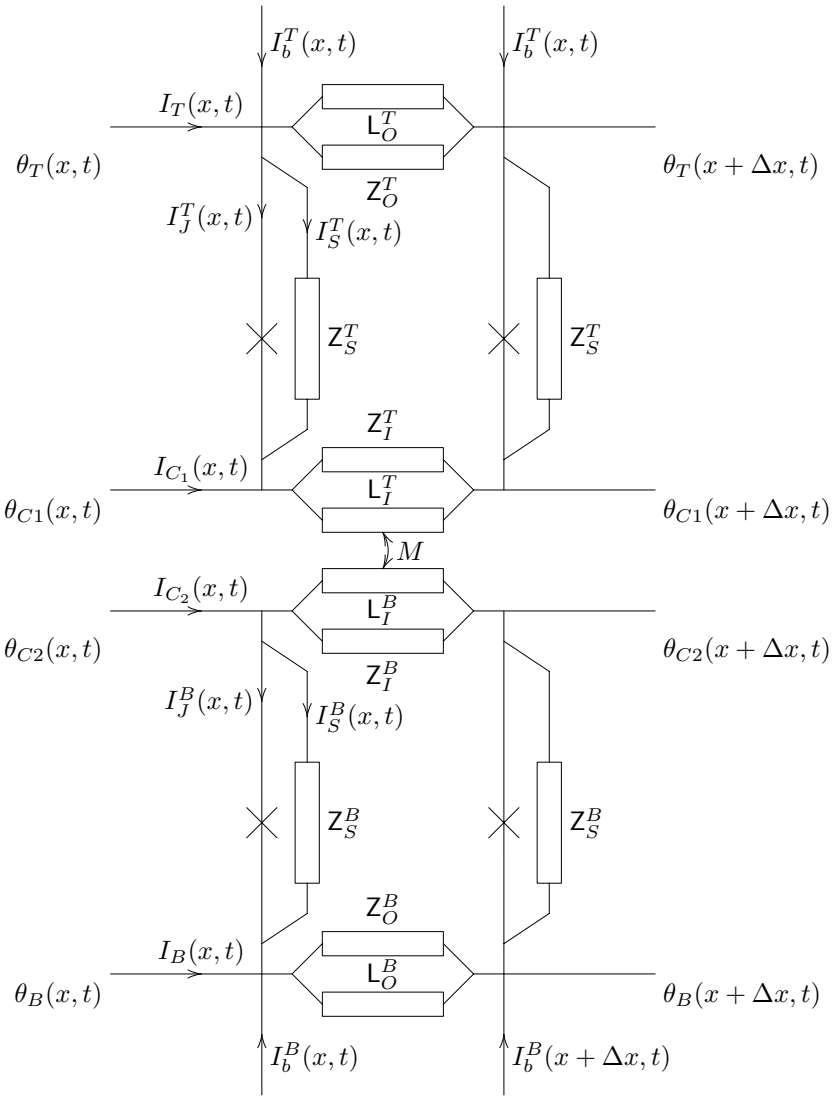

Figure 2.7: The discrete model for a stack of two Josephson junctions

where the constants Δ, C, J and R are all equal to 1 if the two junctions are identical. The parameter σ is the magnetic coupling parameter.

Because of the observation in the previous section that the impedances Z_T and Z_B can be absorbed in one effective impedance Z_e, in [11] it has been assumed that the outer impedances $z_O^T = z_O^B = l_O^T = l_O^B = 0$. These assumptions will be shown to lead to the model

$$\begin{cases} \Phi^T_{xx} - \Phi^T_{tt} - \sin\Phi^T + \sigma\Phi^B_{xx} = \alpha\Phi^T_t - \beta\Phi^T_{xxt} - \gamma^T, \\ \Phi^B_{xx} - \Delta C\Phi^B_{tt} - \Delta\dfrac{\sin\Phi^B}{J} + \Delta\sigma\Phi^T_{xx} = \Delta R\alpha\Phi^B_t - \Delta Z\beta\Phi^B_{xxt} - \gamma^B, \end{cases} \tag{2.3.2}$$

where the parameterβ associated to the quasi-particle flow along the surface of the superconductors is included.

The last assumption we will make in this section is that the surface resistance is not ∞, but still large. We will make this explicit by assuming that the impedances z_I^T, z_I^B, z_O^T and z_O^B scale with $\frac{1}{\epsilon}$. In the final model we will neglect terms of $\mathcal{O}(\epsilon^2)$.

$$\begin{cases} \Phi^T_{xx} - \Phi^T_{tt} + \sigma\Phi^B_{xx} - \sin\Phi^T = \alpha\Phi^T_t - \gamma_T \\ \qquad\qquad -\epsilon\Big(\beta\Phi^T_{xxt} - \delta\cos\Phi^T\Phi^T_t - \eta\Phi^T_{ttt}\Big), \\ \Phi^B_{xx} - \tilde{C}\Phi^B_{tt} + \Delta\sigma\Phi^T_{xx} - \Delta\dfrac{\sin\Phi^B}{J} = \Delta R\alpha\Phi^B_t - \gamma_B \\ \qquad\qquad -\epsilon\Big(B\beta\Phi^B_{xxt} - \delta\Delta\dfrac{\cos\Phi^B}{J}\Phi^B_t - \Delta C\eta\Phi^B_{ttt}\Big), \end{cases} \tag{2.3.3}$$

It is interesting to notice that the two extra terms in the equations, do not contain x-derivatives, although they follow from the presence of a horizontal quasi-particle flow.

The terms of the form $\cos\Phi\Phi_t$ also appear in some models for the short Josephson junction, if a more detailed analysis then the one sketched in chapter 1 is performed. For the short junction these terms are associated to the interaction of the quasi-particle- and supercurrents.

2.3.1 General model

In the manner of section 2.2, we will derive equations for this coupled system. The starting point is again the "conservation of phase". Just as in the single junction case, we can derive an equation for the phase difference, using the AC-Josephson relation. The drop in the phase difference $\Phi(x,t)$ along the junction is related to the potential drop over the impedances $\mathsf{Z}_{T,B}$. For the outer impedances the potential drop only depends on the currents flowing through those impedances. For the inner impedances, there is an extra effect of the coupling. The potential drop over e.g., L_I^B does not only depend on the current through these impedance, but, through the magnetic coupling, also on the current through L_I^T.

Starting from

$$\theta_T(x,t) - \theta_T(x+\Delta x,t) + \theta_T(x+\Delta x,t) - \theta_{C1}(x+\Delta x,t) + \theta_{C1}(x+\Delta x,t) - \theta_{C1}(x,t) + \theta_{C1}(x,t) - \theta_T(x,t) = 0 \quad (2.3.4)$$

we get, after differentiation with respect to t

$$\Delta x \partial_t \partial_x \Phi^T(x,t) = \partial_t \theta_{C1}(x,t) - \partial_t \theta_{C1}(x+\Delta x,t) + \partial_t \theta_T(x+\Delta x,t) + \quad (2.3.5)$$
$$- \partial_t \theta_T(x,t),$$
$$= \frac{2\pi}{\Phi_0}\left[V_T(x+\Delta x,t) - V_T(x,t) + V_{C_1}(x,t) - V_{C_1}(x+\Delta x,t)\right]. \quad (2.3.6)$$

The potential drop in the top layer only depends on the current I_T. The drop in V_{C_1} also depends on the current I_{C_2}, in fact we can derive the following relation for $V^{C_1}(x,t) - V^{C_1}(x+\Delta x,t) = \Delta V^{C_1}(x,t)$ (again, see appendix 2.A for the details)

$$(1 + \mathsf{L}_I^T(\mathsf{Z}_I^T)^{-1})\Delta V_{C_1} = \mathsf{L}_I^T(I_{C_1}) + \mathsf{M}(I_{C_2}) - \mathsf{M}(\mathsf{Z}_I^B)^{-1}\Delta V_{C_2}. \quad (2.3.7)$$

Using the relations (2.3.6) and (2.3.7), as well as the similar relations for the bottom junction, we obtain a relation between the drop in the phase differences along the junction and the surface currents.

$$\begin{cases} (1 + \mathsf{l}_I^T(\mathsf{z}_I^T)^{-1})\partial_t\partial_x\Phi^T = \frac{2\pi}{\Phi_0}\Big[-(1 + \mathsf{l}_I^T(\mathsf{z}_I^T)^{-1})\tilde{\mathsf{z}}_O^T(I_T) + \mathsf{l}_I^T(I_{C_1}) + \\ \qquad \mathsf{m}(I_{C_2}) - \mathsf{m}(\mathsf{z}_I^B)^{-1}(-\frac{\Phi_0}{2\pi}\partial_x\partial_t\Phi^B + \tilde{\mathsf{z}}_O^B(I_B))\Big], \\ (1 + \mathsf{l}_I^B(\mathsf{z}_I^B)^{-1})\partial_t\partial_x\Phi^B = \frac{2\pi}{\Phi_0}\Big[(1 + \mathsf{l}_I^B(\mathsf{z}_I^B)^{-1})\tilde{\mathsf{z}}_O^B(I_B) - \mathsf{l}_I^B(I_{C_2}) \\ \qquad - \mathsf{m}(I_{C_1}) + \mathsf{m}(\mathsf{z}_I^T)^{-1}\big(\frac{\Phi_0}{2\pi}\partial_t\partial_x\Phi^T + \tilde{\mathsf{z}}_O^T(I_T)\big)\Big] \end{cases} \quad (2.3.8)$$

Where we have defined

$$(\tilde{\mathsf{z}}_O^T)^{-1} = (\mathsf{z}_O^T)^{-1} + (\mathsf{l}_O^T)^{-1} \qquad (\tilde{\mathsf{z}}_O^B)^{-1} = (\mathsf{z}_O^B)^{-1} + (\mathsf{l}_O^B)^{-1} \quad (2.3.9)$$

Again, we can derive equations for the x-derivative of the surface currents in terms of the currents across the junctions, from Kirchhoff's current law:

$$\partial_x I_T(x,t) = I_b^T(x,t) - J_c^T \sin\Phi^T(x,t) - \frac{\Phi_0}{2\pi}(\mathsf{z}_S^T)^{-1}(\partial_t\Phi^T(x,t)), \quad (2.3.10a)$$

$$\partial_x I_{C_1}(x,t) = J_c^T \sin\Phi^T(x,t) + \frac{\Phi_0}{2\pi}(\mathsf{z}_S^T)^{-1}(\partial_t\Phi^T(x,t)), \quad (2.3.10b)$$

$$\partial_x I_{C_2}(x,t) = -J_c^B \sin\Phi^B(x,t) - \frac{\Phi_0}{2\pi}(\mathsf{z}_S^B)^{-1}(\partial_t\Phi^B(x,t)), \quad (2.3.10c)$$

$$\partial_x I_B(x,t) = J_c^B \sin\Phi^B(x,t) + \frac{\Phi_0}{2\pi}(\mathsf{z}_S^B)^{-1}(\partial_t\Phi^B(x,t)) - I_b^B(x,t). \quad (2.3.10d)$$

This then completes the model. We will not proceed to derive the full equations with this model. In stead we will immediately neglect the surface currents of quasi-particles and proceed to derive the model for this situation.

2.3.2 Infinite surface resistance

We neglect the quasi particle current along surface of the superconductors. This means that we set $z_I^T = z_O^T = z_I^B = z_I^T = \infty$. We take the resistance infinitely large, to ensure that there is no quasi-particle current through the resistor, no matter what the potential drop over it is. This reduces (2.3.8) to

$$\begin{cases} \partial_t \partial_x \Phi^T(x,t) = \dfrac{2\pi}{\Phi_0}\Big[-\tilde{\mathsf{z}}_O^T(I_T) + \mathsf{I}_I^T(I_{C_1}) + \mathsf{m}(I_{C_2})\Big], \\ \partial_x \partial_t \Phi^B(x,t) = \dfrac{2\pi}{\Phi_0}\Big[\tilde{\mathsf{z}}_O^B(I_B) - \mathsf{I}_I^B(I_{C_2}) - \mathsf{m}(I_{C_1})\Big]. \end{cases} \tag{2.3.11}$$

Now we can use the same arguments as for the single junction in the case of no surface resistance and assume all the impedances in these formulas to be inductors, i.e.,

$$\tilde{\mathsf{z}}_O^T = l_O^T \frac{\mathrm{d}}{\mathrm{d}t}, \qquad \tilde{\mathsf{z}}_O^B = l_O^B \frac{\mathrm{d}}{\mathrm{d}t}, \qquad \mathsf{I}_I^T = l_I^T \frac{\mathrm{d}}{\mathrm{d}t}, \qquad \mathsf{m} = m\frac{\mathrm{d}}{\mathrm{d}t}. \tag{2.3.12}$$

Furthermore, there is a strong relationship between the x-derivative of the currents I_T and I_B on the one side and I_{C_1} and I_{C_2} on the other side. Using this fact (as is done in the appendix) we obtain the equations

$$\begin{cases} \partial_x^2 \Phi^T(x,t) = \dfrac{2\pi}{\Phi_0}\Big[-l_O^T I_b^T + (l_O^T + l_I^T)\partial_x I_{C_1} + m\partial_x I_{C_2}\Big], \\ \partial_x^2 \Phi^B(x,t) = \dfrac{2\pi}{\Phi_0}\Big[-l_O^B I_b^B - (l_O^B + l_I^B)\partial_x I_{C_2} - m\partial_x I_{C_1}\Big]. \end{cases} \tag{2.3.13}$$

Taking the right combinations of these equations and rescaling the x variable, results in the coupled equations

$$\begin{cases} \partial_x^2 \Phi^T(x,t) + \hat{m}\partial_x^2 \Phi^B(x,t) = \dfrac{\partial_x I_{C_1}}{J_c^T} - \gamma_T, \\ \partial_x^2 \Phi^B(x,t) + \Delta\hat{m}\partial_x^2 \Phi^T(x,t) = -\Delta\dfrac{\partial_x I_{C_2}}{J_c^T} - \gamma_B, \end{cases} \tag{2.3.14}$$

where the expressions for $\hat{m}$, γ_T, γ_B and Δ can be found in the appendix (2.A.19) and (2.A.24). Now we substitute (2.3.10) and at the same time make an assumption for $(\mathsf{z}_S^T)^{-1}$ and $(\mathsf{z}_S^B)^{-1}$. Guided by the ideas presented in the previous section, we take

$$(\mathsf{z}_S^T)^{-1}(V) = c^T \frac{d}{dt}V + \frac{1}{r^T}V, \tag{2.3.15}$$

$$(\mathsf{z}_S^B)^{-1}(V) = c^B \frac{d}{dt}V + \frac{1}{r^B}V. \tag{2.3.16}$$

Hence we get after rescaling the time

$$\begin{cases} \partial_x^2 \Phi^T(x,t) + \sigma\partial_x^2 \Phi^B(x,t) = \sin\Phi^T(x,t) + \partial_t^2 \Phi^T(x,t) + \alpha_T \partial_t \Phi^T(x,t) - \gamma_T, \\ \partial_x^2 \Phi^B(x,t) + \Delta\sigma\partial_x^2 \Phi^T(x,t) = \\ \qquad \Delta\dfrac{\sin\Phi^B(x,t)}{J} + \Delta C\partial_t^2 \Phi^B(x,t) + \Delta\alpha_B\partial_t\Phi^B(x,t)\big) - \gamma_B, \end{cases} \tag{2.3.17}$$

where we have defined the following constants

$$C = \frac{c^B}{c^T} \qquad \alpha_T = \frac{\sqrt{\Phi_0}}{r^T\sqrt{2\pi J_c^T c^T}} \qquad \alpha_B = \frac{\sqrt{\Phi_0}}{r^B\sqrt{2\pi J_c^T c^T}} \tag{2.3.18}$$

$$J = \frac{J_c^T}{J_c^B} \qquad \sigma = \frac{m}{l_O^B + l_I^B}. \tag{2.3.19}$$

For most of the constants we have used the notation which is commonly found in literature. However, in literature quite often one sees $-S$ in place of σ, however, this S is then a negative number. Here we chose to use σ instead and let it be positive.

2.3.3 Zero impedance in outer layers

A different model was used by e.g. [11]. Guided by the observation that for the single junction the impedance in the top and bottom layers can be absorbed in one impedance, we could assume the impedances $\tilde{\mathsf{z}}_O^T$ and $\tilde{\mathsf{z}}_O^B$ to be zero. This simplifies the equations (2.3.8) to

$$\begin{cases} (1 + \mathsf{l}_I^T(\mathsf{z}_I^T)^{-1})\partial_t\partial_x\Phi^T = \dfrac{2\pi}{\Phi_0}\Big[\mathsf{l}_I^T(I_{C_1}) + \mathsf{m}(I_{C_2}) + \mathsf{m}(\mathsf{z}_I^B)^{-1}\dfrac{\Phi_0}{2\pi}\partial_x\partial_t\Phi^B\Big], \\ (1 + \mathsf{l}_I^B(\mathsf{z}_I^B)^{-1})\partial_t\partial_x\Phi^B = \dfrac{2\pi}{\Phi_0}\Big[-\mathsf{l}_I^B(I_{C_2}) - \mathsf{m}(I_{C_1}) + \mathsf{m}(\mathsf{z}_I^T)^{-1}\dfrac{\Phi_0}{2\pi}\partial_t\partial_x\Phi^T\Big] \end{cases} \tag{2.3.20}$$

However, doing this means that we should be more careful with the bias current. In the model, currents can flow along the outer surface unhindered. A bias current applied to the system as on the left in figure 2.8 will not affect the system. All the current applied to the system will flow along the outer surface, thus not influencing the system. To overcome this major shortcoming of the model and to force a bias current through each of the layers, we include a current source parallel to the Josephson junction in the discrete model (see figure 2.8). In doing this we prescribe the bias current through each of the junctions separately. In practice, only the total bias current is prescribed.

Using these current sources in the model, changes the equations for I_{C_1} and I_{C_2} as follows

$$\partial_x I_{C_1}(x,t) = J_c^T \sin\Phi^T(x,t) + \frac{\Phi_0}{2\pi}(\mathsf{z}_S^T)^{-1}(\partial_t\Phi^T(x,t)) - J_b^T(x,t), \tag{2.3.21a}$$

$$\partial_x I_{C_2}(x,t) = -J_c^B \sin\Phi^B(x,t) - \frac{\Phi_0}{2\pi}(\mathsf{z}_S^B)^{-1}(\partial_t\Phi^B(x,t)) + J_b^B(x,t). \tag{2.3.21b}$$

Now we use the same assumptions for the surface impedance along the junction, as in [11]. This means, we take the impedances z_I^T and z_I^B to be resistors and the impedances l_I^T and l_I^B to be inductors, with a mutual inductance of m.

$$\mathsf{l}_I^T = l_I^T\frac{\mathrm{d}}{\mathrm{d}t}, \qquad \mathsf{l}_I^B = l_I^B\frac{\mathrm{d}}{\mathrm{d}t}, \qquad \mathsf{z}_I^T = r_I^T \qquad \mathsf{z}_I^B = r_I^B \qquad \mathsf{m} = m\frac{\mathrm{d}}{\mathrm{d}t} \tag{2.3.22}$$

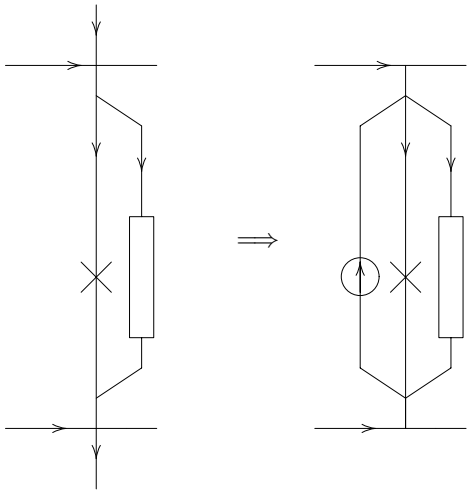

Figure 2.8: A current source parallel to the Josephson junction models the bias current. Note that now the bias current for each of the junctions is prescribed, separately.

Since each term in these equations contains a differentiation with respect to time, we integrate these equations and set the initial conditions to zero. If we then add $\frac{m}{l_I^B}$ times the second equation to the first we obtain

$$\left(1+\frac{l_I^T}{r_I^T}\frac{\mathrm{d}}{\mathrm{d}t}\right)\partial_x\Phi^T+\frac{m}{l_I^B}\left(1+\frac{l_I^B}{r_I^B}\frac{\mathrm{d}}{\mathrm{d}t}\right)\partial_x\Phi^B=\frac{2\pi}{\Phi_0}\left[l_I^T(I_{C_1})-\frac{m^2}{l_I^B}(I_{C_1})\right]+ \\ +\frac{m}{r_I^B}\partial_x\partial_t\Phi^B+\frac{m^2}{l_I^Br_I^T}\partial_x\partial_t\Phi^T. \quad (2.3.23)$$

For Φ^B we have a similar equation. For the current across the junction, we take the RCSJ-model with a parallel current-source (2.3.21).

$$l_{\mathrm{eff}}=\frac{l_I^Tl_I^B-m^2}{l_I^B} \quad (2.3.24)$$

to write the resulting equation as

$$\Phi_{xx}^T-l_{\mathrm{eff}}c^T\Phi_{tt}^T-\frac{2\pi}{\Phi_0}l_{\mathrm{eff}}J_c^T\sin\Phi^T+\frac{2\pi}{\Phi_0}l_{\mathrm{eff}}J_b^T+\frac{m}{l_I^B}\Phi_{xx}^B= \\ \frac{l_{\mathrm{eff}}}{r^T}\Phi_t^T-\frac{l_I^Tl_I^B-m^2}{l_I^Br_I^T}\Phi_{xxt}^T. \quad (2.3.25)$$

In this last equation the terms with Φ_{xxt}^B left and right cancelled, so the only interaction term is the Φ_{xx}^B. The complete model can be written as

$$\begin{cases}\Phi_{xx}^T-\Phi_{tt}^T-\sin\Phi^T+\sigma\Phi_{xx}^B=\alpha\Phi_t^T-\beta\Phi_{xxt}^T-\gamma^T \\ \Phi_{xx}^B-\Delta C\Phi_{tt}^B-\Delta\dfrac{\sin\Phi^B}{J}+\Delta\sigma\Phi_{xx}^T=\Delta R\alpha\Phi_t^B-\Delta Z\beta\Phi_{xxt}^B-\gamma^B\end{cases} \quad (2.3.26)$$

where

$$\sigma = \frac{m}{l_I^B} \qquad \alpha = \frac{\sqrt{\Phi_0}}{r^T\sqrt{2\pi J_c^T c^T}} \qquad \beta = \frac{l_{\text{eff}}}{r_I^T}\sqrt{\frac{2\pi J_c^T}{\Phi_0 c^T}} \qquad \gamma_T = \frac{J_b^T}{J_c^T}$$
$$\Delta = \frac{l_I^B}{l_I^T} \qquad J = \frac{J_c^T}{J_c^B} \qquad R = \frac{r^T}{r^B} \qquad Z = \frac{r_I^T}{r_I^B} \qquad \gamma_B = \frac{J_b^B}{J_c^T}$$

2.3.4 Large surface resistance

The assumption in the previous subsection, that the impedance in the outer layers is zero, can be compared to the discussion about z_e for the single junction. In section 2.2.6 we discussed whether the impedances in the top and bottom superconductor of a junction could be combined into one, which consisted of a inductor parallel to a resistor. It was shown there that this could in principle be done, given the fact that the surface-resistance was sufficiently large.

For the stack case, one should be a bit more careful, since in this case combining both impedances in one, sitting at the inner superconducting layer, has consequences for the coupling. We will show this in the present section.

We will assume the surface resistance to be large (scale $z_{I,O}^{T,B}$ with $\frac{1}{\epsilon}$) and derive a model for this situation, neglecting terms of $\mathcal{O}(\epsilon^2)$. Furthermore we will assume that the ratio of the surface inductance and surface resistance for the inner and outer surfaces will be equal (compare this with (2.2.56)).

To avoid doing all of the algebraic manipulations by hand and to reduce the change of errors in this, use has been made of the computer program Maple to do most of the computations. Starting from the equations (2.3.8), we make the assumptions

$$m = ms \qquad \mathsf{l}_I^T = l_I^T s \qquad \mathsf{l}_I^B = l_I^B s \qquad \mathsf{l}_O^B = l_O^B \qquad \mathsf{l}_O^T = l_O^T \tag{2.3.27}$$
$$\mathsf{z}_I^T = \frac{z_I^T}{\epsilon} \qquad \mathsf{z}_I^B = \frac{z_I^B}{\epsilon} \tag{2.3.28}$$

This means that

$$\tilde{\mathsf{z}}_O^T = \left((\mathsf{z}_O^T)^{-1} + (\mathsf{l}_O^T)^{-1}\right)^{-1} = \mathsf{l}_O^T - \frac{(\mathsf{l}_O^T)^2}{z_O^T}\epsilon + \mathcal{O}(\epsilon^2). \tag{2.3.29}$$

Another assumption we make is that $\frac{\mathsf{L}_O^B}{\mathsf{Z}_O^B} = \frac{\mathsf{L}_I^B}{\mathsf{Z}_I^B}$ (and a similar assumption on the impedances in the "top" layer). This is not stricly necessary, but it seems a reasonable assumption. If we do not make this assumption, we will obtain another coupling term. All other terms remain, but get more complicated.

The worksheet that has been used to derive the equation is given in appendix 2.B.

The equation for Φ^T is given by

$$\sigma\left(\frac{\partial^2}{\partial x^2}\Phi^B(x,t)\right)+\left(\frac{\partial^2}{\partial x^2}\,\Phi^T(x,t)\right)+C_2\varepsilon\left(\frac{\partial^3}{\partial x^2\partial t}\Phi^T(x,t)\right)=\left(\frac{\partial}{\partial x}I_{C1}(x,t)\right)A_2 + A_1\varepsilon\left(\frac{\partial^2}{\partial x\partial t}I_{C1}(x,t)\right))+Ib_TD1+D2\varepsilon\left(\frac{\partial}{\partial t}Ib_T(x,t)\right)+Ib_BE1 + E2\varepsilon\left(\frac{\partial}{\partial t}Ib\_B(x,t)\right) \quad (2.3.30)$$

New in this equation is the term $A_1\varepsilon(\frac{\partial^2}{\partial x\partial t}I_{C1}(x,t))$. In the final equation this will give rise to two new terms. One containing $\cos\Phi^T\partial_t\Phi^T$ and one containing $\partial_t^3\Phi^T$. The new equation can be rescaled to

$$\Phi^T_{xx}-\Phi^T_{tt}+\sigma\Phi^B_{xx}-\sin\Phi^T=\alpha\Phi^T_t-\gamma_T-\epsilon\Big(\beta\Phi^T_{xxt}-\delta\cos\Phi^T\Phi^T_t-\eta\Phi^T_{ttt}\Big) \quad (2.3.31)$$

The coefficients in this equation are given in terms of the model parameters in the appendix section 2.A.4.

The equation for Φ^B can be written as

$$\Phi^B_{xx}-\tilde{C}\Phi^B_{tt}+\Delta\sigma\Phi^T_{xx}-\Delta\frac{\sin\Phi^B}{J}=\Delta R\alpha\Phi^B_t-\gamma_B+ -\epsilon\Big(B\beta\Phi^B_{xxt}-\Delta\delta\frac{\cos\Phi^B}{J}\Phi^B_t-\Delta C\eta\Phi^B_{ttt}\Big), \quad (2.3.32)$$

where the expression for $\tilde{C}$, as well as the relations for δ and η can be found in the appendix on page 36

2.A Detailed derivation of the equations

In this appendix the details of the derivation of the equations are discussed. This is intrinsically a lot of formula manipulation. In the first section we will derive the basic equation (2.2.14) for the single junction. In the next section we will derive the general equations for the stack (2.A.13) and (2.A.14).

2.A.1 Derivation for the single junction

As mentioned in section 2.2.1 an equation for the phase difference $\Phi(x,t)$ can be derived from the conservation of phase formula (2.2.10)

$$\theta_T(x,t)-\theta_T(x+\Delta x,t)+\theta_T(x+\Delta x,t)-\theta_B(x+\Delta x,t)+ +\theta_B(x+\Delta x,t)-\theta_B(x,t)+\theta_B(x,t)-\theta_T(x,t)=0. \quad (2.2.10)$$

We define $\Phi(x,t)=\theta_T(x,t)-\theta_B(x,t)$ and reorder to get

$$\Phi(x,t)-\Phi(x+\Delta x,t)=-\big(\theta_T(x+\Delta x,t)-\theta_T(x,t)\big)+ +\theta_B(x+\Delta x,t)-\theta_B(x,t). \quad (2.A.1)$$

Differentiating this expression with respect to time and using the AC-Josephson relation gives:

$$\begin{aligned}\Phi_t(x,t) - \Phi_t(x+\Delta x,t) &= -\big(\partial_t\theta_T(x+\Delta x,t) - \partial_t\theta_T(x,t)\big) + \\ &\quad + \partial_t\theta_B(x+\Delta x,t) - \partial_t\theta_B(x,t) \\ &= -\frac{2\pi}{\Phi_0}\big(V_T(x+\Delta x,t) - V_T(x,t) - V_B(x+\Delta x,t) + V_B(x,t)\big). \quad (2.A.2)\end{aligned}$$

The potential differences give rise to currents, satisfying (2.2.5), using the in 2.2.1 obtained dependance of the impedances Z on Δx, we obtain

$$\Phi_t(x,t) - \Phi_t(x+\Delta x,t) = \frac{2\pi}{\Phi_0}\Big(\Delta x \mathsf{z}_T\big(I_T(x,t)\big) - \Delta x \mathsf{z}_B\big(I_B(x,t)\big)\Big), \quad (2.A.3)$$

or

$$\frac{\Phi_t(x+\Delta x,t) - \Phi_t(x,t)}{\Delta x} = \frac{2\pi}{\Phi_0}\Big(-\mathsf{z}_T\big(I_T(x,t)\big) + \mathsf{z}_B\big(I_B(x,t)\big)\Big). \quad (2.2.11)$$

This equation relates the drop in the phase difference between the top and bottom superconductor to the surface currents of the superconductors.

We define the current densities J_J and J_S by

$$I_J(x,t) = \Delta x J_J(x,t), \quad (2.A.4a)$$
$$I_S(x,t) = \Delta x J_S(x,t). \quad (2.A.4b)$$

This leads to

$$I_T(x-\Delta x,t) - I_T(x,t) = \Delta x\big(J_J(x,t) + J_S(x,t)\big). \quad (2.A.5)$$

Applying Kirchhoff's current law to the bottom left node in figure 2.2 we can derive a similar expression for the current in the bottom superconductor

$$I_B(x-\Delta x,t) - I_B(x,t) = -\Delta x\big(J_J(x,t) + J_S(x,t)\big). \quad (2.A.6)$$

Combining this with (2.2.11) gives the equation

$$\begin{aligned}&\frac{\Phi_t(x,t) - \Phi_t(x-\Delta x,t)}{\Delta x} - \frac{\Phi_t(x+\Delta x,t) - \Phi_t(x,t)}{\Delta x} = \\ &\qquad \frac{2\pi}{\Phi_0}\Big(-\mathsf{z}_T\big(I_T(x-\Delta x,t) - I_T(x,t)\big) + \mathsf{z}_B\big(I_B(x-\Delta x,t) - I_B(x,t)\big)\Big) \Rightarrow \\ &\frac{-\Phi_t(x-\Delta x,t) + 2\Phi_t(x,t) - \Phi_t(x+\Delta x,t)}{(\Delta x)^2} = \frac{2\pi}{\Phi_0}\big(-\mathsf{z}_e(J_J(x,t) + J_S(x,t)\big). \quad (2.A.7)\end{aligned}$$

In the last line we have written $\mathsf{z}_e = \mathsf{z}_T + \mathsf{z}_B$.

Now taking the limit of (2.A.7) for $\Delta x \to 0$, we obtain the differential equation

$$\Phi_{xxt}(x,t) = \frac{2\pi}{\Phi_0}\mathsf{z}_e\big(J_J(x,t) + J_S(x,t)\big). \quad (2.A.8)$$

The current $J_J(x)$ on the right hand side is the Josephson current, which satisfies the DC-Josephson equation (1.1.4) from chapter 1. The leak current $J_S(x)$ is a current which depends on the potential difference between the top and bottom superconductor. So we can write expression (2.A.8) as

$$\Phi_{xxt}(x,t) = \mathsf{z}_e \left(\frac{2\pi}{\Phi_0} J_c \sin\phi(x,t) + (\mathsf{z}_S)^{-1}\big(\Phi_t(x,t)\big) \right). \tag{2.2.14}$$

2.A.2 Stack of junctions

Most of the derivation is completely analogous to the case of the single junction and will not be copied here. An important difference is the derivation of (2.3.7).

We need to find a relation between the current flowing along the inner surfaces and the potential differences. Due to the presence of the mutual inductance, the potential difference $V^{C_1}(x,t) - V^{C_1}(x+\Delta x,t)$, which we will denote by ΔV^{C_1}, will also depend on the current I_{C_2} flowing along the top of the bottom superconductor. A relation for ΔV^{C_1} can be derived from

$$\begin{aligned} \Delta V_{C_1} &= \mathsf{Z}_I^T(I_{\mathsf{Z}_I^T}) = \mathsf{L}_I^T(I_{\mathsf{L}_I^T}) + \mathsf{M}(I_{\mathsf{L}_I^B}) \\ &= \mathsf{L}_I^T(I_{C_1} - I_{\mathsf{Z}_I^T}) + \mathsf{M}(I_{C_2} - I_{\mathsf{Z}_I^B}) \\ &= \mathsf{L}_I^T(I_{C_1}) - \mathsf{L}_I^T\left((\mathsf{Z}_I^T)^{-1}\Delta V_{C_1}\right) + \mathsf{M}(I_{C_2}) + \\ &\quad - \mathsf{M}\left((\mathsf{Z}_I^B)^{-1}\Delta V_{C_2}\right) \end{aligned} \tag{2.A.9}$$

$$(1 + \mathsf{L}_I^T(\mathsf{Z}_I^T)^{-1})\Delta V_{C_1} = \mathsf{L}_I^T(I_{C_1}) + \mathsf{M}(I_{C_2}) - \mathsf{M}(\mathsf{Z}_I^B)^{-1}\Delta V_{C_2}. \tag{2.3.7}$$

We apply the operator $(1 + \mathsf{L}_I^T(\mathsf{Z}_I^T)^{-1}) = (1 + \mathsf{l}_I^T(\mathsf{z}_I^T)^{-1})$ to the left and right hand side in

$$\Delta x \partial_t \partial_x \Phi^T(x,t) = \frac{2\pi}{\Phi_0}\left[V_T(x+\Delta x,t) - V_T(x,t) + V_{C_1}(x,t) - V_{C_1}(x+\Delta x,t)\right]. \tag{2.3.6}$$

(Also here, lower case letters indicate the impedances divided by Δx.) We use that $V_T(x+\Delta x,t) - V_T(x,t) = -\tilde{\mathsf{z}}_O^T I_T$, where

$$(\tilde{\mathsf{z}}_O^T)^{-1} = (\mathsf{z}_O^T)^{-1} + (\mathsf{l}_O^T)^{-1} \tag{2.A.10}$$

to obtain

$$\begin{aligned} (1 + \mathsf{l}_I^T(\mathsf{z}_I^T)^{-1})\partial_t\partial_x\Phi^T(x,t) = \frac{2\pi}{\Phi_0}\Big[&-(1 + \mathsf{l}_I^T(\mathsf{z}_I^T)^{-1})\tilde{\mathsf{z}}_O^T(I_T) + \mathsf{l}_I^T(I_{C_1}) + \mathsf{m}(I_{C_2}) + \\ &- \mathsf{m}(\mathsf{z}_I^B)^{-1}\Big(\frac{\Delta V_{C_2}(x,t)}{\Delta x}\Big)\Big], \end{aligned} \tag{2.A.11}$$

For the potential difference $\Delta V_{C_2}(x,t)$, we can obtain an expression in terms of Φ^B and V_B from the relation similar to (2.3.6). The "conservation of phase" applied to the bottom circuit gives us the equation

$$\Delta \partial_x \partial_t \Phi^B(x,t) = \frac{2\pi}{\Phi_0}\left[V_{C_2}(x+\Delta x,t) - V_{C_2}(x,t) + V_B(x,t) - V_B(x+\Delta x,t)\right]. \tag{2.A.12}$$

We use this relation to eliminate the $\Delta V_{C_2}(x,t)$ from equation (2.A.11) and obtain

$$(1+\mathsf{l}_I^T(\mathsf{z}_I^T)^{-1})\partial_t\partial_x\Phi^T(x,t) = \frac{2\pi}{\Phi_0}\Big[-(1+\mathsf{l}_I^T(\mathsf{z}_I^T)^{-1})\tilde{\mathsf{z}}_O^T(I_T)+\mathsf{l}_I^T(I_{C_1})+\mathsf{m}(I_{C_2})+ \\ -\mathsf{m}(\mathsf{z}_I^B)^{-1}(-\frac{\Phi_0}{2\pi}\partial_x\partial_t\Phi^B+\tilde{\mathsf{z}}_O^B(I_B))\Big] \tag{2.A.13}$$

In a similar manner we arrive at

$$(1+\mathsf{l}_I^B(\mathsf{z}_I^B)^{-1})\partial_x\partial_t\Phi^B = \frac{2\pi}{\Phi_0}\Big[(1+\mathsf{l}_I^B(\mathsf{z}_I^B)^{-1})\tilde{\mathsf{z}}_O^B(I_B)+ \\ -\mathsf{l}_I^B(I_{C_2})-\mathsf{m}(I_{C_1})+\mathsf{m}(\mathsf{z}_I^T)^{-1}\big(\frac{\Phi_0}{2\pi}\partial_t\partial_x\Phi^T+\tilde{\mathsf{z}}_O^T(I_T)\big)\Big] \tag{2.A.14}$$

This forms together with (2.A.13) equation (2.3.8).

2.A.3 No surface resistance

Now we neglect the surface resistance of the superconductors. This means that we have to set $z_I^T = z_O^T = z_I^B = z_I^T = \infty$. This reduces (2.3.8) to

$$\begin{cases} \partial_t\partial_x\Phi^T(x,t) = \dfrac{2\pi}{\Phi_0}\Big[-\tilde{\mathsf{z}}_O^T(I_T)+\mathsf{l}_I^T(I_{C_1})+\mathsf{m}(I_{C_2})\Big], \\ \partial_x\partial_t\Phi^B(x,t) = \dfrac{2\pi}{\Phi_0}\Big[\tilde{\mathsf{z}}_O^B(I_B)-\mathsf{l}_I^B(I_{C_2})-\mathsf{m}(I_{C_1})\Big] \end{cases} \tag{2.A.15}$$

We assume all the other impedances to be inductors, i.e.,

$$\tilde{\mathsf{z}}_O^T = l_O^T\frac{\mathrm{d}}{\mathrm{d}t}, \qquad \tilde{\mathsf{z}}_O^B = l_O^B\frac{\mathrm{d}}{\mathrm{d}t}, \qquad \mathsf{l}_I^T = l_I^T\frac{\mathrm{d}}{\mathrm{d}t}, \qquad \mathsf{m} = m\frac{\mathrm{d}}{\mathrm{d}t}. \tag{2.A.16}$$

This then leads to (after differentiating with respect to x and integrating over time)

$$\begin{aligned} \partial_x^2\Phi^T(x,t) &= \frac{2\pi}{\Phi_0}\Big[-l_O^T\partial_x(I_T)+l_I^T\partial_x(I_{C_1})+m\partial_x(I_{C_2})\Big], \\ \partial_x^2\Phi^B(x,t) &= \frac{2\pi}{\Phi_0}\Big[l_O^B\partial_x(I_B)-l_I^B\partial_x(I_{C_2})-m\partial_x(I_{C_1})\Big]. \end{aligned} \tag{2.A.17}$$

From the equations (2.3.10) we have

$$\partial_x I_T = I_b^T - \partial_x I_{C_1} \tag{2.A.18a}$$

$$\partial_x I_B = -I_b^B - \partial_x I_{C_2} \tag{2.A.18b}$$

We use these relations to eliminate the $\partial_x I_T$ and $\partial_x I_B$ terms from the equation.

Now we can use the relations for the x-derivatives of the horizontal currents given in (2.3.10) to obtain the final equations. However, to simplify things we will first

define

$$\hat{m} = \frac{m}{l_O^B + l_I^B}, \tag{2.A.19a}$$

$$\Delta = \frac{l_O^B + l_I^B}{l_O^T + l_I^T}, \tag{2.A.19b}$$

$$l_{\text{eff}} = l_I^T + l_O^T - m\hat{m}, \tag{2.A.19c}$$

and rewrite the equations to

$$\begin{cases} \partial_x^2 \Phi^T(x,t) + \hat{m}\partial_x^2 \Phi^B(x,t) = \dfrac{2\pi}{\Phi_0}\Big[l_{\text{eff}}\partial_x I_{C_1} - l_O^T I_b^T - \hat{m} l_O^B I_b^B\Big], \\ \partial_x^2 \Phi^B(x,t) + \Delta\hat{m}\partial_x^2 \Phi^T(x,t) = \dfrac{2\pi}{\Phi_0}\Big[-\Delta l_{\text{eff}}\partial_x I_{C_2} - l_O^B I_b^B - \hat{m} l_O^T I_b^T\Big]. \end{cases} \tag{2.A.20}$$

We can simplify these equations further by rescaling the independent variable x. If we multiply the equations by b and define $\tilde{x} = ax$, the equations become

$$\begin{cases} a^2 b\big(\partial_{\tilde{x}}^2 \Phi^T(\tilde{x},t) + \hat{m}\partial_{\tilde{x}}^2 \Phi^B(\tilde{x},t)\big) = ab\dfrac{2\pi}{\Phi_0} l_{\text{eff}}\partial_{\tilde{x}} I_{C_1} - b\dfrac{2\pi}{\Phi_0}\big(l_O^T I_b^T + \hat{m} l_O^B I_b^B\big), \\ a^2 b\big(\partial_{\tilde{x}}^2 \Phi^B(\tilde{x},t) + \Delta\hat{m}\partial_{\tilde{x}}^2 \Phi^T(\tilde{x},t)\big) = -ab\dfrac{2\pi}{\Phi_0}\Delta l_{\text{eff}}\partial_{\tilde{x}} I_{C_2} - b\dfrac{2\pi}{\Phi_0}(l_O^B I_b^B + \hat{m} l_O^T I_b^T). \end{cases} \tag{2.A.21}$$

We will take a and b such that the resulting equations are as close as possible to the equations for the single junction. Hence we will require $a^2 b = 1$. Since

$$ab\frac{2\pi}{\Phi_0} l_{\text{eff}}\partial_{\tilde{x}} I_{C_1} = b\frac{2\pi}{\Phi_0} l_{\text{eff}}\left(J_c^T \sin\Phi^T + \frac{\Phi_0}{2\pi}(\mathrm{z}_S^T)^{-1}\right)(\partial_t \Phi^T), \tag{2.A.22}$$

we will choose b to be $\frac{\Phi_0}{2\pi l_{\text{eff}} J_c^T}$. This results in

$$\begin{cases} \partial_{\tilde{x}}^2 \Phi^T(\tilde{x},t) + \hat{m}\partial_{\tilde{x}}^2 \Phi^B(\tilde{x},t) = \dfrac{\partial_{\tilde{x}} I_{C_1}}{J_c^T} - \gamma_T, \\ \partial_{\tilde{x}}^2 \Phi^B(\tilde{x},t) + \Delta\hat{m}\partial_{\tilde{x}}^2 \Phi^T(\tilde{x},t) = -\Delta\dfrac{\partial_{\tilde{x}} I_{C_2}}{J_c^T} - \gamma_B, \end{cases} \tag{2.A.23}$$

The constants γ_B and γ_T are defined as

$$\gamma_T = \frac{l_O^T I_b^T + l_O^B \hat{m} I_b^B}{l_{\text{eff}} J_c^T} \tag{2.A.24a}$$

$$\gamma_B = \frac{l_O^B I_b^B + l_O^T \hat{m}\Delta I_b^T}{l_{\text{eff}} J_c^T} \tag{2.A.24b}$$

Now, in each of the two equations, the right hand side contains only one term with the vertical currents. We can immediately substitute the corresponding expressions

from (2.3.10), taking care of

$$\begin{cases} \partial_x^2\Phi^T(x,t) + \hat{m}\partial_x^2\Phi^B(x,t) = \sin\Phi^T(x,t) + \\ \qquad \frac{\Phi_0}{2\pi J_c^T}\big(c^T\partial_t^2\Phi^T(x,t) + \frac{1}{r^T}\partial_t\Phi^T(x,t)\big) - \gamma_T, \\ \partial_x^2\Phi^B(x,t) + \Delta\hat{m}\partial_x^2\Phi^T(x,t) = \Delta\frac{J_c^B\sin\Phi^B(x,t)}{J_c^T} + \\ \qquad \Delta\frac{\Phi_0}{2\pi J_c^T}\big(c^B\partial_t^2\Phi^B(x,t) + \frac{1}{r^B}\partial_t\Phi^B(x,t)\big) - \gamma_B. \end{cases} \tag{2.A.25}$$

Rescaling the time gives

$$\begin{cases} \partial_x^2\Phi^T(x,t) + \hat{m}\partial_x^2\Phi^B(x,t) = \sin\Phi^T(x,t) + \\ \qquad \partial_t^2\Phi^T(x,t) + \frac{\sqrt{\Phi_0}}{r^T\sqrt{2\pi J_c^T c^T}}\partial_t\Phi^T(x,t) - \gamma_T, \\ \partial_x^2\Phi^B(x,t) + \Delta\hat{m}\partial_x^2\Phi^T(x,t) = \Delta\frac{J_c^B\sin\Phi^B(x,t)}{J_c^T} + \\ \qquad \Delta\big(\frac{c^B}{c^T}\partial_t^2\Phi^B(x,t) + \frac{\sqrt{\Phi_0}}{r^B\sqrt{2\pi J_c^T c^T}}\partial_t\Phi^B(x,t)\big) - \gamma_B, \end{cases} \tag{2.A.26}$$

or

$$\begin{cases} \partial_x^2\Phi^T(x,t) + \sigma\partial_x^2\Phi^B(x,t) = \sin\Phi^T(x,t) + \partial_t^2\Phi^T(x,t) \\ \qquad + \alpha_T\partial_t\Phi^T(x,t) - \gamma_T, \\ \partial_x^2\Phi^B(x,t) + \Delta\sigma\partial_x^2\Phi^T(x,t) = \Delta\frac{\sin\Phi^B(x,t)}{J} + \Delta C\partial_t^2\Phi^B(x,t) \\ \qquad + \Delta\alpha_B\partial_t\Phi^B(x,t)\big) - \gamma_B. \end{cases} \tag{2.3.17}$$

2.A.4 Large surface resistance

Assuming the surface resistance to be of order $\frac{1}{\epsilon}$, the equation have been derived using the Maple worksheet in appendix 2.B. Here we give the final equation, resulting from that derivation.

The equation for Φ^T is

$$\begin{aligned} \sigma\frac{\partial^2}{\partial x^2}\Phi^B(x,t) + \frac{\partial^2}{\partial x^2}\Phi^T(x,t) + C_2\varepsilon\frac{\partial^3}{\partial x^2\,\partial t}\Phi^T(x,t) = \frac{\partial}{\partial x}I_{C1}(x,t)A_2 \\ + A_1\varepsilon\frac{\partial^2}{\partial x\partial t}I_{C1}(x,t) + D1I_b^T(x,t) + D2\varepsilon\frac{\partial}{\partial t}I_b^T(x,t) + E1I_b^B(x,t) \\ + E2\varepsilon\frac{\partial}{\partial t}I_b^B(x,t) \end{aligned} \tag{2.A.27a}$$

where

$$A1 = 2\frac{\pi\left(l_O^T + l_I^T\right)}{\Phi_0} - 2\frac{m^2\pi}{\left(l_O^B + l_I^B\right)\Phi_0},$$

$$
\begin{aligned}
A2 &= -2\frac{m^2\pi l_O^T}{\left(l_O^B+l_I^B\right)\Phi_0 z_I^T} - 2\frac{m^2 l_O^B\pi}{z_I^B\left(l_O^B+l_I^B\right)\Phi 0},\\
\sigma &= \frac{m}{l_O^B+l_I^B},\\
C2 &= \frac{l_I^T}{z_I^T} - \frac{m^2}{\left(l_O^B+l_I^B\right)z_I^T},\\
D1 &= -2\frac{\pi l_O^T}{\Phi_0},\\
D2 &= 2\frac{m^2\pi l_O^T}{\left(l_O^B+l_I^B\right)\Phi_0 z_I^T},\\
E1 &= -2\frac{l_O^B\pi m}{\left(l_O^B+l_I^B\right)\Phi_0},\\
E2 &= 2\frac{l_O^B\pi m l_I^B}{z_I^B\left(l_O^B+l_I^B\right)\Phi_0}
\end{aligned}
$$

For Φ^B we get a similar equation

$$
\begin{aligned}
\sigma\frac{\partial^2}{\partial x^2}\Phi^T(x,t) + \frac{\partial^2}{\partial x^2}\Phi^B(x,t) + \hat{C}2s\epsilon\frac{\partial^3}{\partial x^2\partial t}\Phi^B(x,t) = \\
\hat{A}1\frac{\partial}{\partial x}I_{C_2}(x,t) + \hat{A}2\epsilon\frac{\partial^2}{\partial x\partial t}I_{C_2}(x,t) + \hat{D}1I_b^B(x,t) + \epsilon\hat{D}2\frac{\partial}{\partial t}I_b^B(x,t) + \\
\hat{E}1I_b^T(x,t) + \hat{E}2\epsilon\frac{\partial}{\partial t}I_b^T(x,t) \quad \text{(2.A.27b)}
\end{aligned}
$$

where

$$
\begin{aligned}
\hat{A}1 &= -2\frac{\pi\left(l_O^B+l_I^B\right)}{\Phi_0} + 2\frac{m^2\pi}{\left(l_O^T+l_I^T\right)\Phi_0} = -\Delta A_1,\\
\hat{A}2 &= 2\frac{m^2\pi l_O^B}{\left(l_O^T+l_I^T\right)\Phi_0 z_I^B} + 2\frac{m^2 l_O^T\pi}{z_I^T\left(l_O^T+l_I^T\right)\Phi 0} = -\Delta A_2,\\
\hat{\sigma} &= \frac{m}{l_O^T+l_I^T} = \Delta\sigma,\\
\hat{C}2 &= \frac{l_I^B}{z_I^B} - \frac{m^2}{\left(l_O^T+l_I^T\right)z_I^B},\\
\hat{D}1 &= -2\frac{\pi l_O^B}{\Phi_0},\\
\hat{D}2 &= 2\frac{m^2\pi l_O^B}{\left(l_O^T+l_I^T\right)\Phi_0 z_I^B},\\
\hat{E}1 &= -2\frac{l_O^T\pi m}{\left(l_O^T+l_I^T\right)\Phi_0},\\
\hat{E}2 &= 2\frac{l_O^T\pi m l_I^T}{z_I^T\left(l_O^T+l_I^T\right)\Phi_0}
\end{aligned}
$$

The final equations can be written (after rescaling x and t) as

$$\partial_x^2\Phi^T - \partial_t^2\Phi^T + \sigma\partial_x^2\Phi^B - \sin\Phi^T = \alpha\partial_t\Phi^T - \beta\partial_x^2\partial_t\Phi^T + \delta\cos\Phi^T\partial_t\Phi^T + \eta\partial_t^3\Phi^T - \gamma_T, \tag{2.A.28a}$$

$$\partial_x^2\Phi^B - \tilde{C}\partial_t^2\Phi^B + \Delta\sigma\partial_x^2\Phi^T - \Delta\frac{\sin\Phi^B}{J} = \delta R\alpha\partial_t\Phi^B - B\beta\partial_x^2\partial_t\Phi^B + \Delta\delta\frac{\cos\Phi^B}{J}\partial_t\Phi^B + \Delta C\eta\partial_t^3\Phi^B - \gamma_B. \tag{2.A.28b}$$

In these expressions all derivatives with respect to x should be read as derivatives with respect to $\tilde{x} = ax$, and all derivatives with respect to t should be read as being derivatives with respect to $\tilde{t} = ct$. In these equation the tildes have been suppressed to improve readability.

Apart from rescaling the independent variables, we also multiplied both equations with b. We choose a, b and c to have a factor one on $\partial_x^2\Phi^T$, $\partial_t^2\Phi^T$ and $\sin\Phi^T$. This means that a, b and c satisfy

$$\begin{aligned} A_1 b J_c^T &= 1 \\ a^2 b &= 1 \\ \frac{\Phi_0}{2\pi} b c^2 \left(A_1 c^T + \frac{\epsilon A_2}{r^T} \right) &= 1 \end{aligned}$$

The coefficients in (2.A.28a) are then given by

$$\begin{aligned} \alpha &= \frac{A_1\Phi_0 bc}{2\pi r^T} \\ \beta &= \epsilon C_2 c \\ \delta &= \frac{A_2}{A_1}\epsilon c \\ \eta &= \frac{\Phi_0}{2\pi} c^T b c^3 \epsilon A_2 \end{aligned}$$

and all terms containing bias currents are combined in the symbols γ_T and γ_B.

The other constants have their usual meaning

$$C = \frac{c^B}{c^T} \qquad J = \frac{J_c^T}{J_c^B} \qquad R = \frac{r^T}{r^B} \tag{2.A.29}$$

$$\Delta = \frac{l_O^B + l_I^B}{l_O^T + l_I^T} \tag{2.A.30}$$

Only the constant $\tilde{C}$ is new

$$\tilde{C} = \frac{-\hat{A}_1 c^B - \frac{\epsilon\hat{A}_2}{r^B}}{A_1 c^T + \frac{\epsilon A_2}{r^T}} = \Delta C + \epsilon\frac{\Delta A2}{A1}\left(\frac{\frac{1}{r^B} - \frac{c^B}{c^T r^T}}{c^T} \right) + \mathcal{O}(\epsilon^2) \tag{2.A.31}$$

2.B The Maple worksheet to derive the equations (2.A.27)

The equations:

```
> eq1:=(1+l_IT*(z_IT)^(-1))*(diff(Phi_T(x,t),x,t))=
  2*Pi/Phi_0*(-(1+l_IT*z_IT^(-1))*z_OT*(I_T(x,t))+
  l_IT*I_C1(x,t)+m*I_C2(x,t)-m*z_IB^(-1)*
  (-Phi_0/(2*Pi)*diff(Phi_B(x,t),x,t)+z_OB*(I_B(x,t))));
```

$$eq1 := (1+\frac{l_{IT}}{z_{IT}})\,(\frac{\partial^2}{\partial x\,\partial t}\,\Phi_T(x,\,t)) = \frac{2\pi}{\Phi_0}\left(-(1+\frac{l_{IT}}{z_{IT}})\,z_{OT}\,I_T(x,\,t)+l_{IT}\,I_{C1}(x,\,t)+ m\,I_{C2}(x,\,t)+-\frac{m\left(-\frac{1}{2}\,\frac{\Phi_0\,(\frac{\partial^2}{\partial x\,\partial t}\,\Phi_B(x,\,t))}{\pi}+z_{OB}\,I_B(x,\,t)\right)}{z_{IB}}\right)$$

```
> eq2:=(1+l_IB*(z_IB)^(-1))*(diff(Phi_B(x,t),x,t))=
  2*Pi/Phi_0*((1+l_IB*z_IB^(-1))*z_OB*(I_B(x,t))-
  l_IB*I_C2(x,t)-m*I_C1(x,t)+m*z_IT^(-1)*
  (Phi_0/(2*Pi)*diff(Phi_T(x,t),x,t)+z_OT*(I_T(x,t))));
```

$$eq2 := (1+\frac{l_{IB}}{z_{IB}})\,(\frac{\partial^2}{\partial x\,\partial t}\,\Phi_B(x,\,t)) = \frac{2\pi}{\Phi_0}\left((1+\frac{l_{IB}}{z_{IB}})\,z_{OB}\,I_B(x,\,t)-l_{IB}\,I_{C2}(x,\,t)- m\,I_{C1}(x,\,t)+\frac{m\left(\frac{1}{2}\,\frac{\Phi_0\,(\frac{\partial^2}{\partial x\,\partial t}\,\Phi_T(x,\,t))}{\pi}+z_{OT}\,I_T(x,\,t)\right)}{z_{IT}}\right)$$

The assumptions for the impedances

```
> imp_assump1:= m=(m*s),
  l_IT=(l_IT*s),
  l_IB=(l_IB*s),
  l_OB=(l_OB*s),
  l_OT=(l_OT*s):
  imp_assump2:=
  z_IT=z_IT/epsilon,
  z_IB=z_IB/epsilon,
  z_OB=1/(epsilon/(z_OB)+1/l_OB),
  z_OT=1/(epsilon/z_OT+1/l_OT):
```

We substitute the assumptions for the impdeances, and...

```
> eq1_epsilon:=subs(imp_assump1,subs(imp_assump2,eq1)):
```

```
> eq2_epsilon:=subs(imp_assump1,subs(imp_assump2,eq2)):
```

...use the relation between the x-derivative of the currents along the outer and inner surfaces.

```
> rel1:=diff(I_T(x,t),x)=Ib_T-diff(I_C1(x,t),x):
> rel2:=diff(I_B(x,t),x)=-Ib_B-diff(I_C2(x,t),x):
> eq1_IC:=subs(rel1,rel2,diff(eq1_epsilon,x)):
> eq2_IC:=subs(rel1,rel2,diff(eq2_epsilon,x)):
```

We now add a scalar multiple of the second equation to the first, to remove all the terms containing *I_C2* from this first equation. In this way, we will not have coupling terms, containing $\sin(Phi\_B)$ in the first equation. We will only have a coupling via derivatives of *Phi_B*.

```
> sum_eq:=subs(diff(I_C2(x,t),x)=temp,eq1_IC+b*eq2_IC):
```

We assume $\frac{l\_OB}{z\_OB}$ to be equal to $\frac{l\_IB}{z\_IB}$. We substitute this in the sum we defined above and keep only terms up to second order in ε.

```
> coeff_IC2:=subs(l_OB*s/z_OB=l_IB*s/z_IB,map(series,map(coeff,
  sum_eq,temp),epsilon,2));
```

$$coeff\_IC2 := 0 = (2\,\frac{\pi\, m\, s}{\Phi_0} + \frac{2\, b\, \pi\, (-l_{OB}\, s - l_{IB}\, s)}{\Phi_0}) + 2\,\frac{\pi\, m\, s^2\, l_{OB}}{\Phi_0\, z_{IB}}\,\varepsilon + \mathrm{O}(\varepsilon^2)$$

```
> solve(convert(%,polynom),{b});
```

$$\{b = \frac{m\,(z_{IB} + s\, l_{OB}\, \varepsilon)}{z_{IB}\,(l_{OB} + l_{IB})}\}$$

```
> assign(%);
> new_eq1:=subs(l_OB*s/z_OB=l_IB*s/z_IB,l_OT*s/z_OT=l_IT*s/z_IT,
  convert(map(series,eq1_IC+b*eq2_IC,epsilon,2),polynom)):
```

Some useful functions.

To derive the final equations, we will introduce abbriviations for certiain combinations of parameters, like $\sigma = \frac{m}{l\_IB+l\_OB}$. This will more clearly show the form of the terms in the equation. To do this we need to find the coefficients of expressions like $\frac{\partial}{\partial x}$ I_C1$(x,\, t)$ and $\frac{\partial^3}{\partial t\, \partial x^2}$ Phi_B$(x,\, t)$. We define the following functions.

```
> mycoef:=proc(factor,equation,oper) local subseq,coefficient;
> subseq:=subs(factor=temp,equation);
> coefficient:=coeff(oper(subseq),temp);
> end:
```

If *oper*=lhs, this will give the coefficient of *factor* in the left hand side of *equation*. Equivalently for *oper*=rhs.

```
> mycollect:=proc(factor,equation,oper)
> local subseq,collecteq;
```

```
> subseq:=subs(factor=temp,equation);
> collecteq:=collect(oper(subseq),temp); subs(temp=factor,collecteq);
> end:
```

mycollect works as collect on *equation*, it will collect terms of the same order in *factor*. But it will also work if *factor* is an expression like $\frac{\partial}{\partial x}\,\mathrm{I}(x,\,t)$.

```
> coeffs_eq:=proc(factor,equation)
> local coeff_equation;
> coeff_equation:=mycoef(factor,equation,lhs)=mycoef(factor,equation,
  rhs);
> end:
```

coeffs_equation will get the coefficient of *factor* on the left and right hand side and will return them as the equation coefficient_on_left_hand_side=coefficient_on_right_hand_side. Beware that this should not be read as an equation! It only contains the coefficients of a certain term.

```
> lrsubs:=proc(subs_eq,factor,equation)
> subs(subs_eq,mycollect(factor,equation,lhs))=subs(subs_eq,
  mycollect(factor,equation,rhs));
> end:
```

lrsubs will substitute the *subs_eq* on both sides of the "="-sign in the *equation*. Before doing that it will first collect the coefficients of *factor* on the left and right.

Simplifying the equation.

First we look whether the coefficient of I_C2 is really zero: REMARK: The "equation" below is not a real equation. Left of the "="-sign we have the coefficient of I_C2 on the left hand side of equation new_eq1. The same holds of course for the expression to the right of the "="-sign.

```
> coeff_eq1:=coeffs_eq(diff(I_C2(x,t),x),new_eq1);
```

coeff_eq1 :=

$$0 = 2\,\frac{\pi\,m\,s}{\Phi_0}+\frac{2\,m\,\pi\,(-l_{OB}\,s-l_{IB}\,s)}{(l_{OB}+l_{IB})\,\Phi_0}+(2\,\frac{\pi\,m\,s^2\,l_{OB}}{\Phi_0\,z_{IB}}+\frac{2\,m\,l_{OB}\,s\,\pi\,(-l_{OB}\,s-l_{IB}\,s)}{z_{IB}\,(l_{OB}+l_{IB})\,\Phi_0})\,\varepsilon$$

```
> simplify(rhs(coeff_eq1));
```

$$0$$

So, indeed the coefficient of $\frac{\partial}{\partial t}\,\mathrm{I\_C2}(x,\,t)$ is equal to 0. We will substitute this in the equation:

```
> eq1_new2:=lrsubs(rhs(coeff_eq1)=0,diff(I_C2(x,t),x),new_eq1):
> coeff_eq2:=coeffs_eq(diff(I_C1(x,t),x),eq1_new2);
```

$$\mathit{coeff\_eq2} := 0 = 2\,\frac{\pi\,(l_{OT}\,s + l_{IT}\,s)}{\Phi_0} - \frac{2\,m^2\,\pi\,s}{(l_{OB}+l_{IB})\,\Phi_0} + (-2\,\frac{m^2\,\pi\,s^2\,l_{OT}}{(l_{OB}+l_{IB})\,\Phi_0\,z_{IT}} - \frac{2\,m^2\,l_{OB}\,s^2\,\pi}{z_{IB}\,(l_{OB}+l_{IB})\,\Phi_0})\,\varepsilon$$

```
> collect(rhs(coeff_eq2),s);
```

$$(-2\,\frac{m^2\,\pi\,l_{OT}}{(l_{OB}+l_{IB})\,\Phi_0\,z_{IT}} - \frac{2\,m^2\,l_{OB}\,\pi}{z_{IB}\,(l_{OB}+l_{IB})\,\Phi_0})\,\varepsilon\,s^2 + (2\,\frac{\pi\,(l_{OT}+l_{IT})}{\Phi_0} - \frac{2\,m^2\,\pi}{(l_{OB}+l_{IB})\,\Phi_0})\,s$$

The coefficient of $\frac{\partial}{\partial x}\,\mathrm{I\_C1}(x,\,t)$ is of the form $A\_1\,\varepsilon\,s^2 + A\_2\,s$.

```
> eq1_new3:=lrsubs(rhs(coeff_eq2)=A_1*s+A_2*s^2*epsilon,
  diff(I_C1(x,t),x),eq1_new2):
> coeffs_eq(diff(Phi_B(x,t),x,x,t),eq1_new3);
```

$$\frac{m}{l_{OB}+l_{IB}} + (\frac{m\,l_{IB}\,s}{(l_{OB}+l_{IB})\,z_{IB}} + \frac{m\,l_{OB}\,s}{z_{IB}\,(l_{OB}+l_{IB})})\,\varepsilon = \frac{m\,s\,\varepsilon}{z_{IB}}$$

There appear to be terms of the form $B\_1\,(\frac{\partial^3}{\partial t\,\partial x^2}\,\mathrm{Phi\_B}(x,\,t))$ as well as terms of the form $B\_2\,s\,\varepsilon\,(\frac{\partial^3}{\partial t\,\partial x^2}\,\mathrm{Phi\_B}(x,\,t))$, however...

```
> simplify(lhs(%)-rhs(%));
```

$$\frac{m}{l_{OB}+l_{IB}}$$

```
> temp_eq:=subs(diff(Phi_B(x,t),x,x,t)=0,eq1_new3):
> eq1_new4:=lhs(temp_eq)+sigma*diff(Phi_B(x,t),x,x,t)=rhs(temp_eq):
```

Now we turn to the terms containing $\frac{\partial^3}{\partial t\,\partial x^2}\,\mathrm{Phi\_T}(x,\,t)$.

```
> coeffs_eq(diff(Phi_T(x,t),x,x,t),eq1_new4);
```

$$1 + \frac{l_{IT}\,s\,\varepsilon}{z_{IT}} = \frac{m^2\,s\,\varepsilon}{(l_{OB}+l_{IB})\,z_{IT}}$$

```
> temp_eq:=subs(diff(Phi_T(x,t),x,x,t)=0,eq1_new4):
> eq1_new5:=lhs(temp_eq)+(1+C_2*s*epsilon)*diff(Phi_T(x,t),x,x,t)=
  rhs(temp_eq):
```

And finish off by applying the same procedure for Ib_T and Ib_B.

```
> coeffs_eq(Ib_T,eq1_new5);
```

$$0 = -2\,\frac{\pi\, l_{OT}\, s}{\Phi_0} + \frac{2\, m^2\, \pi\, s^2\, l_{OT}\, \varepsilon}{(l_{OB} + l_{IB})\, \Phi_0\, z_{IT}}$$

```
> temp_eq:=subs(Ib_T=0,eq1_new5):
> eq1_new6:=lhs(temp_eq)=rhs(temp_eq)+(D1*s+epsilon*s^2*D2)*Ib_T:
> collect(map(simplify,coeffs_eq(Ib_B,eq1_new6)),s);
```

$$0 = 2\,\frac{l_{OB}\, \pi\, m\, l_{IB}\, \varepsilon\, s^2}{z_{IB}\, (l_{OB} + l_{IB})\, \Phi_0} - \frac{2\, m\, \pi\, l_{OB}\, s}{(l_{OB} + l_{IB})\, \Phi_0}$$

```
> temp_eq:=subs(Ib_B=0,eq1_new6):
```

The final equation is then:

```
> eq1_new7:=lhs(temp_eq)=rhs(temp_eq)+(E1*s+E2*epsilon*s^2)*Ib_B;
```

$$eq1\_new7 := \sigma\,(\frac{\partial^3}{\partial x^2\, \partial t}\,\Phi_B(x,\,t)) + (1 + C_2\, s\, \varepsilon)\,(\frac{\partial^3}{\partial x^2\, \partial t}\,\Phi_T(x,\,t)) =$$
$$(A_1\, s + A_2\, s^2\, \varepsilon)\,(\frac{\partial}{\partial x}\,I_{C1}(x,\,t)) + (\mathrm{D1}\, s + \varepsilon\, s^2\, \mathrm{D2})\, Ib\_T + (E1\; s + E2\, \varepsilon\, s^2)\, Ib\_B$$

Since multiplying with s means differentiating with respect to time, we can integrate the equation left and right with respect to time, to obtain the equation:

```
> sigma*diff(Phi_B(x,t),`$`(x,2))+1*diff(Phi_T(x,t),`$`(x,2)) +
C_2*epsilon*diff(Phi_T(x,t),t,x,x)= A_2*diff(I_C1(x,t),x)+
A_1*epsilon*diff(I_C1(x,t),x,t)+D1*Ib_T+
D2*epsilon*diff(Ib_T(x,t),t)+E1*Ib_B+E2*epsilon*diff(Ib_B(x,t),t);
```

$$\sigma\,(\frac{\partial^2}{\partial x^2}\,\Phi_B(x,\,t)) + (\frac{\partial^2}{\partial x^2}\,\Phi_T(x,\,t)) + C_2\, \varepsilon\,(\frac{\partial^3}{\partial x^2\, \partial t}\,\Phi_T(x,\,t)) = A_2\,(\frac{\partial}{\partial x}\,I_{C1}(x,\,t))$$
$$+ A_1\, \varepsilon\,(\frac{\partial^2}{\partial x\, \partial t}\,I_{C1}(x,\,t)) + \mathrm{D1}\, Ib\_T + \mathrm{D2}\, \varepsilon\,(\frac{\partial}{\partial t}\,I_b^T(x,\,t)) + E1\; Ib\_B$$
$$+ E2\, \varepsilon\,(\frac{\partial}{\partial t}\,I_b^B(x,\,t))$$

Comparing this to the equation that we derived where we assume the outer impedance to be zero, we see that also in this case there is only a coupling term of the form $\frac{\partial^2}{\partial x^2}\,\Phi^{\mathrm{B}}(x,\,t)$. However, where previously we only had a term $\frac{\partial}{\partial x}\,\mathrm{I}_{\mathrm{C}_1}(x,\,t)$ we now also have a term $\frac{\partial^2}{\partial t\,\partial x}\,\mathrm{I}_{\mathrm{C}_1}(x,\,t)$. This term is of the same order as the term containing $\frac{\partial^3}{\partial t\,\partial x^2}\,\Phi^{\mathrm{T}}(x,\,t)$.

Chapter 3

The single Josephson junction

In this chapter we will investigate some of the important aspects of the single Josephson junction. We will mainly focus on the existence of the "fluxon" solutions introduced in chapter 1.

Using perturbation analysis, we are able to show that for small values of the parameters α, β and γ, there exist a fluxon solution. Numerical simulation shows that for fixed α and β, and larger values of γ and the velocity c, there exists a spiral in the (c, γ) plane for which travelling wave solutions exist. We show that this is a consequence of the existence of a heteroclinic cycle.

3.1 Travelling waves

It was noted in the first chapter that the fluxons could travel along the junction. This motivates to look at travelling wave solutions to the equation

$$\Phi_{xx}(x,t) - \Phi_{tt}(x,t) - \sin\Phi(x,t) = \epsilon F(\Phi;\epsilon)(x,t), \tag{3.1.1}$$

where F is an operator containing the perturbation terms. So we assume that the solution only depends on $\xi = x + ct$

$$\Phi(x,t) = \phi(x+ct) = \phi(\xi). \tag{3.1.2}$$

The partial differential equation is, thus, reduced to an ordinary differential equation

$$(1-c^2)\phi''(\xi) - \sin\phi(\xi) = \epsilon\hat{F}(\phi;c,\epsilon)(\xi). \tag{3.1.3}$$

The advantage of this assumption is obvious, since this means reducing the system from an infinite dimensional to a three dimensional one. Also the disadvantage is obvious, since we loose information about the stability of the solution for the PDE. This is important information, since it determines for example whether the solutions we find can actually be observed in the physical system.

To resolve this problem, we will investigate the (linearised) stability problem separately, at the end of this chapter.

3.2 Unperturbed case

In this section we will investigate the possible solutions to the unperturbed sine-Gordon equation. So, we take $\epsilon = 0$.

The travelling wave assumption reduces (3.1.1) to

$$(1 - c^2)\phi'' - \sin\phi = 0. \tag{3.2.1}$$

This is the equation for a pendulum (although the definition of the angle ϕ is different from the conventional one; since the angle $\phi = 0$ corresponds to the situation where the pendulum is standing straight up). The phase portrait of this equation is rather well-known, we will summarise the important aspects.

It is important to note that ϕ is a phase-variable, so increasing its value by 2π does not affect the system in any way. The correct phase space to think of this system is hence $S[0, 2\pi] \times \mathbb{R}$, i.e., one should identify the equilibria which are at a distance $2k\pi$. On this cylinder there are then exactly two equilibria. However, for some discussions and for making pictures, it is quite often easier to "roll-out" the cylinder and draw the pictures in $\mathbb{R}^2$. Using this latter picture, the system contains the equilibria

$$\phi_{2k} = 2k\pi \qquad \phi_{2k+1} = \pi + 2k\pi. \tag{3.2.2}$$

The type of the equilibria is determined by the sign of $1 - c^2$. As long as $|c|$ is smaller than 1, the equilibria ϕ_{2k} are saddle points and the others are centre points. For $|c| > 1$ the role of the two equilibria is reversed. Because ϕ is a phase-variable, connections between a saddle point and the 2π-shifted one, are *homo*clinic orbits.

For $|c| < 1$ there exist periodic orbits around the equilibria ϕ_{2k+1} and connections between the saddles ϕ_{2k} and ϕ_{2k+2}, see figure 3.1. For $|c| > 1$ we get the same phaseportrait, only shifted by π, since the two equilibria reverse role.

The most important for applications are the homoclinic connections between equilibria. These solutions correspond to the fluxons introduced in chapter 1. In the

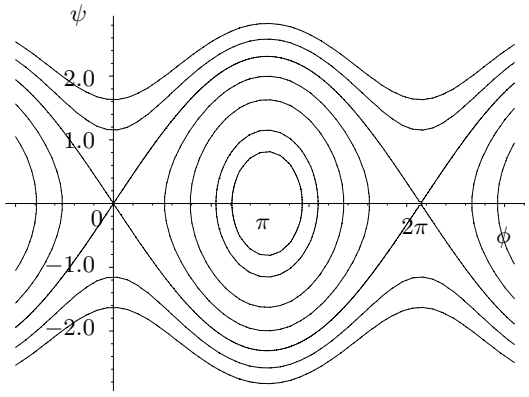

Figure 3.1: The phaseportrait of the sine-Gordon equation

mechanical analogue of the pendulum, these solutions correspond to the motion of the pendulum, where it starts upright and then makes one revolution to end up exactly upright again. With this picture in mind it might be difficult to imagine that these solutions will in fact be stable for the PDE, whereas the small amplitude oscillations around the equilibrium ϕ_1 is not. This is however a consequence of the general result that equilibrium points, which are centres of the ODE when $c = 0$, are unstable equilibria for the PDE, while saddle points of the ODE are stable equilibria of the PDE (see chapter 4).

The homoclinic solution of the unperturbed system is given by

$$\phi_{\xi_0}(\xi) = 4 \arctan\left(e^{\frac{\xi+\xi_0}{\sqrt{1-c^2}}}\right). \tag{3.2.3}$$

This is a solution, for any value of c. For the unperturbed problem travelling kink solutions exist for any speed as long as $|c| \leq 1$. The free constant ξ_0 is a consequence of system (3.2.1) being autonomous.

For $c > 1$, the equilibrium at the origin, becomes a centre. This means that for $c > 1$ there will be travelling wave solutions which are small amplitude oscillations, often called "plasma waves" in physics literature.

For the unperturbed sine-Gordon equation there are clearly separated regions in parameter space for which there exist travelling kink and travelling plasma waves.

The other type of solutions that exist, are the "rotating" solutions. In the case of the pendulum this means a solution where the pendulum has a non-zero velocity in the upright position. The pendulum will continue to rotate. In the (infinite) Josephson junction, this corresponds to an (infinite) series of fluxons, which are equally spaced. This solution is often called a "fluxon train".

In the remainder of this chapter we will focus on the single fluxon solution.

3.3 Perturbation analysis

In this section we will present a general method to find 2π-kink solutions to the perturbed sine-Gordon equation (3.1.1) in the form of a series expansion. A condition which must be satisfied by the perturbation will arise in a natural way in our analysis.

For $\epsilon = 0$, a solution to (3.1.1) under the conditions

$$\lim_{\xi\to-\infty} \phi(\xi) = 0 \qquad \lim_{\xi\to\infty} \phi(\xi) = 2\pi \tag{3.3.1}$$

is given by (3.2.3). We now seek solutions to the perturbed system in the form of a series in ϵ.

$$\phi_\epsilon(\xi) = \phi_0(\xi) + \epsilon\phi_1(\xi) + \epsilon^2\phi_2(\xi) + \mathcal{O}(\epsilon^3), \tag{3.3.2}$$

where each of the $\phi_i(\xi)$ is bounded on $\mathbb{R}$.

Since we assume this perturbation to be small, we can assume that the velocity will stay below $c = 1$ and rescale the independent variable to obtain the equation

$$\phi''(\xi) - \sin\phi(\xi) = \epsilon\tilde{F}(\phi(\xi); c, \epsilon). \tag{3.3.3}$$

The equation that must be satisfied by $U_1 = (\phi_1 \quad \phi_1')^T$ is given by

$$\frac{\mathrm{d}}{\mathrm{d}\xi}U_1 = A(\xi)U_1 + G(\xi) \tag{3.3.4}$$

where

$$A(\xi) = \begin{bmatrix} 0 & 1 \\ \cos\big(\phi_0(\xi)\big) & 0 \end{bmatrix} \qquad G(\xi) = \begin{bmatrix} 0 \\ \tilde{F}(\phi_0(\xi); c, 0) \end{bmatrix}$$

The homogeneous part of this equation is a linear equation $\frac{\mathrm{d}}{\mathrm{d}\xi}U = A(\xi)U$ and has as fundamental solution

$$X(\xi) = \begin{bmatrix} \operatorname{sech}\xi & \frac{1}{2}(\xi\operatorname{sech}\xi + \sinh\xi \\ (\operatorname{sech}\xi)' & \frac{1}{2}(\xi\operatorname{sech}\xi + \sinh\xi)' \end{bmatrix}. \tag{3.3.5}$$

To investigate the bounded solutions of equation (3.3.4), we introduce the following projections. The projection on the stable subspace

$$\{x \in \mathbb{R}^2 \Big| \sup_{t\geq 0} |X(t)x| < \infty\} \tag{3.3.6}$$

will be denoted by P^s. We define the projection $P^u = I - P^s$. In the present case

$$P^s = \begin{bmatrix} 1 & 0 \\ 0 & 0 \end{bmatrix}. \tag{3.3.7}$$

In a similar fashion we define the projection on the unstable subspace

$$\{x \in \mathbb{R}^2 \Big| \sup_{t\leq 0} |X(t)x| < \infty\} \tag{3.3.8}$$

and denote this projection by $\hat{P}^u$, and define $\hat{P}^s = I - \hat{P}^u$. In the present case we have that $P^s = \hat{P}^u$. This is in general not true and is not essential for the present treatment. In fact the theorem we will derive below, will be stated in general. What is important is that the system (3.3.4) possesses both an exponential dichotomy [2] on $\mathbb{R}^+$ (with projections P^s and P^u) and an exponential dichotomy on $\mathbb{R}^-$ (with projections $\hat{P}^s$ and $\hat{P}^u$).

This means that the projections P^s and P^u are such that

$$\begin{cases} |X(t)P^sX^{-1}(s)| \leq Ke^{-\alpha(t-s)} & t \geq s \geq 0, \alpha > 0, \\ |X(t)P^uX^{-1}(s)| \leq Le^{-\beta(s-t)} & s \geq t \geq 0, \beta > 0. \end{cases} \tag{3.3.9}$$

In the present case we can take $\alpha = \beta = 1$. Similar relations hold for the projections $\hat{P}^s$ and $\hat{P}^u$ on $\mathbb{R}^-$.

We have the following theorem for the existence of bounded solutions of (3.3.4)

1 Theorem *If* $\lim_{\xi\to\pm\infty} G(\xi) = 0$, *the equation (3.3.4) has a bounded solution* U_1 *iff*

$$\int_{-\infty}^{0} \hat{P}^sX^{-1}(\tau)G(\tau)\mathrm{d}\tau + \int_{0}^{\infty} P^uX^{-1}(\tau)G(\tau)\mathrm{d}\tau = 0 \tag{3.3.10}$$

Moreover, the solution to (3.3.4) is explicitly given by

$$\begin{cases} X(\xi)\left(\int_0^\xi P^s X^{-1}(\tau)G(\tau)\mathrm{d}\tau + \int_\infty^\xi P^u X^{-1}(\tau)G(\tau)\mathrm{d}\tau\right) & \xi \geq 0 \\ X(\xi)\left(\int_0^\xi \hat{P}^u X^{-1}(\tau)G(\tau)\mathrm{d}\tau + \int_{-\infty}^\xi \hat{P}^s X^{-1}(\tau)G(\tau)\mathrm{d}\tau\right) & \xi < 0 \end{cases} \tag{3.3.11}$$

Proof:
We will construct two bounded solutions to the equation (3.3.4). One solution will be defined on $\mathbb{R}^-$ and the other on $\mathbb{R}^+$. The condition that the value at $\xi = 0$ matches will be the condition that a bounded solution on $\mathbb{R}$ exists.

Applying the variation-of-constants formula to the equation (3.3.4) gives the expression

$$U_1(\xi) = X(\xi)X^{-1}(\sigma)U_1(\sigma) + \int_\sigma^\xi X(\xi)X^{-1}(\tau)G(\tau)\mathrm{d}\tau \tag{3.3.12}$$

First we construct a solution U_1^+ that is bounded on $\mathbb{R}^+$. We introduce the projections

$$P^s(\xi) = X(\xi)P^s X^{-1}(\xi), \tag{3.3.13}$$

$$P^u(\xi) = X(\xi)P^u X^{-1}(\xi). \tag{3.3.14}$$

In the same way we define $\hat{P}^s(\xi)$ and $\hat{P}^u(\xi)$. Now we have

$$U_1^+(\xi) = P^s(\xi)U_1^+(\xi) + P^u(\xi)U_1^+(\xi) \tag{3.3.15}$$

and we will write down expressions for each of these terms. First for the second term.

$$P^u(\xi)U_1^+(\xi) = X(\xi)P^u X^{-1}(\sigma)U_1^+(\sigma) + \int_\sigma^\xi X(\xi)P^u X^{-1}(\tau)G(\tau)\mathrm{d}\tau \tag{3.3.16}$$

We still have the freedom to choose the value of σ. If we choose to let σ go to ∞, the first term will become zero for a solution which is bounded on $\mathbb{R}^+$, since this first term satisfies the inequality

$$|X(\xi)P^u X^{-1}(\sigma)U_1^+(\sigma)| \leq Ke^{-\alpha(\xi-\sigma)}|U_1^+(\sigma) \tag{3.3.17}$$

So we have

$$P^u(\xi)U_1^+(\xi) = \int_\infty^\xi X(\xi)P^u X^{-1}(\tau)G(\tau)\mathrm{d}\tau. \tag{3.3.18}$$

Consequently we have

$$U_1^+(\xi) = X(\xi)P^s U_1(0) + \int_0^\xi X(\xi)P^s X^{-1}(\tau)G(\tau)\mathrm{d}\tau + \int_\infty^\xi X(\xi)P^u X^{-1}(\tau)G(\tau)\mathrm{d}\tau, \tag{3.3.19}$$

Likewise, we have for the solution that is bounded on $\mathbb{R}^-$:

$$U_1^-(\xi) = X(\xi)\hat{P}^u U_1^-(0) + \int_0^\xi X(\xi)\hat{P}^u X^{-1}(\tau)G(\tau)\mathrm{d}\tau + \int_{-\infty}^\xi X(\xi)\hat{P}^s X^{-1}(\tau)G(\tau)\mathrm{d}\tau. \tag{3.3.20}$$

A necessary condition for a bounded solution to exist, is that these two solutions match at $\xi = 0$:

$$U_1^{+1}(0) = U_1^{-}(0) \tag{3.3.21}$$

which is equivalent to

$$\begin{cases} P^s U_1^+(0) = \hat{P}^u U_1^-(0) = P^s U_1^-(0) \\ \displaystyle\int_{-\infty}^{0} \hat{P}^s X^{-1}(\tau) G(\tau) \mathrm{d}\tau + \int_0^{\infty} P^u X^{-1}(\tau) G(\tau) \mathrm{d}\tau = 0 \end{cases} \tag{3.3.22}$$

We impose on U_1 the condition that $P^s U_1(0) = 0$ to get rid of the translation invariance. This means that we require the solution to lie on a section of co-dimension one, transversal to the solution $U_0 = (\phi_0 \quad \phi_0')^T$, at $\xi = 0$. We conclude that provided the second equation of (3.3.22) is satisfied, U_1 is given by (3.3.11).

□

For the case of equation 3.3.4, where the projections P^u and $\hat{P}^s$ are equal, the solvability condition can be written in the simpler form

$$0 = U_1^+(0) - U_1^-(0) = \int_{-\infty}^{\infty} P X^{-1}(\tau) G(\tau) \mathrm{d}\tau, \tag{3.3.23}$$

where $P = P^u = \hat{P}^s$.

When setting up the existence problem in a function space, the solvability condition characterises the range of the linearised operator. Often, and also here, one can fulfill the requirements for application of the Implicit Function Theorem if one can do the "first order" computation. We have chosen to just do this first order computation and to omit the, by now quite standard, details for a rigorous application of the IFT. See for instance [25].

3.4 Travelling kink-solutions

We apply the above theory to find travelling 2π-kink solutions to the equation

$$\Phi_{xx} - \Phi_{tt} - \sin\Phi = \alpha\Phi_t - \beta\Phi_{xxt} - \gamma. \tag{2.2.46}$$

This means we solve this equation under the conditions

$$\begin{cases} \lim\limits_{\xi \to -\infty} \phi(\xi) = \arcsin\gamma \\ \lim\limits_{\xi \to \infty} \phi(\xi) = \arcsin\gamma + 2\pi \end{cases} \tag{3.4.1}$$

We assume all coefficients of the terms on the right hand side to be small, and scale these with ϵ

$$\alpha = \epsilon\tilde{\alpha} \qquad \beta = \epsilon\tilde{\beta} \qquad \gamma = \epsilon\tilde{\gamma} \tag{3.4.2}$$

and rewrite the equation to

$$\Phi_{xx} - \Phi_{tt} - \sin\Phi = \epsilon\Big(\tilde{\alpha}\Phi_t - \tilde{\beta}\Phi_{xxt} - \tilde{\gamma}\Big), \tag{3.4.3}$$

and make the travelling wave assumption

$$(1-c^2)\phi'' - \sin\phi = \epsilon\Big(\tilde{\alpha}c\phi' - \tilde{\beta}c\phi''' - \tilde{\gamma}\Big). \tag{3.4.4}$$

We suppress the tildes on the parameters and rescale the equation to

$$\phi'' - \sin\phi = \epsilon\left(\frac{\alpha c}{\sqrt{1-c^2}}\phi' - \frac{\beta c}{(\sqrt{1-c^2})^3}\phi''' - \gamma\right) \tag{3.4.5}$$

We write $\phi_\epsilon(\xi) = \phi_0(\xi) + \epsilon\phi_1(\xi) + \dots$. The travelling wave solution for $\epsilon = 0$ is known explicitly:

$$\phi_0(\xi) = 4\arctan(e^\xi) \tag{3.4.6}$$

The equation for $\phi_1(\xi)$ reads

$$\begin{cases} \phi_1'' - \cos(\phi_0)\phi_1 = \dfrac{\alpha c}{\sqrt{1-c^2}}\phi_0' - \dfrac{\beta c}{(\sqrt{1-c^2})^3}\phi_0''' - \gamma \\ \lim\limits_{\xi\to-\infty}\phi_1(\xi) = \gamma \qquad \lim\limits_{\xi\to\infty}\phi_1(\xi) = \gamma. \end{cases} \tag{3.4.7}$$

The boundary conditions follow from the condition that $\lim_{\xi\pm\infty}\phi_\epsilon(\xi) = \arcsin\gamma$.

Now, since neither the right hand-side of the equation, nor the boundary conditions, satisfy the requirements of theorem 1 we define $u_1 = \phi_1 - \gamma$. The solvability condition for a bounded solution on $\mathbb{R}$ reads

$$\int_{-\infty}^{\infty} PX^{-1}(\xi)\begin{bmatrix} 0 \\ \frac{\alpha c}{\sqrt{1-c^2}}\phi_0' - \frac{\beta c}{(\sqrt{1-c^2})^3}\phi_0''' - \gamma + \gamma\cos(\phi_0) \end{bmatrix} = 0 \tag{3.4.8}$$

Working out the integrals we obtain a necessary condition for the existence of 2π-kink solutions to the perturbed equation

$$\gamma\pi(1-c^2) - 4\sqrt{1-c^2}\alpha c - \tfrac{4}{3}\frac{\beta c}{\sqrt{1-c^2}} = 0. \tag{3.4.9}$$

This condition is, in fact, a sufficient condition (see [25]). We derived this equation by assuming α and β to be small (of order ϵ). This was not necessary for just this existence condition. The only quantities that matter are the products αc and βc. We could also scale c with ϵ, instead of α and β. This is also from a physical point of view a more intuitive way to derive this equation, since α and β are material constants, whereas γ can be varied (it represents the bias current applied to the system). The speed c is then selected, and it is small if γ is small.

We then obtain the relation

$$\gamma\pi - 4\alpha c - \frac{4}{3}\beta c = 0, \tag{3.4.10}$$

which is equal to (3.4.9) up to $\mathcal{O}(c^2)$.

In physics literature one often sees the "adiabatic perturbation" method, which gives the same relation (3.4.9) between the parameters. The advantage of this method is

that it can be given a clear physical interpretation. However, it cannot be used to actually prove the existence of a solution to the perturbed method. Moreover, the method used in this chapter can also be used to calculate the solution ϕ_1.

The adiabatic perturbation method, start from the observation that the unperturbed system is a Hamiltonian system with Hamiltonian

$$H = \int_{\infty}^{\infty} \left(\frac{1}{2}\Phi_x^2(x,t) + \frac{1}{2}\Phi_t^2(x,t) + 1 - \cos\Phi(x,t) \right) \mathrm{d}x. \tag{3.4.11}$$

This Hamiltonian can be interpreted as the energy contained in the system. For a solution to the perturbed equation, this is still assumed to be total energy in the system. For a solution to the perturbed equation, the energy does not necessarily stay constant and one calculates

$$\begin{aligned}
\frac{\mathrm{d}H}{\mathrm{d}t} &= \int_{-\infty}^{\infty} \Big(\Phi_x(x,t)\Phi_{xt}(x,t) + \Phi_t(x,t)\Phi_{tt}(x,t) + \sin\Phi(x,t)\Phi_t(x,t) \Big) \mathrm{d}x \\
&= \int_{-\infty}^{\infty} \Big(\Phi_t(x,t) \left(\Phi_{tt}(x,t) - \Phi_{xx}(x,t) + \sin\Phi(x,t) \right) \Big) \mathrm{d}x \\
&= \int_{-\infty}^{\infty} \Big(-\alpha\Phi_t^2(x,t) + \beta\Phi_{xxt}(x,t)\Phi_t(x,t) + \gamma\Phi_t(x,t) \Big) \mathrm{d}x \\
&= \int_{-\infty}^{\infty} \Big(-\alpha\Phi_t^2(x,t) - \beta\Phi_{xt}^2(x,t) + \gamma\Phi_t(x,t) \Big) \mathrm{d}x
\end{aligned} \tag{3.4.12}$$

Setting this last equation to zero (after substituting the travelling wave solution), gives the same relation as (3.4.9) between the parameters. Now the terms in the last equation with the α and β can also be seen to be related to energy dissipation, while the γ-term is an energy-input.

It is possible to get an expression for $\phi_1(\xi)$, by working out the integrals in (3.3.11). Since in this case $P^s = \hat{P}^u$, the expression for $\xi > 0$ is identical to the one for $\xi < 0$. We will not write out ϕ_1 here. However, due to the fact that G is in this case even, we can easily see that ϕ_1 must also be even. We will write down the expression for U_1, indicating only which term is even $(+)$, which term is odd $(-)$ and which term is zero:

$$\begin{bmatrix} + & - \\ - & + \end{bmatrix} \left(\int_0^{\xi} \begin{bmatrix} 1 & 0 \\ 0 & 0 \end{bmatrix} \begin{bmatrix} + & - \\ - & + \end{bmatrix} \begin{bmatrix} 0 \\ + \end{bmatrix} \mathrm{d}\tau + \int_{\infty}^{\xi} \begin{bmatrix} 0 & 0 \\ 0 & 1 \end{bmatrix} \begin{bmatrix} + & - \\ - & + \end{bmatrix} \begin{bmatrix} 0 \\ + \end{bmatrix} \mathrm{d}\tau \right) \tag{3.4.13}$$

From this is is easy to see that $U_1 = \begin{bmatrix} + \\ - \end{bmatrix}$, and hence, that ϕ_1 is even.

3.5 Numerical calculations

The relation derived in the previous section is only valid if all parameters are small. We can calculate the parameter combinations for which there exist a homoclinic solution numerically, using the program AUTO[4]. In figure 3.2(a) the numerically

obtained (c, γ) picture (we will refer to these kind of pictures in the future as IV-characteristics, since this is how these pictures are measured in practice) is compared to the prediction for small parameters (3.4.9) derived in the previous section. The numerical values used in these calculations are $\alpha = 0.18$ and $\beta = 0.1$. A good agreement is seen for small values of c and γ. The global picture is as to be expected. If the bias current (driving force) is increased, the fluxon will move at a higher speed. However, near the top of the IV-characteristic, a strange phenomenon takes place. If we zoom in on the top of the IV-characteristic, a spiral shape can be observed (see figure 3.2(b)). Note that this spiral is strongly contracted in one direction, so it may not be immediately clear that this picture actually shows a spiral!

The fact that there exists such a spiral in the parameter plane, can be understood from the discussion in the next section. But first we should define what we mean by a spiral

2 Definition *With a spiral is meant a curve, converging to a a point x_0, which can be parametrised by in polar coordinates around x_0 as $r(\theta)$, where r has the property that for all θ, it holds that $r(\theta + 2\pi) < r(\theta)$. (Or for which it holds that for all θ, $r(\theta + 2\pi) > r(\theta)$.*

A plot showing several solutions for different parameter values along the spiral cruve is given in figure 3.3. The three combinations of parameters for which this picture was calculated, correspond to three consecutive limit points of the curve. This picture shows that if one chooses parametervalues on the spiral close to the centre of the spiral, the solution shows an "overshoot". The closer the parameter values are to

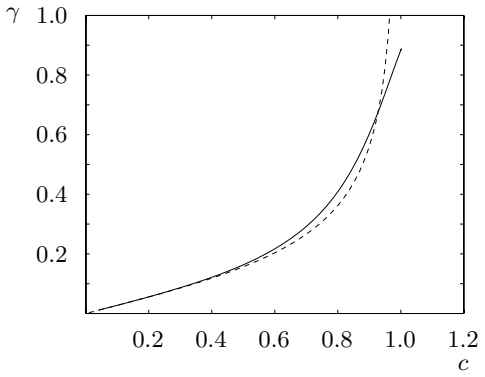

(a) Comparison of the numerically calculated IV-characteristic and the perturbation formula (3.4.9). The solid line is the result of AUTO calculations, the dashed curve is the perturbation method.

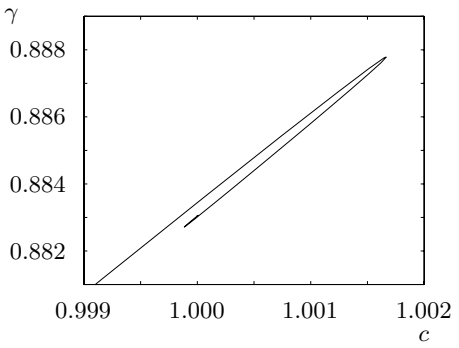

(b) A detail of the IV-characteristic as calculated with AUTO.

Figure 3.2: The IV-characteristic for the single junction

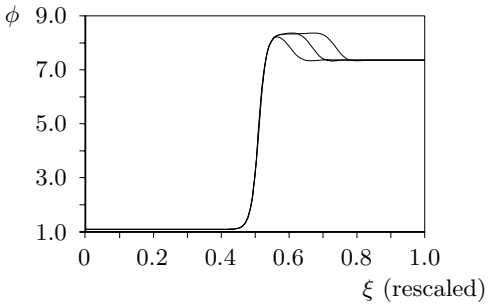

Figure 3.3: Several solutions for different parameters combinations on the spiral.

the centre, the longer the solution stays on a higher level. This higher level is the equilibrium $\phi = \pi - \arcsin\gamma$. This leads to the idea that for the parametervalues in the centre of the spiral, there may exist a heteroclinic solution.

3.6 Heteroclinic cycle breakup

In this section we will show that the existence of the spiral is an immediate consequence of the existence of a heteroclinic cycle in the system combined with the fact that the eigenvalues of one of the equilibria are complex. We will first give a sketch of the situation and how this heteroclinic cycle leads to the spiral. We will formalise this in a theorem. After this we will proof that a heteroclinic connection exists for the system (3.4.4). The centre of the spiral lies at the point $(c, \gamma) = (1, \gamma^*(\alpha, \beta))$. The significance of the value of the wave speed $c = 1$ is that in this case the system has an additional symmetry, i.e. it is reversible.

In the next section we will show that the existence of this heteroclinic cycle leads to the spiral.

3.6.1 Sketch of the situation

Equation (3.4.4) has two equilibria (we identify the 2π shifted equilibria). We will fix the parameters α and β since these are material properties and hence have two free parameters c and γ.

The general picture is that we have an ordinary differential equation in $\mathbb{R}^3$ with a parameter $p \in \mathbb{R}^2$. For a special choice of p the situation is as depicted in Figure 3.4: there is a heteroclinic cycle between the two equilibria. The one dimensional unstable manifold of equilibrium ϕ_1 intersects the one dimensional stable manifold of ϕ_2; this part of the heteroclinic cycle is non-generic (co-dimension 2). Furthermore, the two dimensional manifolds $W^u(\phi_2)$ and $W^s(\phi_1)$ intersect transversally. This intersection does not need to be unique. In [24] uniqueness of such an intersection is proven for the related equation $y''' = y^2 - 1$. To verify the uniqueness of the intersection, it is suggested in [21] to compute a certain time-delay function. In our case transversality is sufficient, since this means that the intersection is isolated.

For parameter values different from this special choice, the unstable manifold of ϕ_1 will no longer intersect the stable manifold of ϕ_2. For specific choices of parameters, the unstable manifold may come close to the intersection of the two dimensional manifolds and intersect the stable manifold of ϕ_1.

We make the following assumptions

H1
$$\begin{aligned}\dim W^u(\phi_1;p) &= 1,\\ \dim W^s(\phi_1;p) &= 2,\\ \dim W^u(\phi_2;p) &= 2,\\ \dim W^s(\phi_2;p) &= 1.\end{aligned}$$

H2 The unstable eigenvalues of ϕ_2 form a complex conjugate pair.

Furthermore we assume that there exists a heteroclinic cycle $\Gamma_0 \cup \Gamma_1$ for $p = 0$:

H3 $$W^u(\phi_1;0) \cap W^s(\phi_2;0) = \Gamma^0,$$

and

H4 $$W^u(\phi_2;0) \cap W^s(\phi_1;0) \supset \Gamma^1,$$

(see Figure 3.4). It is also assumed that $W^u(x_2;0)$ and $W^s(x_1;0)$ intersect transversally, i.e.,

H5 $$T_q W^u(x_2;0) + T_q W^s(x_1;0) = \mathbb{R}^3, \quad q \in \Gamma^1.$$

Hence we have

3 Corollary *For p small enough, there exists a one dimensional intersection of $W^u(x_2;p)$ and $W^s(x_1;p)$. This intersection will be denoted by $\Gamma^1(p)$.*

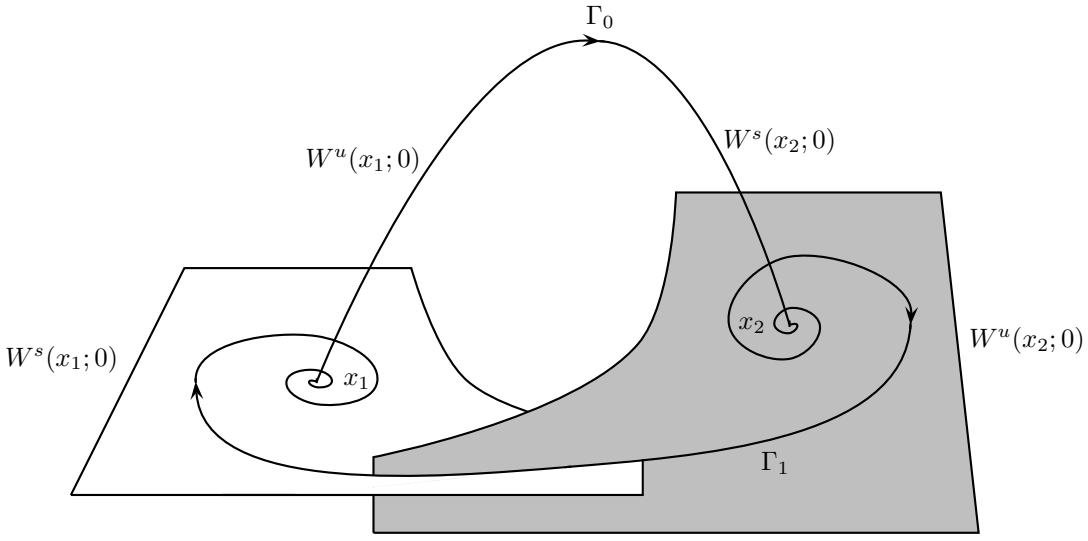

Figure 3.4: Heteroclinic cycle for $p = 0$

The intersection of $W^u(x_1;0)$ and $W^s(x_2;0)$ will in general not persist under perturbations. For small changes in the parameter p, $W^u(x_1;p)$ will still come close to the equilibrium ϕ_2. We will make one assumption on how this manifold depends on p. This will be a non-degeneracy condition formalising that p_1 and p_2 are really two different parameters. For this we need to introduce some notation.

We select a coordinate system around ϕ_2, such that locally the stable manifold of ϕ_2 is the z-axis and the unstable manifold is the (x,y)-plane ($\forall|p|<\delta_2$). We take a transverse intersection of the stable manifold

$$\Sigma = \{(x,y,z)|z=\sigma\}$$

At $p=0$, the unstable manifold of ϕ_1 will intersect Σ at $(0,0,\sigma)$ (see Figure 3.5). We choose δ_2 small enough such that for $|p|<\delta_2$ the unstable manifold of ϕ_1 intersects Σ for the first time at the point $I(p)=(x_I(p),y_I(p),\sigma)$.

Let C_p be the set of parameter values for which there exist an orbit homoclinic to ϕ_1 and let $I(p)$ be the first intersection of $W^u(x_1;p)$ with Σ. If C_Σ denotes the intersection of the homoclinic orbits with Σ, then the relation between C_Σ and C_p is given by $C_p = I^{-1}\big(C_\Sigma\big)$. We assume $p \mapsto I(p)$ to be a bijection:

H6
$$\det \left[\begin{array}{cc} \frac{\partial x_I}{\partial p_1} & \frac{\partial y_I}{\partial p_1} \\ \frac{\partial x_I}{\partial p_2} & \frac{\partial y_I}{\partial p_2} \end{array}\right]\Bigg|_{p=0} \neq 0.$$

We want hypothesis H6 to be satisfied for all small $\sigma>0$. This can be reformulated in a more convenient way by using the solutions to the variation equations, where we

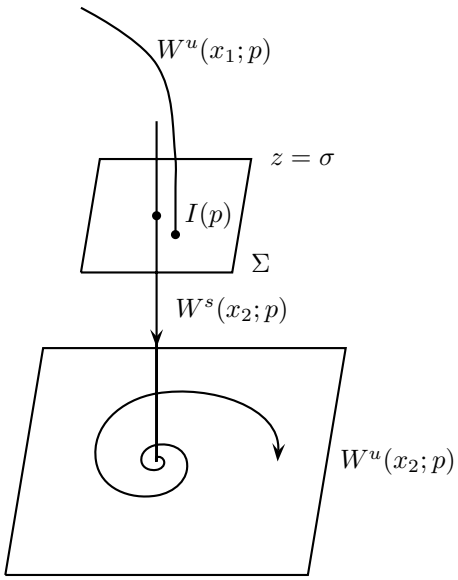

Figure 3.5: The flow near ϕ_2

consider variations around the special heteroclinic orbit Γ_0. We call ϕ_{p_1} the solution of the variation equation of (3.1.3) around Γ_0 for variations in p_1. So, ϕ_{p_1} is the solution to

$$\begin{cases} \dot{y}_1 = D_1 f\big(W^u(x_1;p),p\big)y_1 + \dfrac{\partial}{\partial p_1} f\big(W^u(x_1;p),p\big) \\ \lim\limits_{\xi\to-\infty} y_1(\xi) = \dfrac{\partial}{\partial p_1}\big(\phi_1(p)\big) \end{cases} \tag{3.6.1}$$

at $p = 0$.

Likewise we define ϕ_{p_2}. The solution of the variation equation for variations in time will be denoted by ϕ_t. Assumption H6 will hold if the solutions ϕ_{p_1}, ϕ_{p_2} and ϕ_t are linearly independent, close to the right hand equilibrium, i.e. if H6b holds, where

H6b
$$\lim_{\xi\to\infty} \det \underbrace{\begin{bmatrix}\phi_{p_1} & \phi_{p_2} & \phi_t\end{bmatrix}}_{B} \neq 0$$

If H6b is satisfied then it follows that H6 holds for σ sufficiently small.

Now we will formulate the theorem

4 Theorem *Under the assumptions H1–H5&H6b, there exists $\delta_2 > 0$ and a curve in parameter space $(p_1(\eta), p_2(\eta))$, defined for $|\eta| < \delta_2$ for which there exists an orbit homoclinic to ϕ_1. Furthermore this curve is a spiral.*

Proof:
It is convenient to use cylindrical coordinates. We choose a $\rho > 0$ small enough and a C^1-coordinate transformation such that for $r \le \rho$ and $z \le \sigma$, the system is locally given by

$$\begin{cases} \dot{r} = \mu r, \\ \dot{\theta} = \omega, \\ \dot{z} = -\lambda z. \end{cases} \tag{3.6.2}$$

In the present case C^1-linearisation is possible, see [35].

According to Lemma 3 there exists, for $|p|$ small enough, a connection $\Gamma^1(p)$, which intersects the cylinder $r = \rho$ at the position $Q = (\rho, \theta_0(p), 0)$. Since the intersection of $W^u(x_2;p)$ and $W^s(x_1;p)$ is transversal, there exists a function $\theta^s(z;p)$, such that the stable manifold of ϕ_1 contains the curve $C_1(z) = (\rho, \theta^s(z;p), z)$ for $|z|$ small enough (see Figure 3.6), and $\theta^s(z;p)$ is C^1 for small z and p.

We will now show that for certain values of p the unstable manifold of ϕ_1, intersecting Σ at $I(p) = (r_I(p), \theta_I(p), \sigma)$, (with $r_I < \rho$) will intersect this curve $C_1(z)$.

Because of H6 we can locally write $p(r_I, \theta_I)$.

The curve through $I(p(r_I, \theta_I))$ is for $t \ge 0$ parameterised by

$$\begin{cases} r = r_I e^{\mu t}, \\ \theta = \theta_I + \omega t, \\ z = \sigma e^{-\lambda t}. \end{cases} \tag{3.6.3}$$

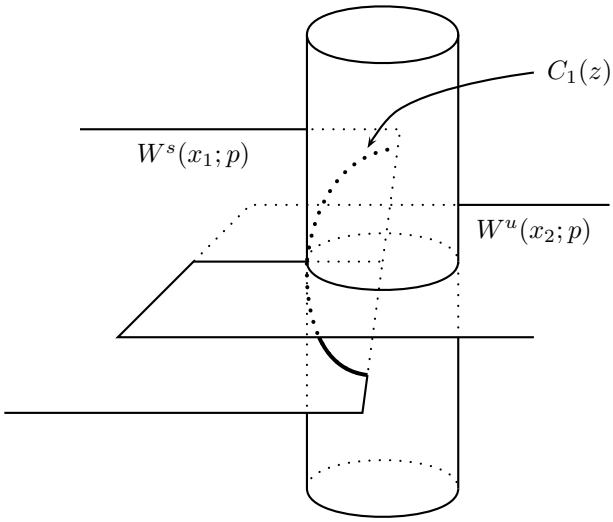

Figure 3.6: The curve C_1 is the intersection of $W^s(x_1;p)$ with a cylinder.

This curve will intersect the cylinder $r = \rho$ at a time

$$t = \frac{\ln \frac{\rho}{r_I}}{\mu} \tag{3.6.4}$$

so the intersection point will be $(\rho, \theta_I + \frac{\omega}{\mu} \ln \frac{\rho}{r_I}, \sigma \left(\frac{\rho}{r_I}\right)^{-\frac{\lambda}{\mu}})$.

Thus this curve will intersect the stable manifold of x_1 if it intersects the curve C_1, i.e.

$$\theta^s(\sigma \left(\frac{\rho}{r_I}\right)^{-\frac{\lambda}{\mu}}; p(r_I, \theta_I)) = \theta_I + \frac{\omega}{\mu} \ln \frac{\rho}{r_I} \mod 2\pi. \tag{3.6.5}$$

The left-hand side of this equation approaches a constant, say $\theta_0 = \theta^s(0;0)$, as $r_I \to 0$. Hence it is easily seen that the (r_I, θ_I) satisfying (3.6.5) form a spiral for small r_I, since we find that, with $\kappa = \min\{1, \frac{\lambda}{\mu}\} > 0$,

$$\theta_I = -\frac{\omega}{\mu} \ln \frac{\rho}{r_I} + \theta_0 + \mathcal{O}(r_I^\kappa) \qquad \text{as } r_I \to 0. \tag{3.6.6}$$

□

3.6.2 Verification of the assumptions

In this subsection we will verify that the system under consideration

$$\beta c \phi''' + (1 - c^2)\phi'' - \alpha c \phi' - \sin\phi + \gamma = 0, \tag{3.6.7}$$

satisfies the assumptions H1–H6b. We rewrite the equation to a system of first order equations

$$\begin{aligned}\phi' &= \psi,\\ \psi' &= \chi,\\ \chi' &= \frac{-(1-c^2)}{\beta c}\chi + \frac{\alpha}{\beta}\psi + \frac{\sin\phi - \gamma}{\beta c}.\end{aligned} \tag{3.6.8}$$

The first two assumptions H1 and H2 are easily checked. For $c = 1$ the equilibrium $\phi = \pi - \arcsin\gamma$ is a saddle-focus if

$$\gamma < \sqrt{1 - \frac{4}{27}\frac{\alpha^3}{\beta}}. \tag{3.6.9}$$

For the numerical values, chosen in figure 3.2, we obtain that $\gamma < 0.995$.

Of course the most difficult to check is the existence of the heteroclinic connection Γ^0. The major part of the present subsection will be dedicated to the proof (thanks to Jan-Bouwe v.d. Berg) of the existence of this connection. Since this is the intersection of two one-dimensional curves in three-dimensional space, such a connection is not to be expected, in general. However, for $c = 1$ the system has a symmetry (the system is reversible), this will help to proof the existence of this connection. The other assumptions will be checked numerically.

Existence of the heteroclinic connection

For $c = 1$ Equation (2.2.46) reduces (after rescaling) to

$$\phi''' - \tilde{\alpha}\phi' = \sin\phi - \gamma, \tag{3.6.10}$$

where $\tilde{\alpha} = \frac{\alpha}{\sqrt[3]{\beta}}$. For the rest of this section we will drop the tilde. This type of equation has been studied in [36]. However, we cannot simply refer to this paper because our right hand side is not sign definite.

The equilibria of (3.6.10) are given by

$$\phi_{2k} = 2k\pi + \arcsin\gamma, \quad \phi_{2k+1} = \pi - \arcsin\gamma + 2k\pi \tag{3.6.11}$$

Equation (3.6.10) is reversible and if $\phi(\xi)$ is a solution then so is $3\pi - \phi(-\xi)$. We will use these symmetries to prove the following result:

5 Theorem *There exists a constant α_0 such that for all $0 < \alpha \leq \alpha_0$ there exists, for some $\gamma \in (0,1)$, a monotone symmetric (with respect to $\frac{3\pi}{2}$) heteroclinic solution connecting ϕ_0 and ϕ_3. Furthermore, $\alpha_0 > 0.65$.*

The linearised equation around ϕ_0 has one positive eigenvalue λ, hence ϕ_0 has a one dimensional unstable manifold for all $\gamma \in [-1,1]$, which varies continuously with γ. We shoot, with γ as the shooting parameter, from this (local) unstable manifold, where we take the orbit in W^u_{loc} which initially increases. Thus, for some small $\varepsilon > 0$

let $\phi(\xi,\gamma)$ be the solution of (3.6.10) with $\phi(0,\gamma) = \phi_0 + \varepsilon$ and $(\phi,\phi',\phi'')(0,\gamma) \in W^u_{\rm loc}(\phi_0,0,0)$.

Since we are looking for a monotone solution, it will be very helpful to use the following formulation. On intervals on which ϕ is monotonically increasing we define

$$t = \phi, \qquad z(t) = \frac{1}{2}\phi'(\xi)^2 \tag{3.6.12}$$

Then $\dot z = \phi''$, where the dot denotes differentiation with respect to t. For the second derivative of z we find, using (3.6.10),

$$\ddot z = \alpha + \frac{\sin t - \gamma}{\sqrt{2z}}. \tag{3.6.13}$$

In the limit $\xi \to -\infty$, we find the initial value for the z-equation:

$$z(\phi_0) = 0, \quad \dot z(\phi_0) = 0, \quad \ddot z(\phi_0) = \lambda^2. \tag{3.6.14}$$

To set up the shooting method we define

$$\xi_1(\gamma) = \sup\{\tilde\xi \,|\, \phi''(\xi,\gamma) > 0 \text{ on } (-\infty,\tilde\xi)\}, \tag{3.6.15}$$

$$\xi_2(\gamma) = \sup\{\tilde\xi \,|\, \phi(\xi,\gamma) < \frac{3\pi}{2} \text{ on } (-\infty,\tilde\xi)\}. \tag{3.6.16}$$

Finally we define

$$\gamma_0 = \sup\{\gamma \in [-1,1] \,|\, \xi_1(\gamma) > \xi_2(\gamma)\}. \tag{3.6.17}$$

That γ_0 is well-defined follows from Lemma 6a below.

First we make some observations. Clearly $\phi'(\xi) > 0$ on $(-\infty,\xi_1]$. It follows from the implicit function theorem that $\xi_2(\gamma)$ depends continuously on γ for $\gamma \le \gamma_0$. Besides, ξ_2 is finite for $\gamma \le \gamma_0$, since ϕ is concave on $(-\infty,\xi]$.

We shall prove the following properties.

6 Lemma *With the above definition of γ_0 one has*
a. γ_0 is well-defined.
b. $\gamma_0 > 0$.
c. $\gamma_0 < 1$ for $0 < \alpha \le \alpha_0$, where $\alpha_0 \gtrapprox 0.65$.

This lemma will be proven in appendix 3.A to this chapter. Here, we will show how this leads to Theorem 5.

7 Lemma *For $\gamma = \gamma_0 \in (-1,1)$ one has $\xi_1 = \xi_2$.*

It follows that $\phi(\xi_1,\gamma_0) = \frac{3\pi}{2}$ and $\phi''(\xi_1,\gamma_0) = 0$, hence using the symmetry we have found for $\gamma = \gamma_0$ a heteroclinic solution as asserted in Theorem 5.

Proof of Lemma 7:
It follows from a continuity argument that $\xi_1(\gamma_0) \le \xi_2(\gamma_0)$. Now suppose, by contradiction, that $\xi_1 < \xi_2$ at γ_0. Then $\phi'(\xi_1) > 0$ and $\phi''(\xi_1) = 0$. From the definition

of ξ_1 we obtain that $\phi'''(\xi_1) \leq 0$ (since $\phi'' > 0$ in a left neighbourhood of ξ_1). From the definition of γ_0 we infer that $\phi'''(\xi_1) = 0$ since otherwise, by the implicit function theorem, $\xi_1 < \xi_2$ for $\gamma \in (\gamma_0 - \delta, \gamma_0)$ for some small positive δ, contradicting the definition of γ_0.

It follows from Equation (3.6.10) that

$$\sin\phi - \gamma = \phi''' - \alpha\phi' < 0, \qquad \text{at } \xi_1, \tag{3.6.18}$$

hence $\phi(\xi_1) \in (\phi_1, \frac{3\pi}{2}) \subset (\frac{\pi}{2}, \frac{3\pi}{2})$; recall that ϕ_1 is the second equilibrium. Differentiating (3.6.10) we obtain

$$\phi'''' = \alpha\phi'' + \phi'\cos\phi < 0, \qquad \text{at } \xi_1. \tag{3.6.19}$$

The fact that $\phi''''(\xi_1) < 0$ implies that $\phi'' < 0$ in a left neighbourhood of ξ_1, contradicting the definition of ξ_1. □

Transversality

Now we will indicate how the assumptions H4 and H5 were checked.

To calculate the intersection of the two manifolds, the calculation was set up as follows. First, using DSTOOL [12], we found a starting point, close to ϕ_2, which lies on a trajectory that passes close to the left hand equilibrium ϕ_1. A solution starting from this point was then used as an initial condition to a boundary value problem for AUTO. The solution was required to start in the unstable eigenspace of the equilibrium ϕ_2 and was calculated, until it hit the stable eigenspace of the equilibrium ϕ_1. In a further step the distance to both equilibria was decreased, hence the solution converged to the heteroclinic solution.

To check the transversality condition, we calculated the linear approximation to both manifolds and the angle θ_M between them. The linear approximation to one of these manifolds is spanned by the direction of the intersection and a solution to the variation equation.

Also in this case we did not directly calculate solutions to the variation equation, since we are only interested in the direction of the solution and these solutions will diverge rapidly. If the intersection is given by $q(\xi)$, the variation equation is given by

$$\dot{y} = Df(q(\xi))y. \tag{3.6.20}$$

We did not solve for y, but defined $v = \frac{y}{|y|}$, similar to what we did to check condition H6b. We calculated two solutions v_l and v_r to the variation equation, where $v_l(0)$ was required to be perpendicular to the intersection and to lie in the stable eigenspace of ϕ_1, whereas $v_r(1)$ was required to lie in the unstable eigenspace of ϕ_2 (time is rescaled so that $\xi = 1$ is the end-point). For every point ξ, the linear approximation to the unstable manifold of ϕ_2 is thus spanned by $\dot{q}(\xi)$ and $v_l(\xi)$. Hence we could calculate the angle θ_M made by the two manifolds at any point and hence check the transversality condition. The angle between the manifolds was always larger than 0.5 rad.

Bijection

Condition H6b was checked by calculating the determinant of the matrix B defined in H6b. However, we did not directly use the solutions to the variation equations. Near the equilibrium ϕ_2, both ϕ_c and ϕ_γ might increase exponentially, while ϕ_t will decrease exponentially (the determinant, however, will remain finite). We defined $\hat{\phi}_t = \frac{\phi_t}{|\phi_t|}$, which is the direction of ϕ_t and which must satisfy

$$\frac{d}{d\xi}\hat{\phi} = A(\xi)\hat{\phi} - \hat{\phi} < A(\xi)\hat{\phi}, \hat{\phi} >, \tag{3.6.21}$$

where $A(\xi) = Df(\Gamma^0(\xi))$ and the vector f represents the right hand side of (3.6.8). For ϕ_c and ϕ_γ we know the growth behaviour near ϕ_2 and define $\hat{\phi}_c = e^{-\lambda\xi}\phi_c$, where λ is the real part of the complex eigenvalues of ϕ_2, and we solve the equation for $\hat{\phi}_c$ instead of ϕ_c (and similarly for ϕ_γ).

In Figure 3.7 the determinant is plotted as a function of ξ (rescaled to lie in the interval [0,1]). The determinant is very small, since the three vectors are almost co-planar. However, as can be seen, the determinant does not vanish near the right hand equilibrium ($\xi \approx 1.0$). Near the right hand equilibrium, the determinant should be constant. In the figure it does not stay constant all the way, but this is caused by numerical errors (numerically the approach to the equilibrium is not *exactly* along the stable eigenvector).

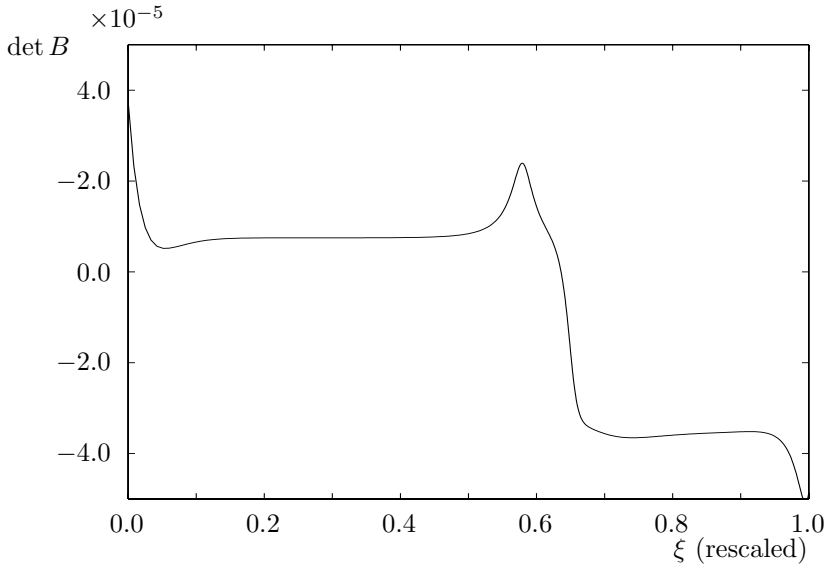

Figure 3.7: The determinant as a function of ξ.

3.7 Other configurations

So far we have only considered the case where there is a single fluxon in the junction. But much more is possible. The whole scala of solutions to expect (as far as travelling waves are concerned) is given by a theorem of Shil'nikov [20, section 6.3], if $\beta \neq 0$. If $\beta = 0$, then all dynamics is also known, since the equation is the driven and damped pendulum see [32].

In parameter-space, close to the heteroclinic orbit, there exist periodic orbits with a large period. These correspond to the existence of fluxon trains, i.e., an infinite number of fluxons with a fixed distance between them. Also 2-periodic solutions exist (or even n-periodic, for any n). This would be a train of "bunched" fluxons, or a solution with an infinite number of fluxons, where the distance between the two fluxons is alternating $\ldots, d_1, d_2, d_1, d_2, \ldots$. Both the d_1 and d_2 can be arbitrarily large. A direct consequence of this is that also a double homoclinic orbit exists, or a solution where there are two fluxons travelling along the junction with a fixed distance between them.

That all these solutions exist, is mainly caused by the β term. (This term forces the system to be three dimensional). *And* the fact that the equilibrium is a saddle-focus. For a saddle, the dynamics would not be so rich. Only single homoclinic orbits would exist.

Two fluxons give rise to a magnetic field pointing in the same direction and would in principle repel one another. The complex eigenvalues cause the solutions to have an oscillating tail. This tail will in the physical system be a wake where currents flow up and down after the fluxon. At certain distances these currents will give rise to a magnetic field, opposite to the one of a fluxon. At these positions a second fluxon could be placed and be trapped [22, 37]. A bunched fluxon state exists. It is interesting to notice the work of Sandstede [33], where he treats the stability of multiple-soliton solutions. His mathematical result, where the the solution of the adjoint equation should point in the "right" direction can be directly related to this physical argumentation.

3.A Proof of Lemma 6

In this section the proof to Lemma 6 will be given. We will first repeat the lemma here:

6 Lemma *With the above definition of γ_0 one has*
a. γ_0 is well-defined.
b. $\gamma_0 > 0$.
c. $\gamma_0 < 1$ for $0 < \alpha \leq \alpha_0$, where $\alpha_0 \gtrapprox 0.65$.

Proof of Lemma 6:
Part a. For $\gamma = -1$ it follows immediately from the z-equation (3.6.13) that $\ddot{z}(t) \geq 0$ for all $t > \phi_0$, hence $\phi''(\xi) > 0$ for all $\xi \in \mathbb{R}$.

Part b. Suppose, by contradiction, that $\gamma_0 \le 0$. Observe that $\phi_1 \ge \pi$, and from Lemma 7 we see that $\dot z(t) > 0$ on $(\phi_0, \frac{3\pi}{2})$. Since $\dot z(\frac{3\pi}{2}) = 0$ we have

$$0 = \int_{\phi_0}^{\frac{3\pi}{2}} \ddot z(t)dt = \int_{\substack{t\in[\phi_0,\frac{3\pi}{2}]\\ \ddot z>0}} \ddot z(t)dt - \int_{\substack{t\in[\phi_0,\frac{3\pi}{2}]\\ \ddot z<0}} |\ddot z(t)|dt. \tag{3.A.1}$$

On the one hand we conclude from the above observations that (we use the notation $(y)_+ \stackrel{\text{def}}{=} \max\{0, y\}$)

$$\begin{aligned}\int\limits_{\substack{t\in[\phi_0,\frac{3\pi}{2}]\\ \ddot z<0}} |\ddot z(t)|\,dt &\le \int_\pi^{\frac{3\pi}{2}} \Big(-\alpha - \frac{\sin t - \gamma_0}{\sqrt{2z(t)}}\Big)_+ dt \le \int_\pi^{\frac{3\pi}{2}} -\frac{\sin t}{\sqrt{2z(t)}}\,dt \\ &< \int_\pi^{\frac{3\pi}{2}} -\frac{\sin t}{\sqrt{2z(\pi)}}\,dt = \frac{1}{\sqrt{2z(\pi)}},\end{aligned} \tag{3.A.2}$$

while on the other hand

$$\begin{aligned}\int\limits_{\substack{t\in[\phi_0,\frac{3\pi}{2}]\\ \ddot z>0}} \ddot z(t)\,dt &\ge \int_{\frac{\pi}{2}}^{\pi} \alpha + \frac{\sin t - \gamma_0}{\sqrt{2z(t)}}\,dt \ge \int_{\frac{\pi}{2}}^{\pi} \frac{\sin t}{\sqrt{2z(t)}}\,dt \\ &> \int_{\frac{\pi}{2}}^{\pi} \frac{\sin t}{\sqrt{2z(\pi)}}\,dt = \frac{1}{\sqrt{2z(\pi)}}.\end{aligned} \tag{3.A.3}$$

These inequalities contradict Equation (3.A.1).

Part c. Suppose, by contradiction, that $\gamma_0 = 1$. Then

$$\dot z(t) \ge 0 \qquad \text{for } t \in [\frac{\pi}{2}, \frac{3\pi}{2}]. \tag{3.A.4}$$

Also, $\ddot z(t) = \alpha + \frac{\sin t - 1}{\sqrt{2z}} \le \alpha$ for $t \in (\frac{\pi}{2}, \frac{3\pi}{2}]$, from which we conclude that

$$z(t) \le \frac{\alpha}{2}(t - \tfrac{\pi}{2})^2. \tag{3.A.5}$$

Now we find that

$$\dot z(\tfrac{3\pi}{2}) = \int_{\frac{\pi}{2}}^{\frac{3\pi}{2}} \ddot z(t)\,dt \le \int_{\frac{\pi}{2}}^{\frac{3\pi}{2}} \alpha + \frac{\sin t - 1}{\sqrt{\alpha}(t - \frac{\pi}{2})}\,dt = \alpha\pi - \frac{C}{\sqrt{\alpha}}, \tag{3.A.6}$$

where

$$C \stackrel{\text{def}}{=} \int_{\frac{\pi}{2}}^{\frac{3\pi}{2}} \frac{\sin t - 1}{(t - \frac{\pi}{2})}\,dt = \int_0^\pi \frac{1 - \cos s}{s}\,ds. \tag{3.A.7}$$

Hence

$$\dot z(\tfrac{3\pi}{2}) < 0 \qquad \text{if} \quad \alpha\pi - \frac{C}{\sqrt{\alpha}} < 0, \text{ i.e. if } \alpha \le \alpha_0 \stackrel{\text{def}}{=} \Big(\frac{C}{\pi}\Big)^{1/3}, \tag{3.A.8}$$

contradicting (3.A.4). Notice that $\alpha_0 \stackrel{\text{def}}{=} (\frac{C}{\pi})^{1/3} \gtrapprox 0.65$. □

Chapter 4

Stability

In this section the linearised stability of the solution is investigated. The partial differential equation (2.2.46) is linearised around a (2π-kink) solution and we analyse the spectral problem. The essential spectrum lies in the left half-plane, for positive damping. To analyse the point spectrum we will make use of the Evans function formulation. For this part we will assume the surface resistance term (β) to be zero. For $\epsilon = 0$ we can explicitly calculate the Evans function and determine the point spectrum. We will analyse the Evans function in the neighbourhood of the point spectrum for ϵ small to determine whether eigenvalues will bifurcate from these points.

4.1 The spectral problem

The sine-Gordon equation

$$\Phi_{xx} - \Phi_{tt} - \sin\Phi = \epsilon(\alpha\Phi_t - \beta\Phi_{xxt} - \gamma) \tag{4.1.1}$$

admits a travelling wave solution ("fluxon solution")

$$\Phi_{x_0}(x,t) = 4\arctan(e^{\frac{x+ct+x_0}{\sqrt{1-c^2}}}) \tag{4.1.2}$$

for α, β, γ all equal to zero. The fluxon can move at any speed, up to $c = 1$. For non-zero values of these parameters, there will be a solution (see section 3.4) moving at a specific speed, so that the dissipation of energy (which dependents on the speed) is in balance with the energy input. We write the equation in a moving coordinate frame, making the transformation $\xi = \frac{x+ct}{\sqrt{1-c^2}}$. This gives the equation

$$\begin{aligned}\Phi_{\xi\xi} - \frac{2c}{\sqrt{1-c^2}}\Phi_{\xi t} - \Phi_{tt} - \sin\Phi = \\ \epsilon\left(\alpha\frac{c}{\sqrt{1-c^2}}\Phi_\xi + \alpha\Phi_t - \beta\frac{c}{(1-c^2)^{\frac{3}{2}}}\Phi_{\xi\xi\xi} - \frac{\beta}{1-c^2}\Phi_{\xi\xi t} - \gamma\right).\end{aligned} \tag{4.1.3}$$

We linearise around the travelling wave solution ϕ_ϵ, which was introduced in section 3.4. We assume $\Phi(\xi,t) = \phi_\epsilon + u(\xi,t)$, and retain the terms linear in u:

$$u_{\xi\xi} - \frac{2c}{\sqrt{1-c^2}}u_{\xi t} - u_{tt} - \cos(\phi_\epsilon)u = \epsilon\left(\alpha\frac{c}{\sqrt{1-c^2}}u_\xi + \alpha u_t - \beta\frac{c}{(1-c^2)^{\frac{3}{2}}}u_{\xi\xi\xi} - \frac{\beta}{1-c^2}u_{\xi\xi t}\right). \quad (4.1.4)$$

We now make the spectral Ansatz $u(\xi,t) = e^{\lambda t}v(\xi)$

$$v_{\xi\xi} - \frac{2c\lambda}{\sqrt{1-c^2}}v_\xi - \lambda^2 v - \cos(\phi_\epsilon)v = \epsilon\left(\alpha\frac{c}{\sqrt{1-c^2}}v_\xi + \lambda\alpha v - \beta\frac{c}{(1-c^2)^{\frac{3}{2}}}v_{\xi\xi\xi} - \frac{\beta\lambda}{1-c^2}v_{\xi\xi}\right). \quad (4.1.5)$$

We can rewrite this last equation in the form

$$\partial_\xi \begin{bmatrix} v \\ v_\xi \\ v_{\xi\xi} \end{bmatrix} = A(\xi,\lambda)\begin{bmatrix} v \\ v_\xi \\ v_{\xi\xi} \end{bmatrix} \quad (4.1.6)$$

where the operator A also depends on the problem parameters. Now the (linear) stability of the solution, around which we linearised, is determined by the spectrum of the operator $T(\lambda)$ defined by

$$T(\lambda) : u \to \frac{\mathrm{d}u}{\mathrm{d}\xi} - A(\xi,\lambda)u. \quad (4.1.7)$$

The spectrum of $T(\lambda)$ are those λ, for which $T(\lambda)$ is not invertible [13, 34]. The spectrum can contain isolated eigenvalues, these form the point spectrum. The complement of the spectrum is called the essential spectrum.

The point spectrum consists of those values of λ for which there exists an eigenfunction, so a solution to (4.1.5) that also satisfies the boundary conditions that $\lim_{\xi\to\pm\infty} v(\xi) = 0$. If the λ for which this solution exists has a real part larger than zero, this clearly gives rise to an instability.

Due to the translational invariance of the equation (4.1.1), reflected in the presence of the parameter x_0 in (4.1.2), there is an eigenvalue $\lambda = 0$, with eigenfunction $v(\xi) = \partial_\xi\phi_\epsilon(\xi)$.

The essential spectrum is related to the equilibria becoming unstable. If the essential spectrum crosses the imaginary axis (hence moving into the right half-plane) this manifests itself often by the appearance of small spatially periodic ripples on the asymptotic state (the state to which the solution convergence for $\xi \to \pm\infty$). If these ripples develop into a stable pattern, this is called a Turing pattern. To analyse the essential spectrum one needs to look only at the operator [13]

$$A_{\pm\infty}(\lambda) = \lim_{\xi\to\pm\infty} A(\xi,\lambda). \quad (4.1.8)$$

Note that this operator A_∞ depends on the value of the equilibrium to which the solution converges. For the 2π-kink solutions we are interested in, this means that $A_{-\infty} = A_\infty$, since this is a homoclinic orbit.

4.2 The essential spectrum

According to [13] the boundary of the essential spectrum is given by those λ for which there exist a solution to $v_\xi = A_\infty(\lambda)v$ of the form $v(\xi) = e^{i\kappa\xi}$, with κ real.

We formulated the spectral problem (4.1.5) in terms of $\xi = \frac{x+ct}{\sqrt{1-c^2}}$. This makes sence for the point spectrum, since the unperturbed solution is a function of ξ. Furthermore, we will restrict ourselves for small values of the perturbation, and hence to small values of c, for the point spectrum. However, for the essential spectrum we will use the transformation $\tilde{\xi} = x + ct$. The spectral problem can then be formulated as (dropping the tilde on ξ)

$$(1-c^2)v_{\xi\xi} - 2cv_{\xi\tau} - v_{\tau\tau} - \cos\big(\phi_\epsilon(\xi)\big)v = \epsilon\left(\alpha c v_\xi + \alpha v_\tau - \beta c v_{\xi\xi\xi} - \beta v_{\xi\xi\tau}\right) \quad (4.2.1)$$

For the solutions converging to the equilibrium $\phi = \arcsin\gamma$, the assumption $v(\xi) = e^{i\kappa\xi}$ leads to the equation

$$\lambda^2 + 2i\lambda c\kappa + \epsilon\alpha(ic\kappa + \lambda) + \epsilon\beta\kappa^2(ic\kappa + \lambda) + \kappa^2(1-c^2) + \sqrt{1-\epsilon^2\gamma^2} = 0 \quad (4.2.2)$$

We substitute $\lambda = \mu - ic\kappa$ and obtain the equation

$$\mu^2 + \left(\epsilon\alpha + \epsilon\beta\kappa^2\right)\mu + \kappa^2 + \sqrt{1-\epsilon^2\gamma^2} = 0 \quad (4.2.3)$$

which is an equation with real coefficients. Since the left hand side is a convex parabola $p(\mu)$, for which it holds that $p(0) > 0$, and $p'(0) > 0$, it is easy to see that there are no solutions to (4.2.3) with the real part of μ positive. The solutions for μ, with κ as parameter are plotted in figure 4.1 The μ values that solve the equation are a half-line starting from $(-\frac{1}{\epsilon\beta}, 0)$ extending into the left half-plane and a part of the circle with centre $(-\frac{1}{\epsilon\beta}, 0)$ and radius almost equal to $\frac{1}{\epsilon\beta}$. We will denote the imaginary part of μ at the edge of the essential spectrum by ω_ϵ, so

$$\omega_\epsilon = \sqrt{\sqrt{1-\epsilon^2\gamma^2} - \frac{\epsilon^2\alpha^2}{4}} \quad (4.2.4)$$

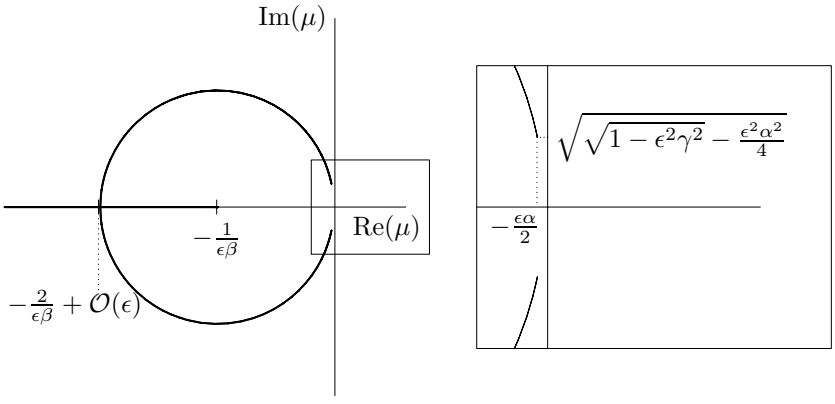

Figure 4.1: The μ satisfying relation (4.2.3).

Since in the equation for μ all coefficients only depend on κ^2, all depicted branches are double, i.e. solutions for μ exist both for a positive and for a negative value of κ. Since we defined $\lambda = \mu - ic\kappa$, we can find the solutions for λ by taking the solutions for μ and subtracting $ic\kappa$. In this way the double branches will separate for λ. A picture of the solutions for λ is given in figure 4.2.

Solutions converging to $\phi = \arcsin\gamma$, can be stable. We cannot conclude that they are stable, before we analyse the point spectrum. The other equilibrium ($\phi = \pi - \arcsin\gamma$) is unstable. Solutions converging to this equilibrium can never be stable, since part of the essential spectrum lies in the right half-plane. For solutions converging to this state, the equation (4.2.3) becomes

$$\mu^2 + \left(\epsilon\alpha + \epsilon\beta\kappa^2\right)\mu + \kappa^2 - \sqrt{1-\epsilon^2\gamma^2} = 0. \tag{4.2.5}$$

A sketch of the solutions to this equation is given in figure 4.3. From the equation (4.2.5) it is obvious that for $\kappa = 0$, there exists a solution to this equation, with μ real and positive. Hence solutions converging to this equilibrium are always unstable.

4.3 The Evans function

In the following sections we will analyse the point spectrum for the operator $A(\xi, \lambda)$. The point spectrum consists of eigenvalues, so, in contrast to the essential spectrum, there must be eigenfunctions solving the equation (4.1.5), also satisfying the boundary conditions

$$\lim_{\xi\to\pm\infty} v(\xi) = 0. \tag{4.3.1}$$

In the limit $\xi \to \pm\infty$, the operator $A(\xi, \lambda)$ is a constant operator $A_\infty(\lambda)$. This means that a solution $v(\xi)$ to the linearised equation, under the conditions (4.3.1 will be an intersection of the unstable and stable manifold of the equilibrium $v = 0$. So we need

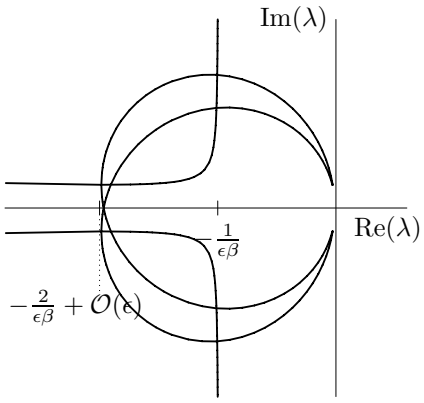

Figure 4.2: The boundary of the essential spectrum.

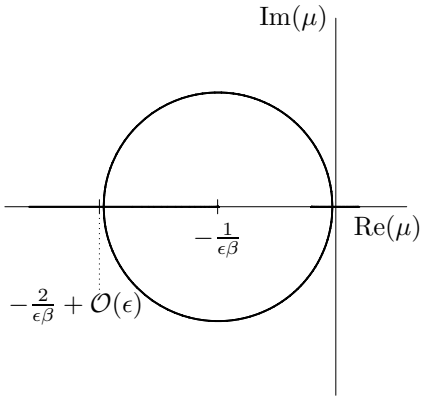

Figure 4.3: The μ satisfying relation (4.2.5). There are solutions with positive real part.

to find for what values of λ these manifolds intersect. This is exactly what can be determined by using the Evans function.

The Evans function as will be used here can be defined for a system in $\mathbb{R}^n$, that depends on a parameter λ. The system is assumed to have two equilibria $u_0(\lambda)$ and $u_1(\lambda)$ (not necessarily different!). It can be used to proof the existence of bounded solutions $U(\xi,\lambda)$ for a certain value of λ with the property that

$$\begin{aligned}\lim_{\xi\to\infty} U(\xi,\lambda) &= u_0(\lambda),\\ \lim_{\xi\to\infty} U(\xi,\lambda) &= u_1(\lambda).\end{aligned} \tag{4.3.2}$$

We assume that the equilibrium u_0 has m eigenvalues with positive real part and the equilibrium u_1 has $n-m$ eigenvalues with negative real part. There are m independent solutions U_i^- satisfying the boundary condition $\lim_{\xi\to-\infty} U(\xi) = u_0$, and $n-m$ solutions U_i^+ satisfying the boundary condition $\lim_{\xi\to\infty} U(\xi) = u_1$. Now we define the Evans function as

$$D(\lambda) = e^{-\int_0^\xi \operatorname{tr}(A(x,\lambda))\mathrm{d}x}\left(U_1^+\wedge\cdots\wedge U_m^+\wedge U_1^-\wedge\cdots\wedge U_{n-m}^-\right)(\xi,\lambda) \tag{4.3.3}$$

If this function $D(\lambda)$ is zero, it means that the manifold spanned by the U^+ intersect the manifold spanned by the U^-, and hence that there exists a solution satisfying both boundary conditions. The exponential factor in front makes the definition of $D(\lambda)$ independent of ξ as a consequence of Liouville's theorem. In the present case the equilibria u_0 and u_1 are both equal to 0.

In the literature several ways to use this Evans function can be found. It is in general not possible to explicitly calculate the Evans function. This is why most of the time the analysis revolves around getting information about this Evans function in two limiting cases. In some cases one can prove the existence of real positive eigenvalues using information for λ close to 0 and for $\lambda\to\infty$. See e.g. [15].

Restricting to travelling wave solutions of autonomous equations, the Evans function for $\lambda = 0$ is always zero, since the derivative of a travelling wave solves the linearised

equation. If the derivative of the Evans function at $\lambda = 0$ is negative and for $\lambda \to \infty$ ($\lambda \in \mathbb{R}$) the Evans function is positive, it must have had a zero in between, so there must be an eigenvalue with positive real part. Note that in this way only *in*stability can be proven. Stability results are often a lot more involved. If the derivative is positive and the Evans function is positive for λ large, this only means that there are an even number of eigenvalues, not necessarily that there are none. Furthermore, one should also take care of possible complex eigenvalues, with positive real part. So one would need to get some information about, e.g., the number of zeros in the right half-plane by integrating around a proper contour, or get information on the Evans function for specific values of λ.

Sometimes it is be possible to get an explicit expression for the Evans function for specific values of the parameters and do some perturbation analysis [16]. In our case, this is possible if we choose $\beta = 0$, since in the work of Mann [23], solutions to the linearised equations have been given and for $\epsilon = 0$, we can calculate the Evans function. The problem with $\beta \neq 0$ is that in that case we have a singularly perturbed problem, for $\epsilon = 0$ we are looking for bounded solutions in a two dimensional space, whereas for $\epsilon \neq 0$, the solutions lie in the $\mathbb{R}^3$. Here, we will treat the system with $\beta = 0$. This β term is the term originating from the resistance experienced by quasi-particles flowing along the surface of the superconductors. This term is normally quite small, but has some important influence as for example in the case of bunching of fluxons [10, 11].

4.4 Analysis with zero surface resistance

With $\beta = 0$, the essential spectrum is a lot simpler (see figure 4.4). It consists of two half-lines, and clearly lies completely in the left half-plane for $\epsilon > 0$. For $\epsilon = 0$, it lies on the imaginary axis.

The edge of the essential spectrum lies at $(\frac{-\epsilon\alpha}{2}, \pm\omega_\epsilon)$, see figure 4.4.

The perturbed equation with $\beta = 0$ is given by

$$\Phi_{xx} - \Phi_{tt} - \sin\Phi = \epsilon(\alpha\Phi_t - \gamma) \tag{4.4.1}$$

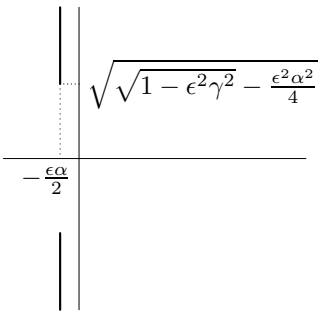

Figure 4.4: The essential spectrum for $\beta = 0$

The linearised equation becomes

$$v_{\xi\xi} = \left(\frac{2\lambda c}{\sqrt{1-c^2}} + \epsilon \frac{\alpha c}{\sqrt{1-c^2}} \right) v_\xi + \left(\lambda^2 + \cos\phi_\epsilon + \epsilon\alpha\lambda \right) v \tag{4.4.2}$$

This can be written as a system of first order equations

$$U_\xi = A(\xi, \lambda, \epsilon) U \tag{4.4.3}$$

where

$$A(\xi, \lambda, \epsilon) = \begin{bmatrix} 0 & 1 \\ \lambda^2 + \cos\phi_\epsilon + \epsilon\alpha\lambda & \frac{2\lambda c}{\sqrt{1-c^2}} + \frac{\epsilon\alpha c}{\sqrt{1-c^2}} \end{bmatrix} \tag{4.4.4}$$

Now, as was indicated in section 4.3, we need to determine whether there is a bounded solution on $\mathbb{R}$. We analyse the system at $\xi = \infty$. The system at infinity $A_\infty(\lambda, \epsilon) = \lim_{\xi\to\infty} A(\xi, \lambda, \epsilon)$, has for $\Re(\lambda) > -\frac{\epsilon\alpha}{2}$, exactly one eigenvalue with positive real part (μ_1) and one with a negative real part (μ_2). So there exist uniquely defined U^+ and U^-, as introduced in that section. For $\Re(\lambda) > -\frac{\epsilon}{2}$, we can use the definition of the Evans function as introduced in section 4.3.

For $|\Im\lambda| < i\omega_\epsilon$one can still use the same definition of the Evans function, since there still exist positive and negative eigenvalues and the associated eigenvectors. A problem occurs if the real part of the eigenvalues vanishes.

Now, if we choose λ in the right half-plane and let it cross the essential spectrum, the eigenvalues μ_1 and μ_2, become purely imaginary for λ in the essential spectrum and change role for λ left of the essential spectrum, i.e., the real part of μ_1 becomes negative and the real part of μ_2 becomes positive. In [16] it has been worked out in detail, how to extend the definition of the Evans function across the essential spectrum. Basically, one takes the analytical extension of the eigenvectors and in this way extend the definition of U^+ and U^-, although for $\lambda \leq 0$, it does not hold anymore that U^+ is exponentially decreasing for $\xi \to \infty$.

A sketch of the eigenvalues in the complex plane for different values of λ is given in figure 4.5. From this picture one can see that the definitions of U^+ and U^- (μ_1 and μ_2) will contradict, if one follows the eigenvalues along the two paths Γ_1 and Γ_2, indicated in the picture.

Along path Γ_1, an eigenvalue starting in the left half-plane would cross the imaginary axis and then move into the right half-plane. Along the path Γ_2, this same eigenvalue would approach the real axis and the move away from it again, all the time staying in the left half-plane.

We need to define cuts in the complex plane to avoid this problem. We will choose these cuts to be the half-lines $\{\lambda \in \mathbb{C} | \Im(\lambda) = \pm i\omega_\epsilon, \Re(\lambda) \leq -\frac{\epsilon\alpha}{2}\}$, indicated with a dashed line in figure 4.5.

As mentioned at the start of this section, for $\epsilon = 0$, we can explicitly write down an expression for the Evans function.

7 Lemma *When $\epsilon = 0$ the Evans function is explicitly given by the relation*

$$D(\lambda, 0) = \frac{2\lambda^2}{1-c^2} \frac{\sqrt{\lambda^2 + 1 - c^2}}{\sqrt{1-c^2}} \tag{4.4.5}$$

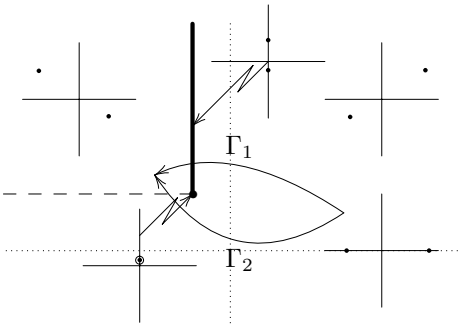

Figure 4.5: The location of the eigenvalues as a function of λ. The large picture is the complex λ-plane. The insets give the position of the eigenvalues of A_∞. The position of the insets shows for which λ values one would find the eigenvalues at these positions.

Proof:
In [23] solutions to the linearised sine-Gordon equation have been given, which can be used to define U^+ and U^-. More explicitly we define

$$U^+(\xi,\lambda,0) = e^{(b_1-b_2)\xi}\begin{bmatrix} b_2+\tanh\xi \\ (b_1-b_2)(b_2+\tanh\xi)+\operatorname{sech}^2\xi \end{bmatrix} \tag{4.4.6}$$

$$U^-(\xi,\lambda,0) = e^{(b_1+b_2)\xi}\begin{bmatrix} b_2-\tanh\xi \\ (b_1+b_2)(b_2-\tanh\xi)-\operatorname{sech}^2\xi) \end{bmatrix} \tag{4.4.7}$$

where,

$$b_1 = \frac{\lambda c}{\sqrt{1-c^2}} \tag{4.4.8}$$

$$b_2 = \frac{\sqrt{\lambda+i\sqrt{1-c^2}}\sqrt{\lambda-i\sqrt{1-c^2}}}{\sqrt{1-c^2}} \tag{4.4.9}$$

In this last equation the square-root is defined as

$$\sqrt{z} = \sqrt{|z|}e^{i\frac{\arg(z)}{2}}, \qquad -\pi < \arg(z) \leq \pi \tag{4.4.10}$$

to incorporate explicitly the cuts in the complex plane.

We have defined U^+ and U_- in such a way that for $\lambda = 0$, they both coincide with the eigenfunction for $\lambda = 0$.

Now, it is a simple matter to substitute these expressions in the formula for $D(\lambda,\epsilon)$. We have

$$\int_0^\xi \operatorname{tr}(A(s,\lambda,0))\mathrm{d}s = \frac{2c\lambda\xi}{\sqrt{1-c^2}} = 2b_1\xi. \tag{4.4.11}$$

Furthermore,

$$U^+(\xi)\wedge U^-(\xi) = 2b_2(b_2^2-1)e^{2b_1\xi}, \tag{4.4.12}$$

thus, the Evans function is given by

$$D(\lambda, 0) = 2b_2(b_2^2 - 1) = \frac{2\lambda^2}{1-c^2}\frac{\sqrt{\lambda^2 + 1 - c^2}}{\sqrt{1-c^2}} \tag{4.4.13}$$

□

From this explicit formula we find the solutions of $D(\lambda, 0) = 0$ to be $\lambda = 0$ (double) and $\lambda = \pm i\sqrt{1-c^2}$. One of the eigenvalues in 0 is, due to the translation invariance of the travelling kink solution. The derivative of the kink, is a solution to the linearised equation. The two zeros of the Evans function at $\pm i\sqrt{1-c^2}$ are not eigenvalues, since there is no eigenfunction satisfying the boundary conditions for these values of λ. This is because the zero of the Evans function lies at the edge of the essential spectrum. Nevertheless, eigenvalues might bifurcate from these points. Around $\lambda = 0$, there is a double eigenvalue and the series expansion of the Evans function looks like

$$D(\lambda, 0) = 2\frac{\lambda^2}{1-c^2} + \mathcal{O}(\lambda^4). \tag{4.4.14}$$

For large values of lambda, the Evans function behaves like

$$D(\lambda, 0) = \mathcal{O}(\lambda^3). \tag{4.4.15}$$

So, eigenvalues cannot bifurcate from ∞.

Here, we have an explicit expression for the Evans function, and hence can calculate the zeros explicitly. If this would not be the case, and we would only have the expressions (4.4.14) and (4.4.15), we could not conclude anything about the (in)stability. Now we know that the solution is (marginally) stable.

4.5 Analysis of the Evans function around $\lambda = 0$.

If $\epsilon \neq 0$, we cannot expect to be able to find an explicit expression for the Evans function. However, given the expression for $\epsilon = 0$, we can analyse whether zeroes move into the right half-plane.

In this section we will proof the following result.

8 Lemma *For the Evans function near $\lambda = 0$ it holds that*

1. $D(0, \epsilon) = 0$,
2. $\frac{\partial}{\partial\lambda} D(0, \epsilon) = \epsilon\alpha \int_{-\infty}^{\infty} e^{\frac{c\epsilon}{\sqrt{1-c^2}}\xi} \left((\phi_\epsilon)_\xi\right)^2 \mathrm{d}\xi$.

This implies that for $\epsilon > 0$, there will be a single eigenvalue at $\lambda = 0$ and that the other eigenvalue will move into the left half-plane. To see this, we need to use that $D(\lambda, 0)$ behaves as $\frac{2\lambda^2}{1-c^2}$ for λ close to 0. For ϵ small, $D(\lambda, \epsilon)$ will be a shifted parabola, with a zero in $\lambda = 0$. Since the derivative of $D(\lambda, \epsilon)$ with respect to λ is positive, the parabola has shifted to the left and down, the other zero, hence, lies in the left half-plane.

Before we turn to the proof of this lemma, we will first prove a lemma that will be of general use in calculations on the Evans function.

9 Lemma *Let the equation*

$$\frac{\partial}{\partial\xi}U(\xi,\nu)=A(\xi,\nu)U(\xi,\nu) \tag{4.5.1}$$

have two solutions $U_1(\xi,\nu)$ and $U_2(\xi,\nu)$, for which it holds that $\lim_{\xi\to-\infty}W(\xi,\nu)=W^-(\nu)$ exists, where

$$W(\xi,\nu)=e^{-\int_0^\xi \operatorname{tr}\left(A(s,\nu)\right)\mathrm{d}s}\left(\frac{\partial}{\partial\nu}U_1(\xi,\nu)\wedge U_2(\xi,\nu)\right). \tag{4.5.2}$$

Then $W(\xi,\nu)$ can be rewritten to

$$W(\xi,\nu)==W^-(\nu)+\int_{-\infty}^{\xi}e^{-\int_0^\tau \operatorname{tr}\left(A(s,\nu)\right)\mathrm{d}s}\left(\frac{\partial}{\partial\nu}A(\tau,\nu)U_1(\tau,\nu)\wedge U_2(\tau,\nu)\right)\mathrm{d}\tau. \tag{4.5.3}$$

Proof:
We differentiate (4.5.2) with respect to ξ

$$\begin{aligned}\frac{\partial}{\partial\xi}W(\xi,\nu)=&-\operatorname{tr}\big(A(\xi,\nu)\big)e^{-\int_0^\xi \operatorname{tr}\left(A(s,\nu)\right)\mathrm{d}s}\left(\frac{\partial}{\partial\nu}U_1\wedge U_2\right)(\xi,\nu)+\\&+e^{-\int_0^\xi \operatorname{tr}\left(A(s,\nu)\right)\mathrm{d}s}\left(\frac{\partial^2}{\partial\nu\partial\xi}U_1\wedge U_2\right)(\xi,\nu)+\\&e^{-\int_0^\xi \operatorname{tr}\left(A(s,\nu)\right)\mathrm{d}s}\left(\frac{\partial}{\partial\nu}U_1\wedge\frac{\partial}{\partial\xi}U_2\right)(\xi,\nu)\end{aligned} \tag{4.5.4}$$

Since U_1 satisfies the differential equation (4.5.1), we have that

$$\frac{\partial}{\partial\nu}\frac{\partial}{\partial\xi}U_1(\xi,\nu)=\frac{\partial}{\partial\nu}A(\xi,\nu)U_1(\xi,\nu)+A(\xi,\nu)\frac{\partial}{\partial\nu}U_1(\xi,\nu). \tag{4.5.5}$$

Using this relation and the fact that U_2 satisfies the same equation, we can rewrite (4.5.4) to

$$\begin{aligned}\frac{\partial}{\partial\xi}W(\xi,\nu)&=e^{-\int_0^\xi \operatorname{tr}\left(A(s,\nu)\right)\mathrm{d}s}\Big(-\operatorname{tr}(A)\frac{\partial}{\partial\nu}U_1\wedge U_2+\\&\qquad+A\frac{\partial}{\partial\nu}U_1\wedge U_2+\frac{\partial}{\partial\nu}U_1\wedge AU_2\Big)(\xi,\nu)+\\&\qquad+e^{-\int_0^\xi \operatorname{tr}\left(A(s,\nu)\right)\mathrm{d}s}\left(\frac{\partial}{\partial\nu}AU_1\wedge U_2\right)(\xi,\nu)\\&\qquad=e^{-\int_0^\xi \operatorname{tr}\left(A(s,\nu)\right)\mathrm{d}s}\left(\frac{\partial}{\partial\nu}AU_1\wedge U_2\right)(\xi,\nu),\end{aligned} \tag{4.5.6}$$

where the last equality follows from the fact that for any two vectors U_1 and U_2 and for any matrix A we have that $AU_1\wedge U_2+U_1\wedge AU_2=\operatorname{tr}(A)U_1\wedge U_2$ (see e.g., [3]). The expression (4.5.3) now follows by integrating this last expression and using $\lim_{\xi\to-\infty}W(\xi,\nu)=W^-(\nu)$. □

10 Remark

1. *This lemma can also be used in case* $\lim_{\xi\to\infty} W(\xi,\nu)$ *exists. A similar relation for* W *can be obtained integrating from* $+\infty$ *to* ξ.
2. *This lemma will be particularly useful for the case that* $\lim_{\xi\to\pm\infty} W(\xi,\nu) = 0$.

Proof of Lemma 8:
We define $V^\epsilon(\xi) = \big((\phi_\epsilon)_\xi, (\phi_\epsilon)_{\xi\xi}\big)^T$. Due to the definition of U^+ and U^-, we have $U^+(\xi,0,\epsilon) = U^-(\xi,0,\epsilon) = V^\epsilon(\xi)$. This implies that $D(0,\epsilon) = 0$.

To find the sign of the Evans function, for λ close to 0, we calculate the derivative of the Evans function with respect to λ and evaluate at $\lambda = 0$.

$$\begin{aligned}\frac{\partial}{\partial\lambda}D(0,\epsilon) &= -e^{-\int_0^\xi \operatorname{tr}\left(A(s,0,\epsilon)\right)\mathrm{d}s}\operatorname{tr}\big(A(\xi,0,\epsilon)\big)\big(U^+\wedge U^-\big)(\xi,0,\epsilon)+\\ &\quad + e^{-\int_0^\xi \operatorname{tr}\left(A(s,0,\epsilon)\right)\mathrm{d}s}\left(\frac{\partial}{\partial\lambda}U^+\wedge U^- + U^+\wedge\frac{\partial}{\partial\lambda}U^-\right)(\xi,0,\epsilon)\\ &= e^{-\int_0^\xi \operatorname{tr}\left(A(s,0,\epsilon)\right)\mathrm{d}s}\left(\frac{\partial}{\partial\lambda}U^+\wedge U^- - \frac{\partial}{\partial\lambda}U^-\wedge U^+\right)(\xi,0,\epsilon) \qquad (4.5.7)\\ &\overset{\text{Lemma 9}}{=} \int_\infty^\xi e^{-\int_0^\xi \operatorname{tr}\left(A(s,0,\epsilon)\right)\mathrm{d}s}\left(\frac{\partial}{\partial\lambda}AU^+\wedge U^-\right)(\xi,0,\epsilon)\mathrm{d}\xi+\\ &\quad -\int_{-\infty}^\xi e^{-\int_0^\xi \operatorname{tr}\left(A(s,0,\epsilon)\right)\mathrm{d}s}\left(\frac{\partial}{\partial\lambda}AU^-\wedge U^+\right)(\xi,0,\epsilon)\mathrm{d}\xi\end{aligned}$$

Now, since $U^\pm(\xi,0,\epsilon) = V^\epsilon(\xi)$, and

$$\frac{\partial}{\partial\lambda}A(\xi,\lambda,\epsilon) = \begin{bmatrix} 0 & 0\\ 2\lambda+\alpha\epsilon & \frac{2c}{\sqrt{1-c^2}}\end{bmatrix}, \qquad (4.5.8)$$

we have that

$$\begin{aligned}\frac{\partial}{\partial\lambda}D(0,\epsilon) = \int_\infty^{-\infty}\begin{bmatrix}0 & 0\\ \epsilon\alpha & \frac{2c}{\sqrt{1-c^2}}\end{bmatrix}\begin{bmatrix}(\phi_\epsilon)_\xi\\ (\phi_\epsilon)_{\xi\xi}\end{bmatrix}\wedge\begin{bmatrix}(\phi_\epsilon)_\xi\\ (\phi_\epsilon)_{\xi\xi}\end{bmatrix}\mathrm{d}\xi =\\ \alpha\epsilon\int_{-\infty}^\infty e^{-\frac{c\epsilon\alpha\xi}{\sqrt{1-c^2}}}\big((\phi_\epsilon)_\xi\big)^2\mathrm{d}\xi > 0\end{aligned} \qquad (4.5.9)$$

□

4.6 Analysis of the Evans function around the points $\lambda = \pm i\sqrt{1-c^2}$

Apart from having an eigenvalue bifurcate from the origin into the right half-plane, instability can also be caused by eigenvalues that bifurcate from the edge of the essential spectrum into the right half-plane, as the unperturbed Evans function vanishes there.

In this section we will analyse the Evans function for λ close to $i\sqrt{1-c^2}$ (the case $\lambda = -i\sqrt{1-c^2}$ is similar) and ϵ close to 0.

The edge of the essential spectrum (the point at which A_∞ has a double eigenvalue) is located at

$$\lambda = i\sqrt{1-c^2} - \frac{\epsilon\alpha}{2} + \tilde{\lambda}(\epsilon), \tag{4.6.1}$$

where

$$\tilde{\lambda}(\epsilon) = i\sqrt{1-c^2}\left(\sqrt{\sqrt{1-\epsilon^2\gamma^2} - \tfrac{\epsilon^2\alpha^2}{4}} - 1\right). \tag{4.6.2}$$

Since this point will move into the left half-plane, we will define a new parameter $\sigma = \lambda + \frac{\epsilon\alpha}{2} - \tilde{\lambda}(\epsilon)$. We define

$$\hat{A}(\xi,\sigma,\epsilon) = A(\xi,\lambda,\epsilon), \tag{4.6.3}$$

$$\hat{D}(\sigma,\epsilon) = D(\lambda,\epsilon), \text{ and} \tag{4.6.4}$$

$$\hat{A}_\infty(\sigma,\epsilon) = \lim_{\xi\to\pm\infty} \hat{A}(\xi,\sigma,\epsilon) \tag{4.6.5}$$

Now $\hat{A}_\infty$ has an eigenvalue at $\sigma = \sigma_0 = i\sqrt{1-c^2}$ of algebraic multiplicity 2 and geometric multiplicity 1, independent of ϵ. The eigenvalue is given by

$$\mu(\epsilon) = ic\sqrt{\sqrt{1-\epsilon^2\gamma^2} - \frac{\epsilon^2\alpha^2}{4}}, \tag{4.6.6}$$

and we denote the eigenvector by $\eta(\epsilon) = \begin{bmatrix} 1 \\ \mu(\epsilon) \end{bmatrix}$.

We define our solutions $U^\pm(\xi,\epsilon)$ in the definition of the Evans function to be

$$U^\pm(\xi,\epsilon) = e^{\mu(\epsilon)\xi}\big(\eta(\epsilon) + w^\pm(\xi,\epsilon)\big), \tag{4.6.7}$$

where, $\lim_{\xi\to\pm\infty} w^\pm(\xi,\epsilon) = 0$. Both $U^\pm(\xi,\epsilon)$ are solutions to the equation

$$U_\xi = \hat{A}(\xi,\sigma_0,\epsilon)U. \tag{4.6.8}$$

Now we will show that the derivative of the Evans function $\hat{D}(\sigma,0)$ with respect to ϵ is zero for $\sigma = \sigma_0$. This means that, *up to order* ϵ no eigenvalues will bifurcate out of the essential spectrum. Since the essential spectrum moves into the left half-plane at a speed of $\mathcal{O}(\epsilon)$, and eigenvalues can only bifurcate out of the essential spectrum at a speed $\mathcal{O}(\epsilon^2)$, these eigenvalues will be in the left half-plane, *for sufficiently small* ϵ.

11 Lemma $\frac{\partial}{\partial\epsilon}\hat{D}(\sigma_0,0) = 0$.

Proof:
Again, we make use of the relation between derivatives of solutions with respect to parameters, and derivatives of the linearised equation, as given in Lemma 9.

$$\frac{\partial}{\partial\epsilon}\hat{D}(\sigma_0,0) = e^{-2\mu(0)\xi}\left(\frac{\partial}{\partial\epsilon}U^+ \wedge U^- + U^+ \wedge \frac{\partial}{\partial\epsilon}U^-\right)(\xi,\sigma_0,0) \tag{4.6.9}$$

$$\overset{\text{Lemma 9}}{=} \int_\infty^{-\infty} e^{-2\mu(0)\xi}\left(\frac{\partial}{\partial\epsilon}\hat{A}U \wedge U\right)(\xi,\sigma_0,0)\,d\xi \tag{4.6.10}$$

$$+ W^+(\sigma_0,0) - W^-(,\sigma_0,0) \tag{4.6.11}$$

where

$$W^{\pm}(\sigma_0, 0) = \lim_{\xi \to \pm\infty} e^{-2\mu(0)\xi} \left(\frac{\partial}{\partial \epsilon} U^{\pm} \wedge U^{\mp} \right) (\xi, \sigma_0, 0). \tag{4.6.12}$$

To use Lemma 9, we must still show that $W^{\pm}$ actually exist. We will show this for W^{+}.

Using that $\mu(\epsilon)$ and $\eta(\epsilon)$ are even functions of ϵ, it is a straightforward calculation to obtain

$$W^{+}(\sigma_0, 0) = \frac{\partial}{\partial \epsilon} w^{+}(\xi, 0) \wedge \big(\eta(0) + w^{-}(\xi, 0)\big) \tag{4.6.13}$$

Now $w^{+}(\xi, \epsilon)$ satisfies $\lim_{\xi \to \infty} w^{+}(\xi, \epsilon) = 0$. To show that W^{+} actually exists and is in fact equal to 0, we need to show that $w^{-}(\xi, 0)$ does not grow exponentially

It holds that $\hat{A}(\xi, \sigma_0, 0)$ in the equation for $U^{-}(\xi, 0)$ can be written as

$$\begin{aligned} \hat{A}(\xi, \sigma_0, 0) &= \begin{bmatrix} 0 & 1 \\ \big(\sigma_0 + \tilde{\lambda}(0)\big)^2 - \frac{\epsilon^2 \alpha^2}{4} + \cos\big(\phi_\epsilon(\xi)\big) & \frac{2c}{\sqrt{1-c^2}} \big(\sigma_0 + \tilde{\lambda}(0)\big) \end{bmatrix} \\ &= \underbrace{\begin{bmatrix} 0 & 1 \\ -\mu(0)^2 & 2\mu(0) \end{bmatrix}}_{A_\infty} + \underbrace{\begin{bmatrix} 0 & 0 \\ \cos\big(\phi_0(\xi)\big) - \sqrt{1 - \epsilon^2 \gamma^2} & 0 \end{bmatrix}}_{\tilde{A}} \end{aligned} \tag{4.6.14}$$

The equation for w^{-} is then given by

$$\partial_\xi w^{-} = \begin{bmatrix} -\mu & 1 \\ -\mu^2 & \mu \end{bmatrix} w^{-} + \tilde{A}\big(\eta(0) + w^{-}\big). \tag{4.6.15}$$

$\tilde{A}$ approaches the zero matrix exponentially fast, hence

$$W^{+} = \lim_{\xi \to \infty} \frac{\partial}{\partial \epsilon} w^{+} \wedge w^{-} = 0 \tag{4.6.16}$$

Now, it follows that

$$\frac{\partial}{\partial \epsilon} \hat{D}(\sigma_0, 0) = \int_{\infty}^{-\infty} e^{-2\mu(0)\xi} \left(\frac{\partial}{\partial \epsilon} \hat{A} U \wedge U \right) (\xi, \sigma_0, 0)\, d\xi. \tag{4.6.17}$$

As

$$\frac{\partial}{\partial \epsilon} \hat{A}(\xi, \sigma_0, 0) = \begin{bmatrix} 0 & 0 \\ -\sin(\phi_0(\xi)) z(\xi) & 0 \end{bmatrix}, \tag{4.6.18}$$

where $z(\xi) = \frac{\partial \phi_\epsilon(\xi)}{\partial \epsilon}\Big|_{\epsilon=0}$ this leads to the expression

$$\frac{\partial}{\partial \epsilon} \hat{D}(\sigma_0, 0) = \int_{\infty}^{-\infty} \sin(\phi_0(\xi)) z(\xi) \tanh^2(\xi)\, d\xi. \tag{4.6.19}$$

The integrand is odd, since $\sin(\phi_0)$ is odd, while $z(\xi) = \phi_1(\xi)$ is even, as was indicated in 3.4. So, the integral vanishes. This concludes the proof. □

Now we can formulate the stability result in a theorem.

12 Theorem *For sufficiently small ϵ the solution $\phi_\epsilon(x+ct)$ is a linearly stable solution to (4.1.1).*

Proof:
A linear instability would manifest itself by the essential spectrum, or a eigenvalue crossing the imaginary axis. The essential spectrum stays in the left half-plane, for all values of ϵ. The above analysis does not rule out that an eigenvalue bifurcates out of the essential spectrum and moves into the right half-plane, but if it does, it can only leave the essential spectrum at a speed of $\mathcal{O}(\epsilon^2)$. The essential spectrum itself, however moves into the left half-plane at a speed of $\mathcal{O}(\epsilon)$, so for small enough ϵ, all eigenvalues will be in the left half-plane. □

Chapter 5

Stacks of Josephson junctions

This chapter focuses on stacks of junctions. In chapter 2 we derived the equations for a stack of two junctions. In general the two junctions can have all parameters different. However, in this chapter we will mainly focus on what happens if the ratio of the critical currents J is not equal to 1. This seems to be the parameter that has the largest influence on the type of solutions to expect.

5.1 Rewriting the equations

Taking all parameters (except for the critical currents) equal, the equations for the travelling waves in the stack are given by

$$\begin{cases} (1-c^2)\ddot{\phi}^A - \sin\phi^A + \sigma\ddot{\phi}^B = \alpha c\dot{\phi}^A - \gamma, \\ (1-c^2)\ddot{\phi}^B - \dfrac{\sin\phi^B}{J} + \sigma\ddot{\phi}^A = \alpha c\dot{\phi}^B - \gamma. \end{cases} \tag{5.1.1}$$

For the calculations we will do, we need to rewrite the system as a first order system. We rewrite (5.1.1) in the form

$$\begin{cases} \dot{\phi^A} = \psi^A \\ \dot{\psi^A} = \dfrac{(1-c^2)\left(\sin\phi^A + \alpha c\psi^A - \gamma\right) + \sigma\left(\frac{\sin\phi^B}{J} + \alpha c\psi^B - \gamma\right)}{(1-c^2)^2 - \sigma^2} \\ \dot{\phi^B} = \psi^B \\ \dot{\psi^B} = \dfrac{(1-c^2)\left(\frac{\sin\phi^B}{J} + \alpha c\psi^B - \gamma\right) + \sigma\left(\sin\phi^A + \alpha c\psi^A - \gamma\right)}{(1-c^2)^2 - \sigma^2}. \end{cases} \tag{5.1.2}$$

When $J = 1$, the system has a Z_2-symmetry as it is equivariant with respect to

$$\eta = \begin{pmatrix} 0 & 0 & 1 & 0 \\ 0 & 0 & 0 & 1 \\ 1 & 0 & 0 & 0 \\ 0 & 1 & 0 & 0 \end{pmatrix}. \tag{5.1.3}$$

Equivariancy with respect to η means that $f(\eta x) = \eta f(x)$, so the differential equation does not change under the change of coordinates $x \to \eta x$. The fixed point space of η, i.e. all the points in $\mathbb{R}^4$ that are invariant under η, is an invariant subspace. On this subspace we have that $\phi^A = \phi^B$ and $\psi^A = \psi^B$, i.e. the junction behave identically.

When $\gamma = 0$ (and J arbitrary), the system has a different Z_2-symmetry, as it is equivariant with respect to

$$\tau = \begin{pmatrix} -1 & 0 & 0 & 0 \\ 0 & -1 & 0 & 0 \\ 0 & 0 & -1 & 0 \\ 0 & 0 & 0 & -1 \end{pmatrix}. \tag{5.1.4}$$

We will call solutions on the fixed point space of $\eta\tau$ anti-symmetric solutions. This requires both $J = 1$ and $\gamma = 0$.

To make these symmetries more apparent, we introduce the new variables $\phi^S = \frac{\phi^A + \phi^B}{2}$ and $\phi^D = \frac{\phi^A - \phi^B}{2}$ and rewrite the equations to

$$\begin{cases} (1 - c^2 + \sigma)\ddot{\phi}^S - \dfrac{\sin\phi^S \cos\phi^D (J+1) + \cos\phi^S \sin\phi^D (J-1)}{2J} = \alpha c \dot{\phi}^S - \gamma, \\ (1 - c^2 - \sigma)\ddot{\phi}^D - \dfrac{\sin\phi^S \cos\phi^D (J-1) + \cos\phi^S \sin\phi^D (J+1)}{2J} = \alpha c \dot{\phi}^D. \end{cases} \tag{5.1.5}$$

In the following section we will first look at the case of identical junctions ($J = 1$) and the symmetric and anti-symmetric solutions. For these cases we recover the equation for the single junction, with different parameter values.

The next section will be dedicated to the single fluxon case, when there is only one fluxon in one of the junctions. The junctions are still taken to be equal. This will prove to be a more interesting situation.

The last (and by far the largest) section of this chapter will be dedicated to a stack of unequal junctions.

5.2 Symmetric solutions

We take both junctions equal, hence equation (5.1.5) reduces to

$$\begin{cases} (1 - c^2 + \sigma)\ddot{\phi}^S - \sin\phi^S \cos\phi^D = \alpha c \dot{\phi}^S - \gamma, \\ (1 - c^2 - \sigma)\ddot{\phi}^D - \cos\phi^S \sin\phi^D = \alpha c \dot{\phi}^D. \end{cases} \tag{5.2.1}$$

If we take ϕ^S equal to zero (the anti-symmetric situation), the first equation reduces to $\gamma = 0$. This anti-symmetric solution can only exist for γ equal to zero. For the case where there is a fluxon in the one junction and an anti-fluxon in the other, this is easy to understand. Since the fluxon and anti-fluxon will be accelerated in opposite directions by the bias-current. The second equation reduces to the equation for the single junction (without β-term). This was discussed already in detail in chapter 3.

Notice, however, that the coefficient of $\ddot{\phi}^D$ is now $1 - c^2 - \sigma$. This means that the maximal velocity is not 1 but slightly lower and given by $c = \sqrt{1-\sigma}$.

The symmetric case ($\phi^D = 0$), reduces the second equation to a trivial one. Now, the first equation reduces to that of the equation for a single junction. The maximal velocity is now given by $c = \sqrt{1+\sigma}$. For the single junction case we had as maximal velocity $c = 1$, for the case of a stack of two junctions, in-phase and out-of-phase solutions have a different maximal velocity. We define

$$c_{\pm} = \sqrt{1 \pm \sigma} \tag{5.2.2}$$

5.3 Identical junctions with a single fluxon

We assume that junction A contains a fluxon, and junction B does not. For small values of the constants (α, β and γ), we can get a relation between the constants for which there exists a 2π-kink solution in the same way as done for the single junction.

We first take $J = 1$ and hence analyse (5.2.1). Of course, we could also use the original equations for ϕ^A and ϕ^B, but it will turn out to be advantageous to look at the equation for ϕ^S and ϕ^D, since in this case only one of the equations becomes singular for $c = c_+$ and the other becomes singular for $c = c_-$.

Using AUTO to calculate the solutions, we obtain the picture that is given in 5.1. For these calculations we chose $\sigma = 0.25$ and $\alpha = 0.18$. Also for this situation we see a spiral in the IV-curve. The pictures of the solutions for parameter combinations along this curve, show a large resemblance to those for the single junction. This indicates that a similar mechanism might be the cause of this spiral. However, in this case there is no "special" value of c or γ to which this curve converges. For the case of the single junction (see figure3.2), the centre of the spiral is located at $c = 1$, the value of c for which the system is reversible. In this case the centre of the spiral appears to lie in $c = 0.8620968$, which is a little below $c_- = 0.8660$.

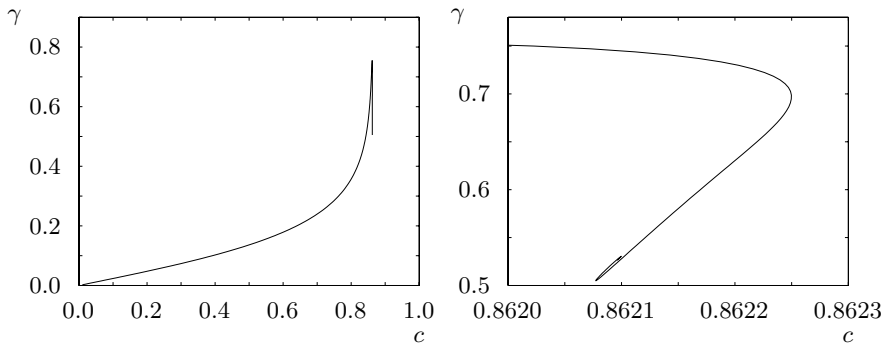

Figure 5.1: The IV-characteristic as calculated for a stack of junctions, which are identical. There is a single fluxon in one of the junctions.

What is more important, the present problem is a four-dimensional one. The key to analysing this problem along the same lines as that for the single junction, is reducing the problem to a three-dimensional invariant manifold. The velocity is close to the critical velocity c_-. For $c = c_-$, the dynamics is confined to a three dimensional invariant manifold. Applying singular perturbation theory, we find that for c close to this critical velocity there still exists a three dimensional invariant manifold close to the manifold for $c = c_-$. On this manifold one might do the same analysis as for the single junction. This is not persued here. We will indicate what should be done to prove the existence of the spiral in this case.

We define $\epsilon = 1 - \sigma - c^2$ and eliminate c from the equation (5.2.1). Written as a first order system, we get

$$\begin{cases} \dot{\phi}^S = \psi^S \\ (2\sigma + \epsilon)\dot{\psi}^S = \sin\phi^S \cos\phi^D + \alpha\sqrt{1-\sigma-\epsilon}\,\psi^S - \gamma \\ \dot{\phi}^D = \psi^D \\ \epsilon\dot{\psi}^D = \cos\phi^S \sin\phi^D + \alpha\sqrt{1-\sigma-\epsilon}\,\psi^D \end{cases} \tag{5.3.1}$$

For $\epsilon = 0$, the system reduces to a three-dimensional one. From the last equation we have

$$\psi^D = \frac{-\cos\phi^S \sin\phi^D}{\alpha\sqrt{1-\sigma}} \tag{5.3.2}$$

So, for $\epsilon = 0$, the dynamics is confined to the three dimensional manifold given by (5.3.2).

If $\epsilon \neq 0$, we can rescale the time in equation (5.3.1) to obtain an equation for the fast dynamics [14]:

$$\begin{cases} \dot{\phi}^S = \epsilon\psi^S \\ (2\sigma + \epsilon)\dot{\psi}^S = \epsilon\left(\sin\phi^S \cos\phi^D + \alpha\sqrt{1-\sigma-\epsilon}\psi^S - \gamma\right) \\ \dot{\phi}^D = \epsilon\psi^D \\ \dot{\psi}^D = \cos\phi^S \sin\phi^D + \alpha\sqrt{1-\sigma-\epsilon}\psi^D \end{cases} \tag{5.3.3}$$

For $\epsilon = 0$ this equation shows that the manifold is normally hyperbolic (it is repelling).

For ϵ small enough there exist a manifold $\mathcal{M}_\epsilon$ which is $\mathcal{O}(\epsilon)$-close to M_0. An expansion in ϵ can easily be given by substituting

$$\psi^D = \frac{-\cos\phi^S \sin\phi^D}{\alpha\sqrt{1-\sigma}} + \sum_{i=1}^{N} \epsilon^i \psi_i^D(\phi^S, \psi^S, \phi^D) + \mathcal{O}(\epsilon^{N+1}) \tag{5.3.4}$$

in (5.3.1) and solving for the coefficients of ϵ^i. For the parameter values used to calculate figure 5.1 we calculated the approximation of the manifold up the third order. It is not immediately clear that this series converges for those parameter values, so if the solution, as calculated with AUTO stays close to the manifold. To get an impression of this we check wether the ψ^D-component of the solution, obtained with AUTO, satisfies (5.3.4). We take a solution $(\phi^S(\xi), \psi^S(\xi), \phi^D(\xi), \psi^D(\xi))$, calculated

with AUTO. For this solution we can calculate ψ^D_{approx} (taking only the first few terms of (5.3.4) by substituting $\phi^S(\xi)$, $\psi^S(\xi)$ and $\phi^D(\xi)$ from the AUTO solution. The difference of this ψ^D_{approx} with the ψ^D from the AUTO calculation is shown in figure 5.2.

The ψ^D_i are of the form $\alpha^{-2i-1}(1-\sigma)^{-i-\frac{1}{2}}\hat{\Psi}_i(\phi^S, \psi^S, \phi^D)$ as can be seen by examining the equations obtained from the assumption (5.3.4). To be able to use theorem 4 we need to be able to reduce the system to a three dimensional one, at least for (c, γ) at the centre of the spiral, but also for a region around this centre. It is not a priori known that the velocity in the centre of the spiral can be made to approach c_- arbitrarily close, by choosing the parameters α and S.

To prove the existence of the spiral for this case, we would need to prove that all the assumptions that were made to prove theorem 4 are satisfied. The assumptions about the eigenvalues and dimension of the manifolds H1 and H2 are easily seen to be satisfied. The co-dimension zero part of the heteroclinic cycle H4 and the transversality thereof and H5, could be calculated in the same way as was done in chapter 3. Also the non-degeneracy condition on the parameters H6b can be shown to hold in the same way. The important assumption H3 will be difficult to prove and this will not be attempted here. Due to the fact that we cannot make use of any (reversibility) symmetry this will be very hard to prove.

5.4 Unequal junctions

An interesting situation occurs if the two junctions forming the stack, are not identical. We will focus here on the situation that all parameters, except for the critical current are equal. This means that the parameter J from equation (5.1.1) is not equal to 1. The other parameters have a less drastic influence on the dynamics.

Having $J > 1$ will show the "back bending" phenomenon, first mentioned in [9].

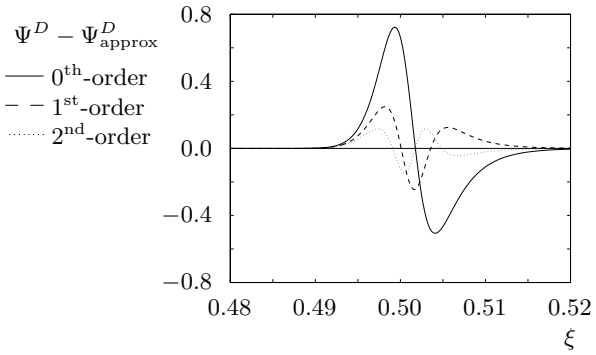

Figure 5.2: The convergence of the approximations to M_ϵ on increasing the order of the approximation

5.4.1 The case $J > 1$

In experiments and numerical calculations on the PDE for a stack of junctions, an interesting phenomenon has been observed. For $J > 1$ the IV-curve "bends" back, as shown in figure 5.3. This picture is the result of numerical computations on the partial differential equation. What happens is that the image of the fluxon in the "empty" junction, grows. Hence, the gradients increase drastically. The dissipation is proportional to $c\phi'$, so to balance the energy dissipation and the energy input, the velocity decreases. When the bias current is increased further, at a certain moment the stack switches to the resistive state with a much higher voltage across the stack.

That the velocity $c = c_-$ cannot be reached can be explained from singular perturbation theory. This argument has been used in [8], but without reference to singular perturbation theory. The second equation of (5.1.5) becomes singular for $c \to c_-$. For c equal to this velocity, there exists an invariant manifold given by

$$\sin\phi^S \cos\phi^D (J-1) + \cos\phi^S \sin\phi^D (J+1) + 2\alpha c J \psi^D = 0, \tag{5.4.1}$$

which can be written as

$$J \sin\phi^A = \sin\phi^B + 2J\alpha c(\psi^A - \psi^B) \tag{5.4.2}$$

If $\alpha = 0$, one can see that the case where there is a fluxon in junction A (which means that $\sin\phi^A$ runs over all values from -1 to 1) and no fluxon in ϕ^B, can only exist if $J < 1$.

To understand why the stack switches to the resistive state and how to model this phenomenon, one should know exactly what happens at the top. People have suggested [7] that the solution becomes unstable at that point. Another possibility would be that the solution ceases to exist for higher bias-currents. Using AUTO, we have been able to calculate the complete branch of solutions in figure 5.4. From this picture it is clear that the solution does not exist for values of the bias current above a certain threshold. The calculations of AUTO and the PDE-solver coincide nicely on the right half of the branch. Using the PDE-solver it is not possible to follow the solution "over the top" of the IV-curve. To do this one should operate the device in

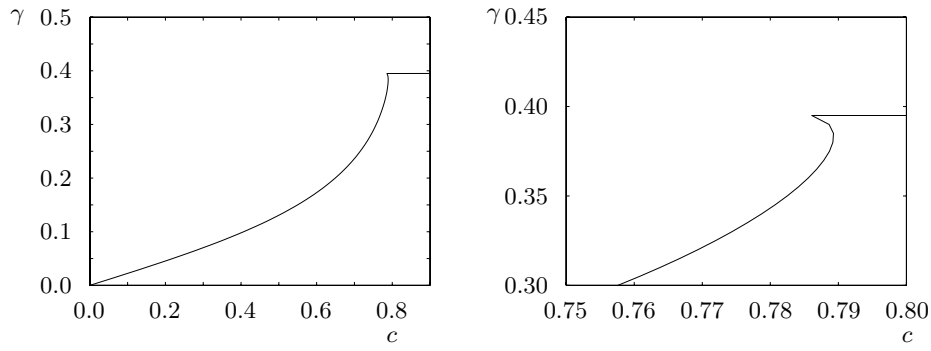

Figure 5.3: The IV-characteristic, calculated using the PDE-solver

the so-called voltage-bias mode, i.e. apply a certain voltage to the system and measure the current. This is in practice already difficult to do, but using this PDE-solver impossible, since the voltage is determined by an integral over the x-coordinate of the solution. One would need to handle this problem in a different way, numerically.

Using AUTO it is no problem to calculate the whole branch, since AUTO treats the two parameters c and γ in an equivalent manner.

Seeing two solutions with a different speed, but for the same bias current, raises the question what would be the difference between these two solutions, and of course whether the solutions on the left branch could be observed in experiments and what properties they would have.

In figure 5.5 two solutions for the same value of γ (0.17) are plotted. In junction A (the one containing the fluxon) there is hardly any change. However, in junction B there is a big difference. On the right branch there is only a small "image" in junction B, of the fluxon in junction A. On the left branch, this disturbance has grown to a large peak. If one would continue to decrease γ on the left branch, this peak will first become higher, reaching its maximum value of 2π and then broaden. In the limit $\gamma = 0$, there will be a fluxon in junction A and a fluxon/anti-fluxon pair in junction B. The fluxon in junction A and the anti-fluxon in junction B will be at the same position in the stack, while the fluxon in junction B will be as far away as possible.

That the distance between the fluxon and anti-fluxon increases, may be understood by the fact that the fluxon and the anti-fluxon attract each other. The driving γ induces a Lorenz force on the fluxon and anti-fluxon, pushing the two away from one another. To maintain a balance between these two forces, the fluxon and anti-fluxon have to be at a larger distance, if the driving is less.

Stability

Having found these solutions, the most important question is whether these are stable. If this is the case, it would be interesting to get some experimental confirmation of these calculations.

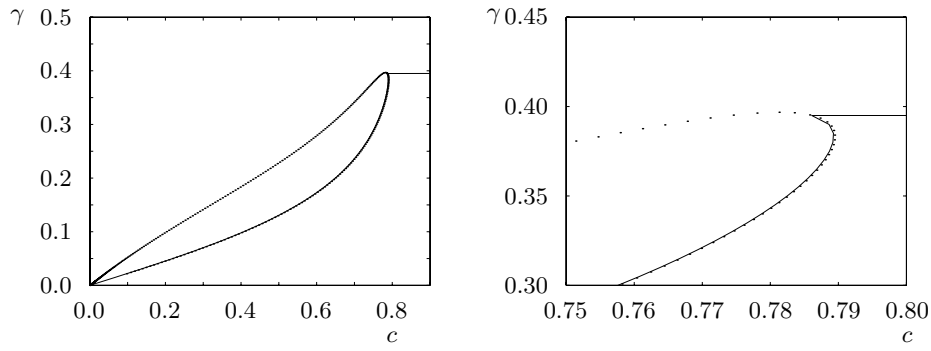

Figure 5.4: Comparison of the results of the PDE-solver and AUTO.

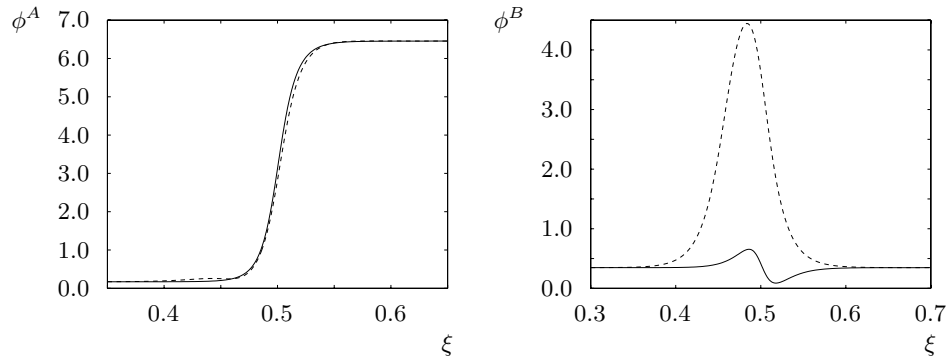

Figure 5.5: Comparison of two solutions to (5.1.5) for $J = 2$ and $\gamma = 0.17$ on the left and right branch.

To test the stability, we took the solution, as calculated with AUTO and used this as initial solution to the PDE-solver. The results of this simulation show that the solution on the left branch is unstable.

That the solutions near $\gamma = 0$ are unstable is quite clear, since the distance between the fluxon and anti-fluxon is determined by a balance of forces. The attracting force depends on the distance between the fluxon and anti-fluxon, while the Lorenz force is not. If the distance would increase or decrease slightly, the balance is destroyed. If the distance decreases the attracting force will become stronger and they would approach each other and annihilated. If the distance increases, the attracting force becomes smaller and they would move away. For γ values near the top the analysis is much more involved, since the solution in junction B cannot be approximated very well as a fluxon/anti-fluxon pair. However, attempts have been made [7] to explain the shape of the IV-characteristic near the top, using the assumption that also there the solution for ϕ^B can be approximated by a fluxon/anti-fluxon pair.

It seems that the left branch of solutions forms a sort of separatrix. We use a solution on the left branch as initial solution to the PDE-solver. After some time this either develops into a situation where there is a fluxon/anti-fluxon pair, or it approaches the solution on the right branch. Starting from the solution for $\gamma = 0.48$, the profile develops into the solution of the right-hand branch. The solid curve in figure 5.6 is the L^2-norm of the difference between $\Phi(x,t)$ and $\phi_{\text{right}}(x+ct)$, where $\Phi(x,t)$ is the solution that is calculated using the PDE-solver and $\phi_{\text{right}}(x+ct)$ is the solution on the right branch, calculated with AUTO. To be able to compare the shape of the solutions (although $\Phi(x,t)$ moves at a different speed than ϕ_{right}), we first shift the solutions, so that the maximum value of $\Phi^A_x(x,t)$ and $\dot{\phi}^A(x+ct)$ are assumed at the same position. Since there is only a single fluxon in junction A there will be a clearly defined peak. Then the L^2-norm is calculated.

Starting from $\gamma = 0.4$, the solution calculated with the PDE-solver, develops into a situation where there is a fluxon/anti-fluxon pair in junction B. The fluxons move in the same direction, and the anti-fluxon moves in the other direction.If we start from the solution on the left branch for $\gamma = 0.4$, but use $\gamma = 0.399$ in the PDE-solver,

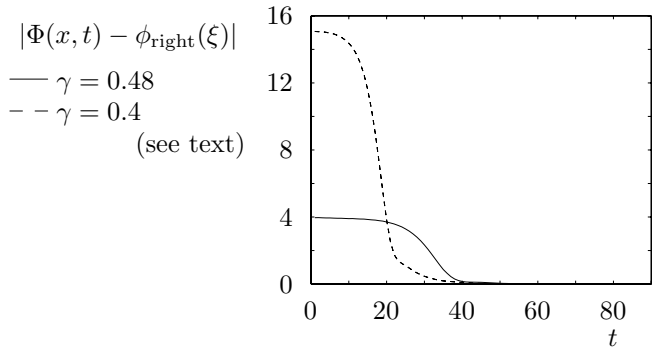

Figure 5.6: The L^2-norm for the difference of the solution $\Phi(x,t)$ calculated with the PDE-solver and the solution ϕ_{right}, on the right branch of the (c,γ)-graph calculated with AUTO.

the solution actually goes to the solution on the right branch. The L^2-norm for this calculation is represented by the dashed line in figure 5.6.

Slope in the IV-characteristic

Analogously to what we have done for the single junction, we can also calculate an approximation to the IV-characteristic for the stack case. Again we make use of the exponential dichotomy and the projections on the stable and unstable manifolds. We now scale α, β, γ and σ with ϵ. The equations for the travelling wave are now given by

$$\begin{cases} \ddot{\phi}^A - \sin\phi^A = \epsilon\left(\dfrac{\alpha c\dot{\phi}^A}{\sqrt{1-c^2}} - \gamma - \sigma\ddot{\phi}^B\right) \\ \ddot{\phi}^B - \dfrac{\sin\phi^B}{J} = \epsilon\left(\dfrac{\alpha c\dot{\phi}^B}{\sqrt{1-c^2}} - \gamma - \sigma\ddot{\phi}^A\right) \end{cases} \tag{5.4.3}$$

For the lower branch the unperturbed solution is given by

$$\begin{cases} \phi_0^A(\xi) = 4\arctan(e^\xi) \\ \phi_0^B(\xi) = 0 \end{cases} \tag{5.4.4}$$

Just as in the single junction case we can try to find a series expansion for $\phi^A = \phi_0^A + \epsilon\phi_1^A + \dots$ and similarly for ϕ^B. Theorem 1 immediately generalises to four dimensions. Just as in the single junction case we define $U_1 = (\phi_1^A - \gamma\ \psi_1^A\ \phi_1^B - \gamma\ \psi_1^B)^T$. Where the γ's are subtracted to have the solution go to zero for $\xi \to \pm\infty$, so that the right hand side goes to zero, which was one of the conditions for theorem 1 to hold. The equations for U_1 is given by

$$\frac{\mathrm{d}}{\mathrm{d}\xi}U_1 = A(\xi)U_1 + G(\xi) \tag{5.4.5}$$

where

$$A(\xi) = \begin{bmatrix} 0 & 1 & 0 & 0 \\ \cos(\phi_0^A(\xi)) & 0 & 0 & 0 \\ 0 & 0 & 0 & 1 \\ 0 & 0 & \frac{\cos(\phi_0^B(\xi))}{J} & 0 \end{bmatrix} \tag{5.4.6}$$

and

$$G(\xi) = \begin{bmatrix} 0 \\ \frac{\alpha c}{\sqrt{1-c^2}}\dot{\phi}_0^A - \gamma - \frac{\sigma}{1-c^2}\ddot{\phi}_0^B + \gamma\cos\phi_0^A \\ 0 \\ \frac{\alpha c}{\sqrt{1-c^2}}\dot{\phi}_0^B - \gamma - \frac{\sigma}{1-c^2}\ddot{\phi}_0^A + \gamma\cos\phi_0^B \end{bmatrix}. \tag{5.4.7}$$

A solution to the homogeneous equation is given by

$$X = \begin{bmatrix} \operatorname{sech}(\xi) & \frac{1}{2}(\xi\operatorname{sech}(\xi) + \sinh(\xi)) & 0 & 0 \\ (\operatorname{sech}(\xi))' & \frac{1}{2}(\xi\operatorname{sech}(\xi) + \sinh(\xi))' & 0 & 0 \\ 0 & 0 & e^{-\xi/\sqrt{J}} & e^{\xi/\sqrt{J}} \\ 0 & 0 & -e^{-\xi/\sqrt{J}} & e^{\xi/\sqrt{J}} \end{bmatrix} \tag{5.4.8}$$

The projection P^u is in this case given by

$$P^u = \begin{bmatrix} 0 & 0 & 0 & 0 \\ 0 & 1 & 0 & 0 \\ 0 & 0 & 0 & 0 \\ 0 & 0 & 0 & 1 \end{bmatrix}. \tag{5.4.9}$$

In this case the projection $\hat{P}^s$ is not the same as P^u:

$$\hat{P}^s = \begin{bmatrix} 0 & 0 & 0 & 0 \\ 0 & 1 & 0 & 0 \\ 0 & 0 & 1 & 0 \\ 0 & 0 & 0 & 0 \end{bmatrix}. \tag{5.4.10}$$

Now, since the first component of both $P^s U_1^+(0)$ and $\hat{P}^u U_1^-(0)$ are zero, the condition that $U_1^+(\xi)$ and $U_1^-(\xi)$ match at $\xi = 0$ will give a single necessary condition for existence of a bounded solution on $\mathbb{R}$.

The solvability condition requires in this case

$$\Big\{ 4\sqrt(1-c^2)\alpha c - \gamma\pi + \gamma\pi c^2 = 0 \tag{5.4.11}$$

This equation is the same as for the single junction. Hence, the slope in the IV-characteristic will be independent of σ, for σ small enough.

This same relation can also be obtained by using the "adiabatic perturbation" method. The unperturbed system is a Hamiltonian system with Hamiltonian

$$H = \int_{-\infty}^{\infty} \left(\frac{1}{2}(\Phi_x^T)^2 + \frac{1}{2}(\Phi_x^B)^2 + \frac{1}{2}(\Phi_t^T)^2 + \frac{1}{2}(\Phi_t^B)^2 + 2 - \cos\Phi^T - \frac{\cos\Phi^B}{J} + \sigma\Phi_x^T\Phi_x^B \right) \mathrm{d}x \quad (5.4.12)$$

Calculating $\frac{\mathrm{d}H}{\mathrm{d}t}$ as was done in 3.4 for the single junction case, we obtain

$$\frac{\mathrm{d}H}{\mathrm{d}t} = \int_{-\infty}^{\infty} \alpha(\Phi_t^T)^2 - \gamma\Phi_t^T + (\alpha\Phi_t^B)^2 - \gamma\Phi_t^B \mathrm{d}x \quad (5.4.13)$$

For the unperturbed solution on the lower branch we use

$$\begin{cases} \Phi^T(x,t) = 4\arctan(e^{\frac{x+ct}{\sqrt{1-c^2}}}) \\ \Phi^B(x,t) = 0 \end{cases} \quad (5.4.14)$$

resulting in the same relation (5.4.11).

On the upper branch the solution can be approximated (as motivated by the AUTO calculations) by

$$\begin{cases} \Phi^T(x,t) = 4\arctan(e^{\frac{x+ct}{\sqrt{1-c^2}}}) \\ \Phi^B(x,t) = 4\arctan(e^{\frac{x+ct+L}{\sqrt{1-c^2}}}) - 4\arctan(e^{\frac{x+ct}{\sqrt{1-c^2}}}) \end{cases} \quad (5.4.15)$$

Substituting this in the expression for $\frac{\mathrm{d}H}{\mathrm{d}t}$ and requiring this to be zero, gives the relation (for $L \to \infty$):

$$12\sqrt{1-c^2}\alpha c - \gamma\pi + \gamma\pi c^2 = 0 \quad (5.4.16)$$

This agrees very well with the numerically obtained values.

5.5 Numerical experiments

So far, only the situation where there is a single fluxon in one of the junctions (junction A) and "only" an image in the other (junction B) has been discussed. Bifurcating from this solution, we have already seen solutions where junction B, contains a fluxon/anti-fluxon pair. We have seen numerical experiments indicating that those types of solutions are in fact unstable. A generalisation of the Evans function to the stack case, seems promising, but is not within the scope of this thesis.

However, some results are presented here that may be interesting as a starting point to investigate in a more analytical way. Often there is already some idea about the physics behind the (in)stability and this might lead to ideas to treat the mathematical problem.

First we take the situation of the in-phase solution. For the case of two identical junctions the existence of the solutions reduces to the existence problem of solutions for a single junction. There is evidence that for velocities below c_-, these solutions are unstable [10]. This may seem not surprising, since both fluxons have the same polarity and will repel each other. In figure 5.7, the velocities of the two fluxons is shown. They start at the same position and travelling at the same velocity. After perturbing this situation (at $t = 100$), the fluxons move away, and take up positions at maximal distance (eventually, not in picture). If one starts from a situation, where the velocity is larger than c_-, however, the in-phase solution is stable. It would be interesting to get a better understanding of this.

For junction which are not equal, however, the in-phase solution will be unstable (assuming the γ's for both junction to be identical). The driving force on the one fluxon is larger than the force on the other one and they will split up. Using the PDE-solver this situation has been investigated, and one can indeed see that the fluxon in the junction with the higher critical current (junction B in equation 5.1.2, with J=0.5) has a lower velocity than the fluxon in junction A. Since the program uses periodic boundary conditions, the fluxon in junction B will approach the other fluxon from behind after some time, and will try to pass the other fluxon. In figure 5.8 a picture is given of the velocities of the two fluxons in the two junctions.

Both fluxons have the same polarity and will repel each other. If the fast-moving fluxon approaches the other one, it will slow down because of this. The other fluxon will be pushed by the faster fluxon and speed up itself. If the bias current is not too high a stable configuration can be formed where both fluxons move with the same velocity, although the parameters for both junctions are different.

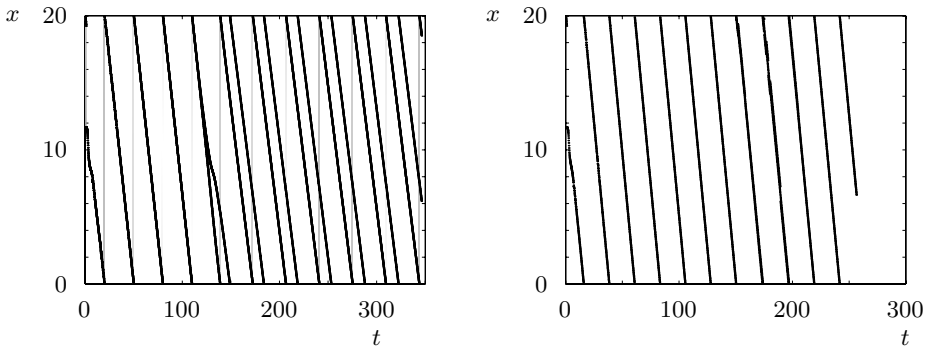

(a) Position of the two fluxons, starting from a situation where they are at the same position. $\gamma = 0.17$ and the velocity is at the start equal to $c = 0.668 < c_-$.

(b) The same situation, but now using $\gamma = 0.3$, which causes the initial velocity to be $c = 0.893 > c_-$.

Figure 5.7: Graphs showing the position of the fluxons in the separate junctions as a function of time.

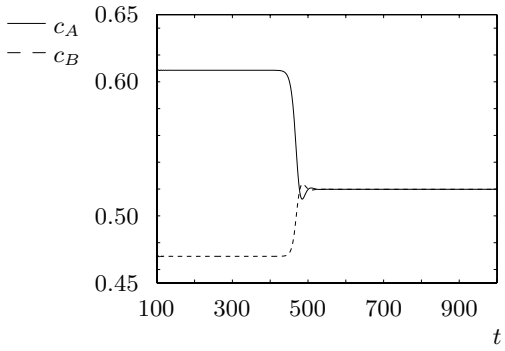

Figure 5.8: A plot of the velocity of the fluxon in junction A (—) and the one in junction B (- -).

5.A The PDE-solver

In this appendix we will discuss the main aspects of the program that was used to simulate the partial differential equation.

5.A.1 The numerical scheme

Since the problem is only one-dimensional in space and one-dimensional in time, it is not very difficult to obtain a numerical scheme. Time is not a very important issue, so we did not strive for the most optimal scheme, but rather resortet to a simple treatment where space and time are separated. The equation can be written in the form

$$\partial_t \Phi = \mathcal{F}(\Phi). \tag{5.A.1}$$

where $\mathcal{F}$ is an operator, containing only derivatives in space. This enables us to discretize the right-hand side independent from the left-hand side. The problem then transforms to an integration in time and we use the Runge-Kutta-4 scheme.

For the equation (2.3.1), we have that

$$\Phi = \begin{bmatrix} \Phi^A \\ \Psi^A \\ \Phi^B \\ \Psi^B \end{bmatrix} \qquad \mathcal{F} = \begin{bmatrix} \Psi^A \\ \Phi^A_{xx} - \sin\Phi^A - S\Phi^B_{xx} - \alpha\Psi^A - \gamma \\ \Psi^B \\ \Phi^B_{xx} - \frac{\sin\Phi^B}{J} - S\Phi^A_{xx} - \alpha\Psi^B - \gamma \end{bmatrix}. \tag{5.A.2}$$

To simulate the infinitely long junction, we used periodic boundary conditions with a sufficiently large period (of the order of 10 times the size of a fluxon) such that the interaction of the fluxon with itself can be neglected. The second derivatives in space are calculated using a central scheme on three points.

Chapter 6

Conclusions and recommendations

The treatment of long Josephson junctions in this thesis is necessarily incomplete. Some important phenomena have been discussed. Effort has been taken to derive a model, based on a discrete electrical analogue, that is as complete as possible. For the single junction this gives no new results, only a confirmation of the existing model, including the β-term. For a stack of junctions, however, our analysis shows two new terms that may be important.

We analysed the existence part for the single fluxon case for the single junction completely. The spiral in (c, γ)-parameter space has been analysed. The linearised stability problem for $\beta = 0$ has been considered.

For a stack of two junctions, we restricted to two different situations. The case of two identical junctions is reduced to the problem of a single junction, by restricting to in- or out-of-phase solutions. For non-identical junctions we investigated the situation where "backbending" occurs.

6.1 Modelling

The aim of chapter 2 was to give an overview of different models that have been proposed and to derive a slightly more general model. For the single long junction there seems to be agreement on the "correct" model. The model as given in equation (2.2.46)

$$\Phi_{xx} - \Phi_{tt} - \sin\Phi = \alpha\Phi_t - \beta\Phi_{xxt} - \gamma \tag{6.1.1}$$

seems to be the model that describes the observed phenomena to a high degree of accuracy.

It was noted in the chapter that actually this β-term is just an approximation. In fact also the quasi-particle current gives rise to a magnetic field, and hence an inductor included in series with the resistor would seem a necessary extension. The fact that

the model works so well is, that for not too high temperatures, the resistance will be very high, and consequently the current through the resistor is very small and the addition of the inductor will not have a large effect on the system. Mathematically this can be analysed using singular perturbation theory.

The higher-order terms which are introduced by taking an impedance in series with the resistor all contain factors β^n, with $n \geq 2$.

The derivation of the equations for a stack of long junctions shows that a direct generalization of the model for the single long junction, gives rise to some additional terms, not included in any previous model the author is aware of. For the single junction, it turned out that the surface impedance of the outer and inner layer could be combined in one effective impedance. One can extend this idea to a stack of junctions and combine the surface impedance on the outer and inner layer into one effective impedance. This is what has been done in section 2.3.3. To model the coupling, this effective impedance should, of course, be taken at the inner surface. A drawback of this is that the current that flows along the outer surface is treated in the same way as the one flowing along the inner surface, although the coupling between currents flowing along the outer surface would be negligible.

The model derived in 2.3 shows some new terms, which are of comparable order of magnitude as the β-term. In this thesis these have not been investigated, but one should get at least get some idea of their importance. Possibly these terms give rise to new dynamics, or influence the stability of the solutions.

6.2 Single long junction

For the single long junction the point to start the investigation in this thesis, is the observed spiral in parameter space (figure 3.2(b)). The fact that at the centre of this spiral the velocity has the special value $c = 1$, and the fact that the system is reversible for this value of c, seems to be important.

The existence of this spiral is a result of the existence of a heteroclinic cycle connecting two equilibria, and the fact that one of these equilibria is a saddle-focus. This heteroclinic cycle consists of a co-dimension two heteroclinic connection and a connection of co-dimension zero. The special value of c is related to the existence of this co-dimension two connection. For $c = 1$ and some value of $\gamma^\star$ that depends on α and β there exists a monotonic connection between the two equilibria. The one-dimensional manifold of the one equilibrium intersects the one-dimensional manifold of the other equilibrium.

It is important to note that the value $c = 1$ is only important for the existence of the co-dimension two intersection. If the two one-dimensional manifolds would intersect for a different value of c and γ, one would also expect a spiral around this point in parameter space, since the co-dimension zero intersection would generically still exist and the local analysis does not change at all (as long as the one equilibrium is still a saddle-focus).

The stability of the travelling kink solutions has been investigated using the Evans function formulation. The boundary of the essential spectrum is easy to calculate

and resides in the left half-plane, so this will not give rise to (linear) instabillity. The point spectrum is less trivial.

For the unperturbed system ($\alpha = \beta = \gamma = 0$), the point spectrum can be given, using the results of [23]. For $\beta = 0$ the point spectrum has been investigated in this thesis. It has been shown that for small enough perturbations, no eigenvalues will move in the right half-plane.

6.3 Stacks of junctions

In a stack of two (equal) junctions there has also been observed a spiral. This spiral can be explained along the same lines, as for the single junction with β-term. The four-dimensional system can be reduced to a three-dimensional one, for velocities close to $c = c_- = \sqrt{1+\sigma^2}$, using singular perturbation theory. The existence of a heteroclinic connection for this case is much more difficult, since the system does not have an obvious symmetry to help proving it. Still, there is numerical evidence that in fact, such a connection does exist. The existence of the spiral in parameter space than immediately follows from the theorem in chapter 3, since all conditions of the theorem are met.

Furthermore, we have investigated the effect of a difference in the critical current of the two junctions. If this this ratio is larger than 1, this gives rise to what has been called the effect of "backbending"[9]. If this ratio becomes smaller than 1, on the other hand, a different effect occurs. The velocity c_- is no longer forms a boundary. Travelling wave solutions exist for velocities larger than c_-.

At the end of chapter 5, some effects observed in numerics and experiments have been indicated, that will be interesting for further research.

Bibliography

[1] A. Barone and G. Paternò. *Physics and Applications of the Josephson Effect*. Wiley-Interscience, 1982.

[2] W.A. Coppel. *Dichotomies in Stability Theory*. Lecture Notes in Mathematics. Springer-Verlag, 1978.

[3] M. Crampin and F.A.E. Pirani. *Applicable differential geometry*, volume 59 of *London Mathematical Society lecture notes series*. Cambridge University Press, 1986.

[4] E.J. Doedel, A.R. Champneys, et al. *AUTO 97: Continuation and bifurcation software for ordinary differential equation (with HomCont HomCont)*. Concordia University, Canada, `ftp.ca.concordia.ca/pub/doedel/auto`.

[5] N. Fenichel. Geometric singular perturbation theory for ordinary differential equations. *J. Differential Equations*, 31(1):53–98, 1979.

[6] R.P. Feynman. *The Feynman lectures on physics*, volume III: Quantum mechanics. Addison-Wesley, 1965.

[7] E. Goldobin. personal communication.

[8] E. Goldobin, B.A. Malomed, and A.V. Ustionv. Maximum velocity of a fluxon in a stack of coupled Josephson junctions. *Physics Letters A*, 266(1):67–75, 2000.

[9] E. Goldobin, A. Wallraff, et al. Cherenkov radiation from fluxon in a stack of coupled long Josephson junctions. *Journal of Low Temperature Physics*, 119(5/6):589–614.

[10] N Grønbech-Jensen, D Cai, et al. Stability of bunched fluxons in magnetically coupled Josephson junctions. *Physical Review B*, 48(21):16160–16163, 1993.

[11] N. Grønbech-Jensen, M.R. Samuelsen, et al. Bunched soliton states in weakly coupled sine-Gordon systems. *Physical Review B*, 42(7), 1990.

[12] J. Guckenheimer, M.R. Myers, et al. *DsTool: A Dynamical System Toolkit with an Interactive Graphical Interface*.

[13] D. Henry. *Geometric theory of semilinear parabolic equations*, volume 840 of *Lecture notes in mathematics*. Springer-Verlag, 1981.

[14] C.K.R.T. Jones. Geometric singular perturbation theory. In *Dynamical systems*, pages 44–118. Springer, 1995.

[15] T. Kapitula. Stability criterion for bright solitary waves of the perturbed cubic-quintic Schrödinger equation. *Physica D*, 116:95–120, 1998.

[16] T. Kapitula and B. Sandstede. Stability of bright solitary-wave solutions to perturbed nonlinear Schrödinger equations. *Physica D*, 124(1–3):58–103, 1998.

[17] R. Kleiner, P. Müller, et al. Dynamic behaviour of Josephson-coupled layered structures. *Physical Review B*, 50(6):3942–3952, 1994.

[18] V.P. Koshelets, S.V. Shitov, et al. First implementation of a superconducting integrated receiver at 450 GHz. *Applied Physics Letters*, 68(9):1273–1275, 1996.

[19] V.P. Koshelets, S.V. Shitov, et al. Linewdith of frequency locked flux flow oscillators for sub-mm wave receivers. *IEEE Transactions on Applied Superconductivity*, 7(2):2905–2908, 1997.

[20] Y.A. Kuznetsov. *Elements of Applied Bifurcation Theory*, volume 112 of *Applied Mathematical Sciences*. Springer.

[21] Y.-T. Lau. The "coccon" bifurcations in three-dimensional systems with two fixed points. *Int. J. of Bifurcation and Chaos*, (3):543–558, 1992.

[22] B.A. Malomed. Bunching of fluxons in a long Josephson junction with surface losses. *Physical Review B*, 47(2):1111–1112, 1993.

[23] E. Mann. Systematic perturbation theory for sine-Gordon solitons without the use of inverse scattering methods. *Journal of Physics A*, 30(4):1227–1241, 1997.

[24] C.K. McCord. Uniqueness of connecting orbits in the equation $y^{(3)} = y^2 - 1$. *J. of Math. Analysis and Applications*, (114):584–592, 1986.

[25] K Palmer. Exponential dichotomies and transversal homoclinic points. *J. Differential Equations*, (55):225–256, 1984.

[26] R.D. Parmentier. Fluxons in long Josephson junctions. In K. Lonngren and A. Scott, editors, *Solitons in Action*, pages 173–199. Academic Press, Inc., 1978.

[27] N.F. Pedersen. Solitons in Josephson transmission lines. In S.E. Trullinger et al., editors, *Solitons*. Elsevier Science Publishers, B.V., 1986.

[28] G.P. Pepe, G. Peluso, et al. Pulse-induces switches in a Josephson tunnel stacked device. *Applied Physics Letters*, 79(17):2770–2772, 2001.

[29] G.P. Pepe, R. Scaldaferri, et al. Low-t_c three-terminal structures for new superconducting devices. *Superconductor Science and Technology*, 14:987–993, 2001.

[30] A.V. Sakai, S. Ustinov et al. Theory and experiment on electromagnetic-wave-propagation velocities in stacked superconducting tunnel structures. *Physical Review B*, 50(17), 1994.

[31] S. Sakai, P. Bodin, and N.F. Pedersen. Fluxons in thin-film superconductor-insulator superlattices. *Journal of Applied Physics*, 73(5), 1993.

[32] J. A. Sanders and R. Cushman. Limit cycles in the Josephson equation. *SIAM Journal on Mathematical Analysis*, 17(3):495–511, 1986.

[33] B. Sandstede. Stability of multiple-pulse solutions. *Transaction of the American Mathematical Society*, 350(2):429–472, 1998.

[34] B. Sandstede and A. Scheel. Absolute and convective instabilities of waves on unbounded and large bounded domains. *Physica D*, 145(3–4):233–277, 2000.

[35] S. Sternberg. Local contractions and a theorem of Poincaré. *American Journal of Mathematics*, 79:809–824, 1957.

[36] J.F. Toland. Existence and uniqueness of heteroclinic orbits for the equation $\lambda u''' + u' = f(u)$. *Proceedings of the Royal Society of Edinburgh*, 109A:23–26, 1988.

[37] A.V. Ustinov, R.P. Doderer, et al. Dynamics of sine-Gordon solitons in the annular Josephson junction. *Physical review letter*, 69(12):1815–1818, 1992.

[38] A. Wallraff, E. Goldobin, and A.V. Ustinov. Numerical analysis of the cohernet radiation emission by two stacked Josephson flux-flow oscillators. *Journal of Applied Physics*, 80(11):6523, 1996.

[39] Y. Zhang and Gupta D. Low-jitter on-chip clock for RSFQ circuit applications. *Superconductor Science and Technology*, 12(11):769–772, 1999.

Summary

or various reasons people have been interested in Josephson junctions. Ranging from "understanding nature" to building quantum computers. In this thesis we focus on a special type of junction (the long junction) and to a special type of problem (fluxon dynamics).

After the introduction, we start in chapter 2 by modelling the long Josephson junction. Although this has been done many times over the years, we found it necessary to carefully investigate this topic again. We model the long Josephson junction using a discrete model, the final equations are obtained on taking the limit of the cell size to zero. We use different discrete models to obtain more general models.

In the most general case treated here, we assume the resistance experienced by quasi-particles flowing along the surface of the superconductors to be very large (of order $\frac{1}{\epsilon}$). The well-known β-term in the partial differential equation is then of order ϵ. In our model we obtain two more terms, both of order ϵ. One assumption made in this derivation is that the ratio of the resistance and inductance experienced by currents flowing along the surface of the superconductors is equal for both superconductors forming a junction. If one would derive the equations without making this assumption, one would get more (coupling) terms.

Important for applications is to understand the behaviour of travelling fluxons, for example what the maximum speed of these fluxons is, and what the maximum driving current can be. The answer to these questions is related to both the existence and stability problem of the travelling 2π-kink solutions. In the third chapter the existence problem for these solutions is addressed. Numerical simulations with AUTO indicate that there is an upper bound on both γ and the velocity c for the existence of these travelling kink solutions. In the (c, γ) parameter plane, the combinations for which a travelling wave exists lie on a spiral. In this chapter it is shown that this is the consequence of the existence of a heteroclinic cycle.

The linearised stability problem is discussed in chapter 4. The essential spectrum is analysed in general, and is shown to lie in the left half-plane. The point spectrum is analysed using the Evans function. For the unperturbed sine-Gordon equation the Evans function is given explicitly. For small perturbations we calculate how the Evans function perturbs. We show that for small enough perturbations, no eigenvalues can move into the right half-plane.

The last chapter before the conclusions is dedicated to a stack of two junctions. Here, again, we necessarily have to restrict our attention to some specific topics. For equal

junctions it makes sense to look at symmetric solutions. The existence problem is reduced to the problem for a single junction. The stability of this in-phase solution depends on the speed as is shown numerically in section 5.5.

Interestingly, also for a stack of junctions a spiral is observed, if there is a single fluxon in one of the junctions. It is motivated briefly how this four dimensional case can be compared to the three-dimensional case analysed in chapter 3. We finish off the chapter with some numerical experiments to spark further research.

Samenvatting

osephson juncties zijn in de afgelopen tijd om verschillende redenen een object van studie geworden. Enerzijds is een motivatie geweest om puur het fenomeen en de fysica te begrijpen, anderzijds wordt deze techniek al gebruikt voor snelle elektronische schakelingen en mogelijk in de toekomst voor quantumcomputers. In dit proefschrift beperken we ons tot een specifiek type junctie, nl. de lange junctie. Verder beperken we ons tot de dynamica van fluxonen.

Na een korte introductie beginnen we in hoofdstuk 2 met het modelleren van de lange juncties. Hoewel dit door de jaren heen al vele malen is gedaan, vonden we het toch nodig om dit onderwerp nogmaals nauwkeurig te bestuderen. We maken in dit proefschrift gebruik van een discreet model om vergelijkingen af te leiden. Door de afmeting van de discrete cellen naar nul te laten gaan, verkrijgen we een partiële differentiaalvergelijking. Voor verschillende discrete modellen worden vergelijkingen afgeleid.

In het meest algemene geval dat hier aan bod komt, wordt aangenomen dat de quasideeltjes die langs het oppervlak van de supergeleiders stromen, een zeer grote weerstand ondervinden (van orde $\frac{1}{\epsilon}$). De in de literatuur bekende β-term in de partiële differentiaalvergelijking is dan van orde ϵ. Het model dat hier wordt afgeleid bevat nog twee termen, die niet in de literatuur voorkomen die tevens van orde ϵ zijn. Een van de aannames die gemaakt wordt is dat de verhouding van de weerstand en de inductie die de oppervlaktestromen ondervinden gelijk is voor beide supergeleiders in een junctie. Als men vergelijkingen afleidt zonder deze aanname, zal dit tot nieuwe (koppelings-)termen leiden.

Voor toepassingen is het belangrijk om te weten wat de maximale snelheid van een fluxon is en wat de maximale stroom is waarbij fluxonen nog bestaan. Om een antwoord op deze vraag te vinden moet zowel de existentie als de stabiliteit van oplossingen worden onderzocht. De existentie wordt behandeld in hoofdstuk 3. Numerieke berekeningen met het programma AUTO laten zien dat er maximale waarden voor de snelheid c en de stroom γ bestaan. In het (c, γ)-parametervlak liggen de combinaties van parameterwaarden, waarvoor een lopende golf bestaat, op een spiraal. In dit hoofdstuk wordt aangetoond dat dit een gevolg is van het bestaan van een heterocliene cykel.

Het gelineariseerde stabiliteits probleem wordt in hoofdstuk 4 behandeld. Hiertoe wordt het spectrum geanalyseerd. Het essentiële spectrum ligt geheel in het linker halfvlak (voor algemene verstoringen). Het puntspectrum wordt geanalyseerd voor

kleine verstoringen, met behulp van de Evans functie. Voor de ongestoorde sine-Gordon vergelijking wordt een expliciete uitdrukking gegeven. Voor kleine verstoringen van de vergelijking wordt geanalyseerd hoe de nulpunten van de Evans functie verstoord worden. We tonen aan dat als de verstoring voldoende klein is, er geen eigenwaarden het rechter halfvlak in bewegen.

In het laatste hoofdstuk voor de conclusies wordt een stapel van twee juncties behandeld. Als de twee juncties waaruit de stapel bestaat identiek zijn, is het zinvol om naar symmetrische oplossingen te zoeken. Het existentie probleem voor deze oplossingen kan gereduceerd worden tot het existentie probleem in een enkele junctie. De stabiliteit van deze in-fase oplossingen hangt af van de snelheid, zoals numeriek wordt aangetoond in paragraaf 5.5.

Indien zich maar in een van beide juncties een fluxon bevindt, is er wederom een spiraal in het (c, γ) parametervlak gevonden. Deze situatie wordt gerelateerd aan de situatie in hoofdstuk 3. Dit hoofdstuk wordt afgesloten met enkele numerieke experimenten, bedoeld om punten voor vervolgonderzoek aan te stippen.

Curriculum Vitae

Timco Visser was born on the 3rd of November 1973 in Hengelo, the Neterlands. He finished his secondary education at the "Ichthus College" Enschede in 1992. In the summer of that same year, he was one of the six members of the team that represented The Netherlands at the International Mathematical Olympiad in Moskow, Russia.

In September 1992, he started to study both Applied Mathematics and Applied Physics at the University of Twente. During the final phase of these studies, a practical training was performed at the "Von Karman Institute for Fluid Dynamics" in Rhode Saint Genèse, Belgium. Under supervision of Prof. G Degrez and D. Vanden Abeele he worked on the "Implementation of General Formulas for Transport Coefficient Calculations". Back in the Netherlands, he started his master's project on "Kinematic Simulation with Vortex Tubes", under supervision of Dr. ir. A. Biesheuvel en Dr. ir. B. Geurts. He received his Master's degree for both Applied Mathematics and Applied Physics in February 1998.

In March 1998 he started his PhD research under supervision of Prof. dr. E. van Groesen and Dr. S.A. van Gils. The result of this research can be found in this thesis. Part of this work was performed in the group of Prof. dr. A.V. Ustinov in Erlangen.